Zoological Journal of the Linnean Society, 2021, **193**, 31–77. With 24 figures.

Integrative taxonomy of giant crested *Eusirus* in the Southern Ocean, including the description of a new species (Crustacea: Amphipoda: Eusiridae)

MARIE L. VERHEYE[1,2,*] and CÉDRIC D'UDEKEM D'ACOZ[1]

[1]*Royal Belgian Institute of Natural Sciences, O.D. Nature, Rue Vautier 29, B-1000 Brussels, Belgium*
[2]*Université de Liège, Laboratoire d'Océanologie, Quartier Agora, Allée du 6 Août 11, B-4000 Liège, Belgium*

Received 25 March 2020; revised 16 September 2020; accepted for publication 10 October 2020

Among Antarctic amphipods of the genus *Eusirus*, a highly distinctive clade of giant species is characterized by a dorsal, blade-shaped tooth on pereionites 5–7 and pleonites 1–3. This lineage, herein named 'crested *Eusirus*', includes two potential species complexes, the *Eusirus perdentatus* and *Eusirus giganteus* complexes, in addition to the more distinctive *Eusirus propeperdentatus*. Molecular phylogenies and statistical parsimony networks (*COI*, *CytB* and ITS2) of crested *Eusirus* are herein reconstructed. This study aims to formally revise species diversity within crested *Eusirus* by applying several species delimitation methods (Bayesian implementation of the Poisson tree processes model, general mixed Yule coalescent, multi-rate Poisson tree processes and automatic barcode gap discovery) on the resulting phylogenies. In addition, results from the DNA-based methods are benchmarked against a detailed morphological analysis of all available specimens of the *E. perdentatus* complex. Our results indicate that species diversity of crested *Eusirus* is underestimated. Overall, DNA-based methods suggest that the *E. perdentatus* complex is composed of three putative species and that the *E. giganteus* complex includes four or five putative species. The morphological analysis of available specimens from the *E. perdentatus* complex corroborates molecular results by identifying two differentiable species, the genuine *E. perdentatus* and a new species, herein described as ***Eusirus pontomedon* sp. nov.**

ADDITIONAL KEYWORDS: alpha taxonomy – cryptic species – genetics – molecular systematics – phylogenetic systematics.

INTRODUCTION

It is now recognized that the diversity of Antarctic continental shelves exceeds that of the Arctic, and is comparable with temperate and even some non-reef tropical shelves (Clarke, 2008). Taxonomic lists of described Antarctic marine species currently include > 8200 records (Griffiths, 2010; De Broyer *et al.*, 2011). However, it has been predicted that the total number of macrozoobenthic species on the shelf alone could be > 17 000 (Gutt *et al.*, 2004). Such numbers suggest that the vast majority of the Antarctic marine diversity remains unknown to science. Many of these new species will probably come from undersurveyed areas of Antarctica, such as the zone between the Bellingshausen Sea/Amundsen Sea and the Ross Sea, the Western Weddell Sea, large parts of the East Antarctic and the deep sea, which are poorly sampled because of the logistic constraints attached to sampling in such heavily ice-covered and/or remote places (Griffiths, 2010; De Broyer *et al.*, 2011). However, many new species also come from regions showing the highest level of sampling and recorded species, such as the islands of the Scotia Sea, the West Antarctic Peninsula, the eastern Weddell Sea, the Ross Sea and Prydz Bay (Griffiths, 2010; d'Udekem d'Acoz & Verheye, 2017).

Documenting this poorly known biodiversity is becoming even more pressing in the light of the many

*Corresponding author. E-mail: mverheye@naturalsciences.be
[Version of record, published online 26 December 2020; http://zoobank.org/ urn:lsid:zoobank.org:pub:055688C7-A2E1-4C0D-BE45-57058B3AB67A]

threats that the region is currently facing. Regional warming, alterations to sea-ice concentration and distribution, changes in seasonality, ocean acidification and industrial fishing are negatively impacting Antarctic marine ecosystems (Orr *et al.*, 2005; Clarke *et al.*, 2007; Barnes & Peck, 2008; Griffiths, 2010; Schloss *et al.*, 2012; Chown *et al.*, 2012, 2015; Gutt *et al.*, 2015; Hernando *et al.*, 2015; Xavier *et al.*, 2016). In such a context, alpha taxonomic studies are needed to document the current state of Antarctic marine biodiversity in order to be able to assess alterations in faunal composition and distributions related to local and global change processes and, thereby, assist in conservation programmes (Costello *et al.*, 2013; Xavier *et al.*, 2016).

The development of molecular techniques notably led to a substantial increase in the number of known Antarctic marine species. Using one or more genes, cryptic species and species complexes have been inferred in almost every Antarctic taxon that has been investigated (Grant *et al.*, 2011), including macrobenthic and generally well-studied organisms, such as molluscs (Linse *et al.*, 2007; Allcock *et al.*, 2011), pycnogonids (Mahon *et al.*, 2008; Krabbe *et al.*, 2010), echinoderms (Janosik & Halanych, 2010; Hemery *et al.*, 2012), isopods (Held, 2003; Held & Wägele, 2005; Raupach & Wägele, 2006; Raupach *et al.*, 2007; Leese & Held, 2008) and amphipods (Lörz & Held, 2004; Lörz *et al.*, 2009; Havermans *et al.*, 2011, 2013; Verheye *et al.* 2016; d'Udekem d'Acoz & Verheye, 2017). Molecular systematics, phylogeography and DNA barcoding studies are currently revealing 'candidate species' at a faster pace than results can be followed up by taxonomic descriptions (Padial *et al.*, 2010). However, in order to translate such DNA-based entities into formal species, the use of additional lines of evidence is increasingly being advocated (Schlick-Steiner *et al.*, 2009; Padial *et al.*, 2010). In an integrative taxonomic framework, additional non-DNA (e.g. morphological, ecological, behavioural and biogeographical) data can provide the background knowledge corroborating the evolutionary interpretation of the DNA data (DeSalle *et al.*, 2005; Will *et al.*, 2005; Vogler & Monaghan, 2007).

Including a total of 945 currently recorded species (Griffiths *et al.*, 2011; De Broyer *et al.*, 2020), amphipods are among the most species-rich macrobenthic organisms in Antarctic and sub-Antarctic waters (De Broyer *et al.*, 2007; De Broyer & Jażdżewska, 2014). They perfectly exemplify the general underestimation of Antarctic diversity, because recent morphological and/or molecular studies have revealed a considerable number of new species, even among large-bodied forms (e.g. d'Udekem d'Acoz, 2008; Krapp-Schickel & De Broyer, 2014). For instance, putative species-level clades were uncovered by molecular methods within the giant nominal species *Eurythenes gryllus* (Lichtenstein in Mandt, 1822) (Havermans *et al.*, 2013). Using a combination of DNA-based methods and morphology, the number of known Antarctic species within the large and iconic genus *Epimeria* Costa, 1851 has been doubled, with the description of 28 new species (Verheye *et al.*, 2016; d'Udekem d'Acoz & Verheye, 2017). Likewise, a previous molecular study suggests that the nominal species of giant (50–80 mm, or even larger) amphipods, *Eusirus perdentatus* Chevreux, 1912 and *Eusirus giganteus* Andres, Lörz & Brandt, 2002, might also be complexes of several species (Baird *et al.*, 2011).

Eusirus perdentatus, *E. giganteus* and *Eusirus propeperdentatus* Andres, 1979 together form the most distinctive lineage within Antarctic *Eusirus* Krøyer, 1845. It is herein termed 'crested *Eusirus*', because all these species have six body segments (pereionites 5–7 and pleonites 1–3) adorned with a strong, laterally compressed crest posteriorly produced into a tooth, whereas other Antarctic *Eusirus* have only two or three toothed body segments. *Eusirus giganteus* is morphologically similar to *E. perdentatus*, but with a longer and more slender propodus on ambulatory pereiopods 3 and 4. As a result of this high morphological similarity, the two species have been extensively confused in previous records (e.g. by Klages, 1993; Emison, 2000). *Eusirus perdentatus* is reported to be a benthic to benthopelagic (possibly, also temporarily sympagic) carnivorous predator (Klages & Gutt, 1990; Klages, 1993; Emison, 2000; Dauby *et al.*, 2001; Graeve *et al.*, 2001; Nelson *et al.*, 2001; Nyssen *et al.*, 2005; Krapp *et al.*, 2008). *Eusirus giganteus* is presumed to have a similar lifestyle (Andres *et al.*, 2002). However, because of the past confusion with *E. perdentatus*, it is unclear which ecological observations were based on which species. *Eusirus propeperdentatus* is a strictly pelagic species and morphologically distinct from other crested *Eusirus* (for morphological differences, see Emison, 2000: table 6).

The unrooted concatenated (*COI*, *CytB* and ITS2) phylogeny of crested *Eusirus* (excluding *E. propeperdentatus*) of Baird *et al.* (2011) showed four maximally supported clades within *E. giganteus*, termed G1–G4, and three maximally supported clades within *E. perdentatus*, termed P1–P3. Using a 95% connection limit, all these clades corresponded to unconnected statistical parsimony networks, with two clades within G4 (G4a and G4b) even corresponding to unconnected *COI* and *CytB* networks, but a single one for ITS2. Such statistical parsimony analysis separates groups of sequences into different networks if haplotypes are connected by comparatively long branches that have a > 5% probability to be affected by homoplasy. Although

homoplasious connections do not necessarily correspond to species boundaries, the interruption of gene flow associated with speciation events is indeed expected to produce large observed genetic discontinuities, and the 95% connection limit in statistical parsimony networks was suggested to be a consistent quantitative standard of such genetic differentiation (Wiens & Penkrot, 2002; Morando *et al.*, 2003; Cardoso & Vogler, 2005; Hart *et al.*, 2006; Pons *et al.*, 2006; Hart & Sunday, 2007; Chen *et al.*, 2010). Unconnected statistical networks, non-overlapping intra- and interclade distances and the sympatric distribution of some of these clades led to the conclusion that the clades P1–P3 and G1–G4 are likely to corresponded to cryptic species, with G4 even potentially including two recently diverged species, G4a and G4b (Baird *et al.*, 2011).

In the present study, we add new sequences (*COI*, *CytB* and ITS2), mostly of *E. perdentatus s.l.* specimens, but also some *E. giganteus* (*COI*), collected off the Antarctic Peninsula, in the Eastern Weddell Sea and along the Adélie Coast, to the datasets of Baird *et al.* (2011). Molecular phylogenies and statistical parsimony networks are reconstructed based on these larger datasets. The aims of this study are as follows: (1) to formally explore species boundaries within the whole crested *Eusirus* clade by applying several species delimitation methods [Bayesian implementation of the Poisson tree processes model (bPTP), general mixed Yule coalescent (GMYC), multi-rate Poisson tree processes (mPTP) and automatic barcode gap discovery (ABGD)] to the resulting phylogenies/genetic distances; (2) to revise the geographical distributions of putative species; and (3) within the *E. perdentatus* complex, to integrate molecular results with a detailed morphological analysis, including colouration data. This leads to the redescription of *E. perdentatus* and the formal description of a new species, *Eusirus pontomedon*.

MATERIAL AND METHODS

Sampling

Most of the material was collected during various Antarctic cruises of the R.V. *Polarstern*, using Agassiz trawls and Rauschert dredges. Colour photographs of some living specimens were taken during ANT-XXIII/8, whereas all collected specimens were sorted out systematically on board by colour morph during ANT-XXIX/3. Coordinates of the *Polarstern* stations have been extracted from the cruise reports: PS61, ANT-XIX/3–4, ANDEEP I and II (Fütterer *et al.*, 2003); PS65, ANT-XXI/2, BENDEX (Arntz & Brey, 2005); PS69, ANT-XXIII/8 (Gutt, 2008); PS71, ANT-XXIV/2, ANDEEP-SYSTCO (Bathmann, 2010); PS77, ANT-XXVII/3, CAMBIO (Knust *et al.*, 2012); PS81, ANT-XXIX/3, LASSO (Gutt, 2013); and PS82, ANT-XXIX/9 (Knust & Schröder, 2014). Samples from the CEAMARC and RSS *James Ross* were loaned by, respectively, the Muséum national d'Histoire naturelle, Paris, France and the British Antarctic Survey, Cambridge, UK. Voucher specimens are deposited at the Royal Belgian Institute of Natural Sciences (RBINS, Brussels, Belgium) and the Muséum national d'Histoire naturelle (MNHN, Paris, France).

Molecular systematics

Taxon sampling

A total of 42 additional specimens of the *E. perdentatus* complex, collected off the Antarctic Peninsula area, the Adélie Coast and in the eastern Weddell Sea, were sequenced for this study and added to the datasets of Baird *et al.* (2011), which included 71 specimens from this species complex. In the *E. giganteus* complex, 14 specimens collected in the Peninsula area, the Adélie Coast and the eastern Weddell Sea were newly sequenced and added to the datasets of Baird *et al.* (2011), which included 56 specimens from this species complex. Additionally, two *E. propeperdentatus* from the Adélie Coast were newly sequenced (*COI*). Four specimens of the *Eusirus* complex *antarcticus* Thomson, 1880 were used as the outgroup in the *COI* phylogeny. All specimens newly sequenced for this study are listed in the Supporting Information (Table S1), along with their sampling details.

DNA sequencing

DNA was extracted from one or two pleopod(s) using a DNAeasy Blood & Tissue kit (Qiagen, Antwerp, Belgium), following the manufacturer's protocol for animal tissues. The DNA was eluted in 100 µL of sterile distilled H_2O (RNase free) and stored at –20 °C.

Partial segments of the mitochondrial cytochrome *c* oxidase subunit I (*COI*; 577 bp), cytochrome B (*CytB*; 368 bp) and internal transcribed spacer 2 (ITS2; 553 bp) were amplified by polymerase chain reaction (PCR). Amplifications were performed in 25 µL reaction mix, which contained 0.26 µL Taq DNA Polymerase (5 U μL^{-1}; Qiagen), 2.5 µL CoralLoad PCR Buffer (Qiagen), 2.5 µL dNTPs mix (250 µM of each), 2.5 µL of each primer (2 µM), 13 µL of RNase-free water and 2 µL of DNA extract.

The *COI* fragment was amplified using two different pairs of primers. First, the universal primers LCO1490 and HCO2198 of Folmer *et al.* (1994) were used, with the same thermal cycling protocol as described by

Baird *et al.* (2011). Later, another pair of primers was tested, which amplified a longer fragment (~850 bp): COCF, CHACRAAYCAYAAA-GATATTGGWAC and COCR, RAARTARTGTCGDTRTCTAC. The thermal cycling protocol began with 1 min at 94 °C, followed by 38 cycles of 50 s at 94 °C, 50 s at 51 °C, 50 s at 72 °C, and a final elongation at 72 °C for 10 min. The *CytB* and ITS2 fragments were amplified using the same primers (151F/270R and ITS4/ITS5, respectively) and the same thermal cycling conditions as described by Baird *et al.* (2011).

The PCR products were visualized under blue light on 1% agarose gels stained with MIDORI^{Green} Advance (NIPPON Genetics Europe, Dueren, Germany), with a comigrating 200 bp ladder molecular-weight marker to confirm their correct amplification. Before sequencing, PCR products were purified using Exonuclease I (20 U μL^{-1}) and FastAP thermosensitive alkaline phosphatase (1 U μL^{-1}) (ThermoFisher Scientific, Waltham, MA, USA), following the manufacturer's protocol.

Forward and reverse strands were sequenced with fluorescence-labelled dideoxynucleotide terminators (BigDye 3.1; Applied Biosystems, Foster City, CA, USA). Both fragments were sequenced using the PCR primers.

Phylogenetic analyses

Sequence chromatograms were checked, and forward and reverse sequence fragments were assembled using CODONCODE ALIGNER v.3.7.1 (CodonCode Corporation; available at http://www.codoncode.com/aligner/). All sequences have been deposited in GenBank (Supporting Information, Table S1).

Sequences were aligned with CLUSTALW in MEGA7 (Kumar *et al.*, 2016), using default settings. In order to prevent inclusion of pseudogenes in the analyses, amino acid translations of both mitochondrial fragments were checked for stop codons. ITS2 sequences contained indels. Treating gaps as missing data could discard useful phylogenetic information, and treating them as a fifth character would weigh each indel event too strongly. We therefore recoded gaps as single characters representing the presence or absence of a single event using FASTGAP v.1.2 (Borchsenius, 2009), according to the method described by Simmons & Ochoterena, 2000.

The best-fitting models of DNA substitution were selected in PARTITIONFINDER (Lanfear *et al.*, 2012). The Bayesian information criterion (BIC) was used on the concatenated dataset partitioned by gene and by codon position (for *COI* and *CytB*), with a distinct partition for the recoded gaps of ITS2, and assuming a single set of underlying branch lengths (Table 1).

Table 1. Best substitution models selected for each partition based on the Bayesian information criterion

Gene partition	Substitution model
CytB_pos1, CytB_pos2, ITS2	K80+I
CytB_pos3, COI_pos3	K80+G
COI_pos1	SYM+G
COI_pos2	F81

In order to evaluate the congruence between genes, preliminary phylogenetic trees were inferred using Bayesian inference (BI) on each separate dataset (*COI*, *CytB* and ITS2). Bayesian inference and maximum likelihood (ML) were then used to reconstruct phylogenetic relationships based on the *COI* dataset and a *CytB*–ITS2 dataset concatenated with SEQUENCEMATRIX (Vaidya *et al.*, 2011).

Bayesian inference trees were reconstructed using MRBAYES v.3.2. (Ronquist & Huelsenbeck, 2003) on the CIPRES portal (Miller *et al.*, 2010). Bayesian inference analyses included two runs of 10^7 generations. Substitution model parameters were set according to the results of PARTITIONFINDER, as indicated in Table 1. Indels that had been recoded as single events in the ITS2 sequence were treated as binary data, adjusting for the ascertainment bias that indels present or absent in all taxa cannot be observed. Trees were sampled every 1000 generations, using four Markov chains and default heating values. Convergence was assessed by the standard deviation of split-frequencies (< 0.01) and by examining the trace plots of log-likelihood scores in TRACER v.1.7 (Rambaut *et al.*, 2018). The first 50% of trees were discarded as burn-in, and the remaining trees (5000) were used to reconstruct a 50% majority rule consensus tree and estimate the posterior probabilities (PP). Nodes with a posterior probability (PP) ≥ 0.95 were considered as significantly supported.

Maximum likelihood trees were estimated using RAXML-HPC v.8 (Stamatakis, 2014) on the CIPRES portal (Miller *et al.*, 2010). A rapid bootstrapping analysis (1000 replicates) and search for the best ML tree was performed in one single run (option f a). A GTRGAMMA model of substitution was used for the nucleotide data (partitioned per gene, in addition to codon positions for the mitochondrial genes), whereas a BINGAMMA model was used for the ITS2 indels re-coded as binary data, and using a Lewis correction for the ascertainment bias. RAXML only supports the GTR substitution model for nucleotide data. Although this might potentially over-parameterize the substitution model of a partition, it has been found that the influence of model over-parameterization on

the results of phylogenetic inferences is likely to be mild (Dornburg *et al.*, 2008). Nodes with a bootstrap values (BV) ≥ 70 were considered as meaningful.

Haplotype networks

Genealogical relationships among haplotypes in relationship to their geographical locations were represented using haplotype networks. TCS v.1.21 (Clement *et al.*, 2000) was used to create maximum parsimony networks for each gene fragment with 95% connection limits. The presence of missing data can lead to misleading statistical parsimony networks. In TCS, a sequence with missing data that has a distance of zero with several distinct sequences will be grouped with the sequence that appears first in the matrix, leading to order-dependent results (Joly *et al.*, 2007). Therefore, sequences including too many ambiguous sites, and then the remaining positions of the alignment including ambiguous sites, were deleted before analysis. The online tool tcsBU (Múrias dos Santos *et al.*, 2016; available at https://cibio.up.pt/software/tcsBU/) was used to improve the network layout and facilitate visualization. The geographical locations of specimens were overlaid on the networks.

Species delimitation

We first analysed single gene trees using the Bayesian implementation of the Poisson tree processes model (bPTP; Zhang *et al.*, 2013). This method estimates the mean expected number of substitutions per site between two branching events, using the branch length information of a phylogeny. The assumption is that the number of substitutions between species is significantly higher than the number of substitutions within species, resulting in two different branch length classes, modelled as two independent classes of Poisson processes (for intra- and interspecific branching events). The algorithm will search for a delimitation pattern maximizing the likelihood of this mixed model describing speciation and diversification processes as two independent Poisson process classes across the search space, i.e. sets of species hypotheses. In the Bayesian implementation, a Markov chain Monte Carlo (MCMC) sampler is used to produce PPs for the species delimitations. The analyses were conducted on the web server for bPTP (available at http://species.h-its.org/ptp/) using the BI phylogenies and the following settings: 500 000 generations, thinning set to 100 and burn-in at 10%. The *COI* phylogeny was rooted with the *E.* cf. *antarcticus* outgroup, which was excluded from the species delimitation analysis. Given that no suitable outgroup was available for *CytB* and ITS2, these phylogenies were rooted at the position of the most basal divergence event as determined by the BEAST analyses (see next paragraph), which was identical in both cases. Defined as such, the latter outgroups were included in the species delimitation analyses.

Secondly, we used the general mixed Yule coalescent (GMYC) model on single gene trees (Pons *et al.*, 2006; Fujisawa & Barraclough, 2013). This method models speciation via a pure birth process and within-species branching events as neutral coalescent processes. It identifies the transition points between inter- and intraspecies branching rates on a time-calibrated ultrametric tree by maximizing the likelihood score of the model. All lineages leading from the root to the transition point are then considered as different species. We built the ultrametric trees required to run the GMYC algorithm for each of our individual datasets in BEAST v.2.6. Identical sequences (haplotypes) were pruned to a single copy before implementation, because zero-length terminal branches hamper the likelihood estimation (Monaghan *et al.*, 2009; Fujisawa & Barraclough, 2013). The phylogenetic analyses were performed under a relaxed lognormal clock set to an evolutionary rate of 1.0 (i.e. no attempt to estimate divergence time). We used a coalescent tree prior, because it is considered a more adequate option, given that the GMYC uses coalescence as a null model (Monaghan *et al.*, 2009). Analyses were run for 1×10^6 (*CytB* dataset) and 1×10^7 (ITS2 and *COI* datasets) MCMC generations, sampled every 1000th (*CytB*) and 10 000th (ITS2 and *COI*) generation, and the first 10% of the samples were discarded as burn-in. TRACER v.1.7 (Rambaut *et al.*, 2018) was used to check for minimum effective sample sizes (ESS) of 200 and visually inspect stationarity and convergence by plotting likelihood values. The resulting trees were summarized into a target maximum clade credibility tree using TreeAnnotator v.1.8.0. The GMYC analysis was carried out in R v.3.0.1 using the splits (Ezard *et al.*, 2009) and ape (Paradis *et al.*, 2004) packages under the single-threshold method and excluding the outgroup for the *COI* phylogeny (Fujisawa & Barraclough, 2013). The Akaike information criterion (AIC)-based support values for the species clusters were calculated, in order to account for delineation uncertainty (Powell, 2012).

Thirdly, the new algorithm based on PTP, the multi-rate PTP (mPTP), was implemented (Kapli *et al.*, 2017). By assuming a distinct exponential distribution for the branching events of each of the delimited species, mPTP allows interspecific variation to be taken into account in coalescence rates. Although the speciation rate can be assumed as constant between sister species, the intraspecific coalescence rate and, consequently, genetic diversity can vary significantly even among sister species. We performed ML analyses

on the individual RAXML trees, because the method requires fully bifurcating topologies, using the mPTP webserver (https://mptp.h-its.org). The trees were rooted as for the bPTP analyses.

Lastly, the automatic barcode gap discovery (ABGD) method was used on individual genetic distance matrices. This approach aims to identify the 'barcode gap', which separates intraspecific and interspecific genetic distances even when the two distributions overlap. The pairwise genetic distances are first ranked from smallest to largest. A local slope function is computed for a given window size to detect peaks of slope values, with the significantly highest peak being the barcoding gap. A primary partition is defined based on this barcoding gap. The procedure is then repeated recursively on each group of the primary partition to obtain secondary partitions until no further gaps can be defined (Puillandre *et al.*, 2012a). Distance matrices were computed in MEGA7 (Kumar *et al.*, 2016). The BIC in JMODELTEST v.0.1 (Posada, 2008) was used to determine the best-fitting model of substitution available in MEGA for each gene fragment separately, not partitioned by codon position. By this method, the K80+G model was selected for *CytB*, with a gamma shape value of 0.18, TrNef+G was selected for *COI*, with a gamma shape value of 0.15 and, finally, Tamura-3-parameters+G was selected for ITS2, with a gamma shape value of 0.22. Distance matrices were computed in MEGA7 and uploaded to the ABGD webserver (available at https://bioinfo.mnhn.fr/abi/public/abgd/abgdweb.html). The parameters were set to default (X = 1.5, Pmin = 0.001, Pmax = 0.100, steps = 10 and number of bins = 20).

MORPHOLOGICAL SYSTEMATICS

The specimens used for photographic illustration had their colour pattern recorded on board the research vessel (as 'marbled form' or 'spotted form'). Photographs of the preserved specimens were made using the stacking technique (Brecko *et al.*, 2014; d'Udekem d'Acoz & Verheye, 2017). Crested *Eusirus* species are exceedingly similar to each other and differ only in the proportions of a few body parts. Stacking photography allows such differences to be documented objectively with the required precision, and this technique is more time efficient than line drawings. Contrasts were adjusted, and the photographic plates were mounted with ADOBE Photoshop CS3. After this procedure, if the contrast on some portions of the pictures was still too low, the outlines were inked with an INTUOS 3 graphic tablet. The holotype of *E. perdentatus* was examined at the Muséum national d'Histoire naturelle, Paris, where it was illustrated by line drawings.

The model of description is derived from that of Andres *et al.* (2002), with modifications. The following abbreviations were used in the list of examined material: extr., extraction code; reg. number, registration number; sta., station; sp(s), specimen(s). The following abbreviations were used in the captions of the figures: A1, antenna 1; A2, antenna 2; Ep1–Ep3, epimeral plates 1–3; Gn1, gnathopod 1; Gn2, gnathopod 2; Md, mandible; Mx1, maxilla 1; Mx2, maxilla 2; Mxp, maxilliped; P3–P7, pereiopods 3–7; U1–U3, uropods 1–3. In the descriptions, the term 'tooth' is used for non-articulated, pointed ectodermic structures, 'spine' for stout, inflexible, articulated structures, and 'seta' for slender, flexible, articulated structures. For a discussion on the pertinence of this terminology, see d'Udekem d'Acoz (2010). Nomenclature of the setae of the mandibular palp follows Lowry & Stoddart (1993). In the genus *Eusirus*, sex is difficult to determine except for adult or near-mature females. For other specimens, identifying sex is time consuming and requires potentially damaging manipulations. Considering that it is not essential data, because the sexual dimorphism is weak, the sex of the specimens was not determined systematically.

RESULTS

MOLECULAR ANALYSES

Data overview

For the *E. perdentatus* complex, we obtained 41 *COI*, 37 *CytB* and 32 ITS2 sequences, in addition to the 57 *COI*, 64 *CytB* and 50 ITS2 sequences already available from Baird *et al.* (2011). For the *E. giganteus* complex, 14 *COI*, one *CytB* and one ITS2 sequence were obtained and added to the 52 *COI*, 52 *CytB* and 48 ITS2 already available from Baird *et al.* (2011). An additional two *COI* sequences of *E. propeperdentatus* were obtained, as were four *COI* sequences of *E.* cf. *antarcticus* specimens, used as the outgroup.

For the mitochondrial genes, this resulted in a *COI* alignment 633 bp long, including a total of 177 taxa, with 190 variable sites (179 parsimony informative), and a *CytB* alignment 371 bp long, including a total of 154 taxa, with 97 variable sites (90 parsimony informative). The ITS2 nucleotide alignment length, excluding gap regions, was 406 bp, to which was appended a partition of 47 binary characters indicating the presence/absence of gaps, resulting in a total of 453 positions, with 95 variable sites (84 parsimony informative) and 131 taxa.

After removal of some sequences and sites (columns) containing ambiguous positions, in order to prevent

ambiguities in collapsing sequences into haplotypes, the *COI* dataset used for network reconstruction was 581 bp long and included 168 taxa and 57 unique haplotypes. The *CytB* dataset was 368 bp long and included 143 taxa and 42 unique haplotypes. The ITS2 dataset was 451 bp long and included 128 taxa and 36 unique haplotypes.

Intra- and interspecific distances (both uncorrected *p*-distances and corrected), computed in MEGA for each dataset by using the best-fitting models as determined by JMODELTEST, are presented in the Supporting Information (Table S2).

Congruence between gene trees and methods

An examination of the unrooted tree topologies resulting from BI analyses performed on the separate datasets shows that *CytB*, ITS2 and *COI* do not exhibit any supported incongruences. In contrast to *CytB* and ITS2 phylogenies, specimens of the new species *E. pontomedon* (described below) do not all cluster together in the *COI* phylogeny. However, the phylogenetic relationships within the *E. perdentatus* species complex are unsupported (PP < 0.95, BV < 70) in the latter gene tree. Given this discrepancy, and the greater number of *COI* sequences available (notably in the *E. giganteus* complex and the outgroup, *E.* cf. *antarcticus*), the *CytB* and ITS2 datasets were concatenated (Fig. 1) and the *COI* phylogeny is presented separately (Fig. 2). Differences between the topologies of the different reconstruction methods used (MRBAYES, BEAST2 and RAXML) are minimal. In all cases, ambiguities affected only unsupported nodes.

Concatenated (CytB + ITS2*) phylogeny and haplotype networks*

Although the concatenated phylogeny is unrooted, we use the same terminology as for rooted trees in the present section, because the rooted *COI* phylogeny (see next section) shows that the placement of the root does not compromise any of the discussed clusters, which are therefore interpreted as clades.

All specimens of the *E. perdentatus* complex form a clade, supported by both BI and ML (0.96/85). All sequences of the *E. perdentatus* complex produced for the present study fall into clades 'P2' (here identified as the genuine *E. perdentatus*; PP = 1.00, BV = 100) and 'P3' (herein described as the new species *E. pontomedon*; PP = 0.96, BV = 57) of Baird *et al.* (2011). An additional clade, including specimens not available for this study, comprises only *E.* aff. *perdentatus* from the Ross Sea (P1; PP = 1.00, BV = 100). With a maximum parsimony connection limit set at 95%, these three clades correspond to unconnected statistical parsimony networks for all three genes (Fig. 3).

Similar to the results of Baird *et al.* (2011), four clades are supported by BI within the *E. giganteus* complex (G1–G4). These clades are also supported by ML in the present analysis (Fig. 1). Additional sequences (*CytB* and ITS2) of one *E.* cf. *giganteus* specimen from the Antarctic Peninsula produced in this study fall into G1 (in bold in Fig. 1), thereby extending the geographical distribution of this putative species. These four clades (1–4) correspond to unconnected statistical parsimony networks (connection limit = 95%), with two clades within G4 even corresponding to distinct *CytB* networks (but only one ITS2). Slight differences that can be observed in the resulting networks when compared with those of Baird *et al.* (2011) are attributable to differences in taxon sampling, but also in the number of alignment positions used in TCS analyses. In the present study, some columns were deleted owing to ambiguous sites (Fig. 3).

COI *phylogeny and haplotype networks*

The *COI* phylogeny supports the monophyly of all specimens from the *E. perdentatus* complex (PP = 0.95, BV = 77). The *E. perdentatus* clade (P2) and clade P1 are supported by both methods (PP = 1.00/BV = 98 and PP = 1.00/BV = 100, respectively). In contrast, P3 specimens (*E. pontomedon*) do not form a clade in the *COI* phylogeny, but these relationships are unsupported by both BI and ML (Fig. 2). *Eusirus perdentatus*, *E. pontomedon* and P1 all correspond to unconnected *COI* statistical parsimony networks (connection limit = 95%; Fig. 3).

All *E.* cf. *giganteus* sequences produced for the present study fall into clades 'G1' (not supported here; PP = 0.79/BV < 50), 'G2' (PP = 1.00/BV = 100), 'G3' (PP = 1.00/BV = 99) and 'G4' (PP = 1.00/BV = 90) from the study by Baird *et al.* (2011). Clade 'G4' is itself divided into two well-supported clades: 'G4a' (PP = 1.00/BV = 99) and 'G4b' (PP = 1.00/BV = 94). Clades G1–G3, G4a and G4b all correspond to unconnected statistical parsimony networks (connection limit = 95%; Fig. 3). Phylogenetic relationships with *E. propeperdentatus* are not supported. This species also forms a distinct *COI* haplotype network (connection limit = 95%; Fig. 3).

Geographical structure

The present taxon sampling extends the known geographical distribution of several of the inferred species. The true *E. perdentatus* (P2) is now newly recorded from the Adélie Coast, in addition to the eastern Weddell Sea, Peninsula area and Tressler Bank. The new species, *E. pontomedon* (P3), is circum-Antarctic, being present in the same locations as *E. perdentatus*, and also in the Ross Sea (Fig. 3). The two

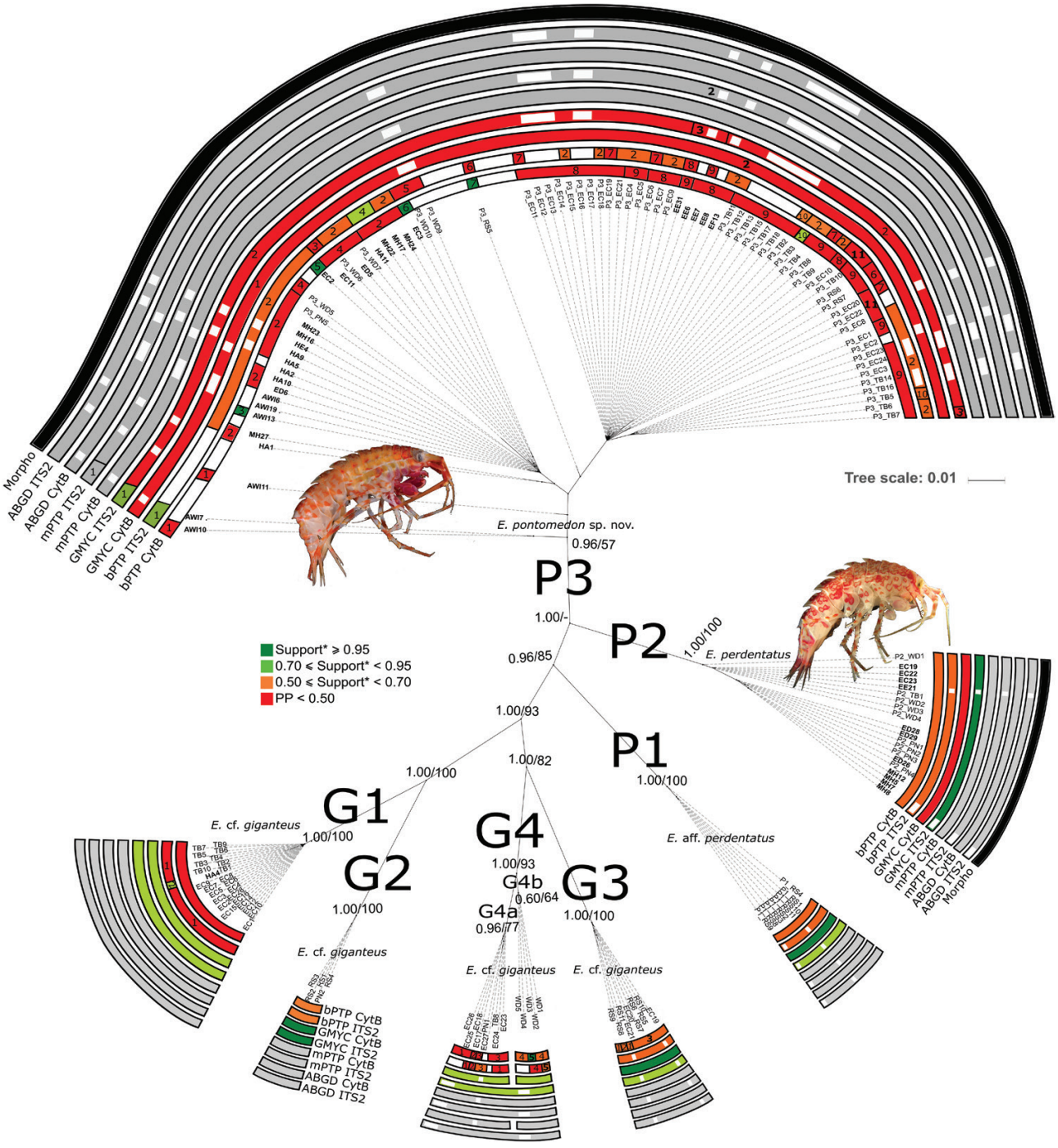

Figure 1. Unrooted Bayesian phylogenetic tree of the concatenated *CytB* + ITS2 dataset. Posterior probabilities and bootstrap values (> 50) from the maximum likelihood analysis are indicated at the corresponding nodes. Putative species identified by DNA-based species delimitation methods [Bayesian implementation of the Poisson tree processes model (bPTP), general mixed Yule coalescent (GMYC), multi-rate Poisson tree processes (mPTP) and automatic barcode gap discovery (ABGD)] applied on the *CytB* and ITS2 trees/distance matrices are indicated by bars on the concatenated tree. Colour codes indicate the support of each putative species. *Posterior probability (PP) for bPTP and Akaike information criterion (AIC)-based support for GMYC. White patches indicate missing data. Whenever some delimited putative species were non-monophyletic on the concatenated tree, numbers on the bars indicate which taxa were identified together as one putative species. In addition, results from the morphological analysis are indicated with black bars for P2 and P3.

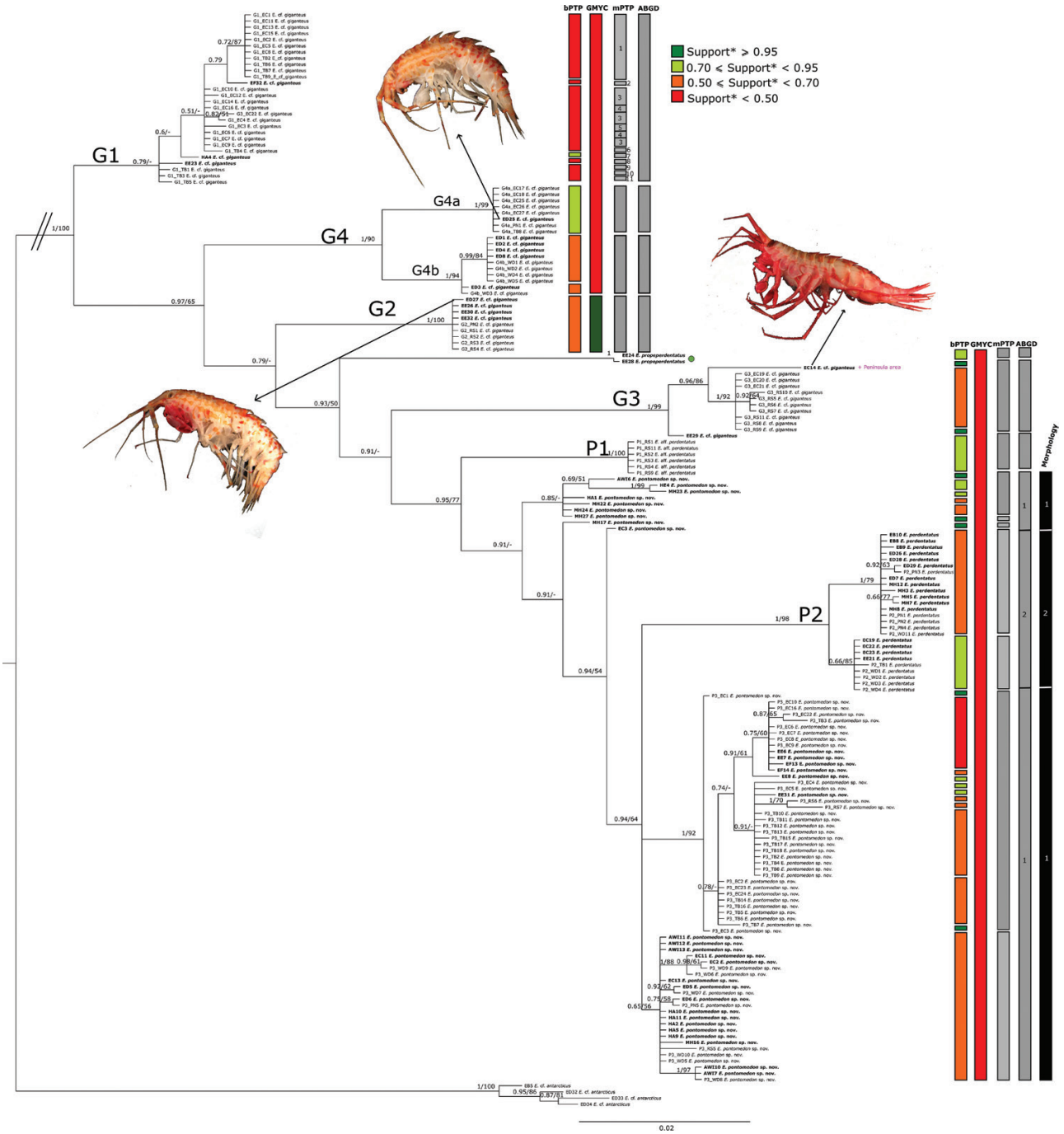

Figure 2. Bayesian phylogenetic tree of the *COI* dataset. Posterior probabilities and bootstrap values (> 50) from the maximum likelihood analysis are indicated above the nodes. Putative species identified by DNA-based species delimitation methods [Bayesian implementation of the Poisson tree processes model (bPTP), general mixed Yule coalescent (GMYC), multi-rate Poisson tree processes (mPTP) and automatic barcode gap discovery (ABGD)] applied on the *COI* tree/distance matrix are indicated by bars on the tree. Colour codes indicate the support of each putative species. *Posterior probability (PP) for bPTP and Akaike information criterion (AIC)-based support for GMYC. Whenever the delimited putative species were non-monophyletic on the tree, numbers on the bars indicate which taxa were identified together as one putative species. In addition, results from the morphological analysis are indicated with black bars for P2 and P3.

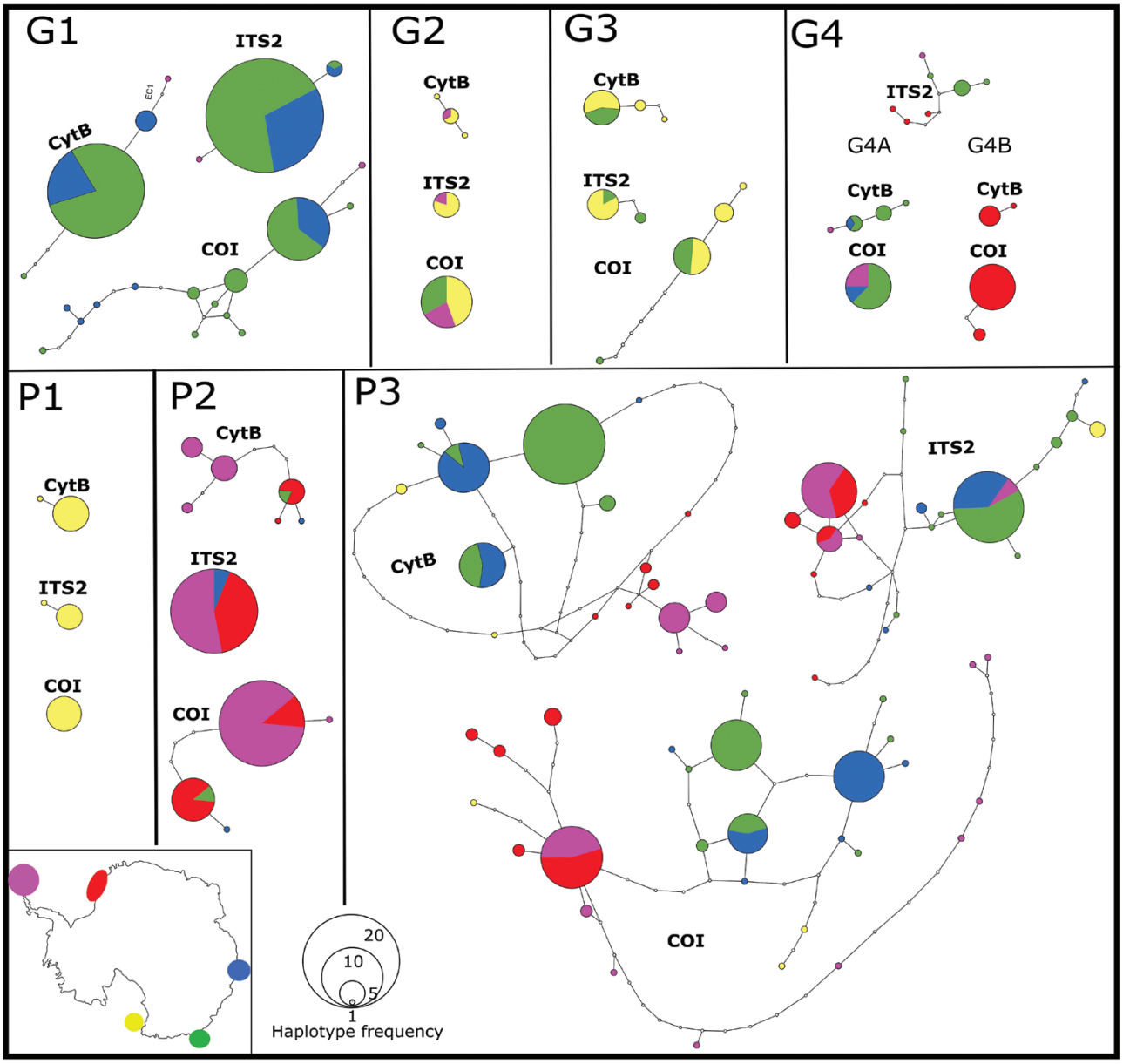

Figure 3. TCS statistical parsimony haplotype subnetworks of the three genes (*COI*, *CytB* and ITS2), including geographical information (colour code).

species were found in sympatry in the Tressler Bank (Baird *et al.*, 2011). They are now also both recorded from station 193-8 (ANT-XXIX/3) in the Bransfield Strait, where they were collected during the same trawling event (Supporting Information, Table S1).

Eusirus cf. *giganteus* 'G1' was known from the Adélie Coast and Tressler Bank and is now found also to occur in the Peninsula area. An identical *COI* haplotype of *E.* cf. *giganteus* 'G2' was found in the Peninsula and the Ross Sea, and is now also found in the Adélie Coast. *Eusirus* cf. *giganteus* 'G3' includes specimens from the Ross Sea and Adélie Coast. The newly sequenced specimen EC14, collected in the Peninsula area, is part of that clade, but was not included in the haplotype network because of ambiguous sites (Fig. 2). Specimens of *E.* cf. *giganteus* 'G4b' and 'G2' were found in sympatry, collected in the same trawl in station 700-2 (ANT-XXIII/8) in Larsen B (Supporting Information, Table S1).

Species delimitation

The bPTP analyses resulted in high numbers of poorly supported putative species. The bPTP analysis of the

CytB Bayesian phylogeny gave a total of 23 putative species. However, all of these delimited entities are unsupported (PP < 0.95), except for some single sequences delimited as putative species. The bPTP analysis of the ITS2 Bayesian phylogeny resulted in a total of 22 unsupported putative species (PP < 0.95). Applied on the *COI* Bayesian phylogeny, bPTP returned a total of 36 putative species. However, all are unsupported by PPs (< 0.95), except for some single sequences delimited as putative species (Figs 1, 2; results on individual BI gene trees are presented in Supporting Information, Fig. S1).

The GMYC analysis of the *CytB* phylogeny returned nine (confidence interval 7–15) 'ML entities' (= putative species). The log-likelihood ratio test suggested that this model was a significantly better fit for the data than the single-species model (likelihood ratio = 14.65, $P = 0.0006$). Within the *E. giganteus* complex, the clades G1, G2, G3, G4a and G4b are each delimited as single putative species (AIC-based support: 0.82, 1.00, 1.00, 0.90 and 0.90, respectively). Within the *E. perdentatus* complex, P1 and P2 are delimited each as single species, although P2 is poorly supported (AIC-based support: 1.00 and 0.40), whereas P3 is delimited as two poorly supported putative species (AIC-based support: 0.03 and 0.27).

The GMYC analysis of ITS2 resulted in nine 'ML entities' (confidence interval 4–20), and the log-likelihood ratio test suggested that this model was a marginally significantly better fit for the data than the single-species model (likelihood ratio = 7.42, $P = 0.02$). Within the *E. giganteus* complex, the clades G1, G2, G3 and G4 are each delimited as single putative species, with AIC-based support of 0.73, 1.00, 0.88 and 0.50, respectively. Within the *E. perdentatus* complex, P1 and P2 are each delimited as single species, with AIC-based support of 0.80 and 1.00, respectively, whereas P3 is delimited as three putative species, two of them being poorly supported (AIC-based support: 0.24, 0.13 and 0.80).

For *COI*, the GMYC analysis returned three (confidence interval 3–31) 'ML entities', and the log-likelihood ratio test suggested that this model was a marginally significantly better fit for the data than the single-species model (likelihood ratio = 7.97, $P = 0.02$). G2 is delimited as a single putative species with a support of 0.87. The two remaining delimited entities received poor AIC-based support: G1 is grouped with G4 with a support of 0.15, and G3 is grouped with P1–P3 with a support of 0.01 (Figs 1, 2; results for each individual ultrametric gene trees are presented in Supporting Information, Fig. S2).

When applied to the *CytB* ML tree, the mPTP algorithm returned seven putative species corresponding to the clades P1, P2, P3, G1, G2, G3 and G4. The mPTP analysis of the ITS2 ML tree returned a total of eight delimited species, including P1, P2, two within P3 (with just the two specimens AWI7 and 10 identified as one separate species), G1, G2, G3 and G4 (Figs 1, 2). Lastly, the mPTP analysis of the *COI* ML tree resulted in 24 putative species, two within P2, five within P3 and 11 within G1, whereas P1, *E. propeperdentatus*, G2, G3, G4a and G4b were each delimited as single putative species (Figs 1, 2; results on individual ML gene trees are presented in Supporting Information, Fig. S3).

Although there is still a lack of consensus on how to interpret discordant ABGD results (Kekkonen & Hebert, 2014), previous studies advocate using a *P*-value of ~0.01 (Puillandre *et al.*, 2012a). For *CytB* and ITS2 distance matrices, the delimitation corresponding to a *P*-value of ~0.01 was also the most stable across all tested *P*-values and was therefore selected. For the *COI* distance matrix, no predominant scheme was observed, and the delimitation corresponding to a *P*-value of ~0.01 was retained (which was also the highest *P*-value resulting in more than one putative species). The complete set of ABGD delimitation schemes is presented in the Supporting Information (Fig. S4). The ABGD analysis of the *COI* TrNef+G pairwise distances matrix, using the highest *P*-value (initial partitioning), suggested a total of nine putative species, including G1, G2, G3, G4a, G4b, P1, P2, P3 and *E. propeperdentatus*. The ABGD analysis of the *CytB* K80+G pairwise distances matrix reported eight putative species, including G1, G2, G3, G4a, G4b, P1, P2 and P3, consistently across all *P*-values (initial partitioning), except for the highest one, which resulted in five putative species, grouping together P2, P3 and G4. The most stable delimitation scheme across *P*-values (initial partitioning) obtained with the ABGD analysis of the Tamura-3-parameters+G pairwise distance matrix of ITS2 sequences was seven putative species, including G1, G2, G3, G4, P1, P2 and P3.

TAXONOMY

Order Amphipoda Latreille, 1816

Superfamily Eusiroidea Stebbing, 1888

Family Eusiridae Stebbing, 1888

Genus *Eusirus* Krøyer, 1845

Eusirus perdentatus Chevreux, 1912

(Figs 4–14)

Eusirus perdentatus Chevreux, 1912: 10. – Chevreux, 1913: 163, figs 50–52. – K.H. Barnard, 1930: fig. 4.6a [presumably, in part]. – K.H. Barnard, 1932: 188 [in

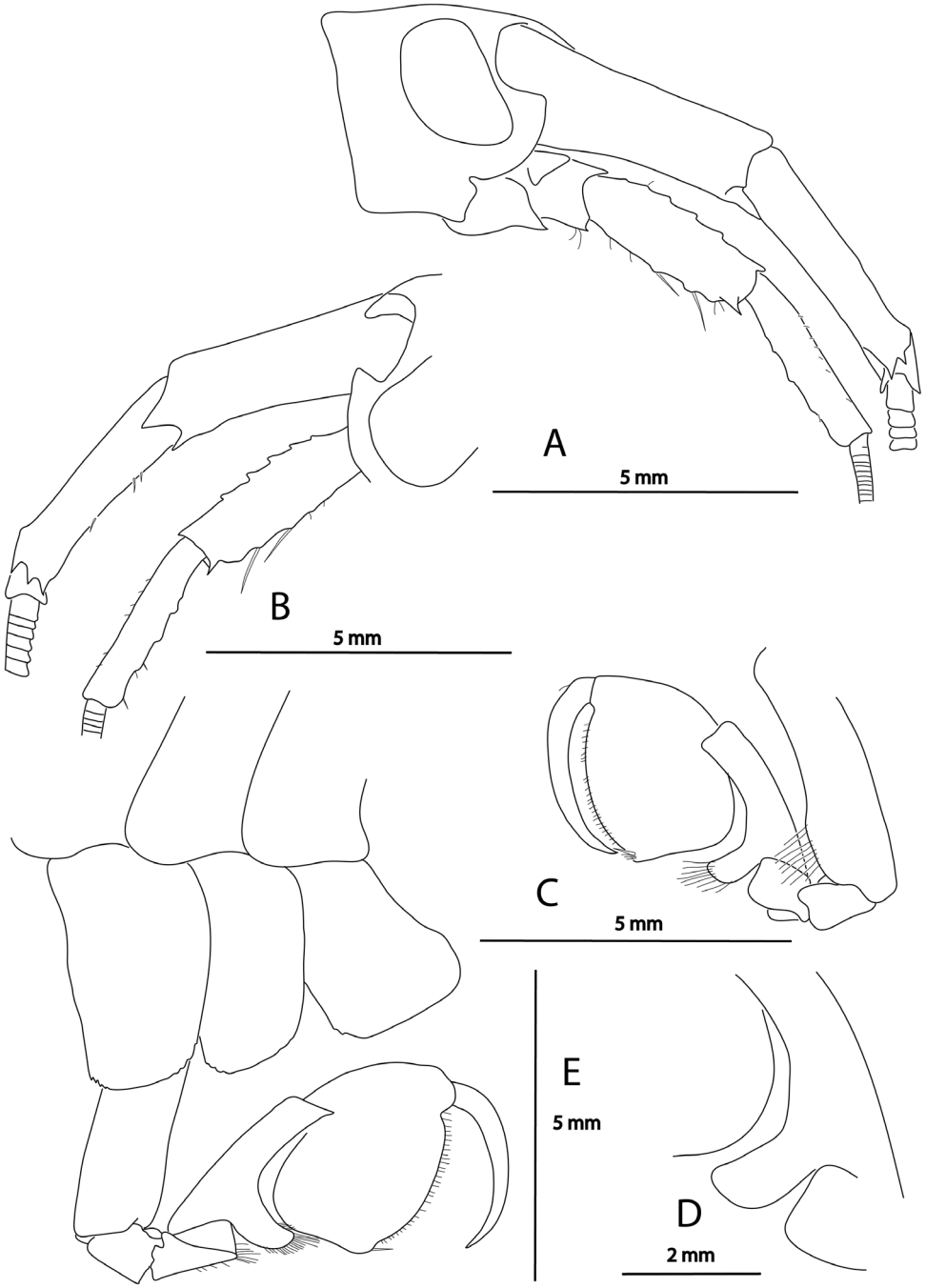

Figure 4. *Eusirus perdentatus*, ♀ holotype, RV *Pourquoi Pas?*, dredging station 15, Palmer Archipelago, *MNHN AM 831*. A, head (right side) and right antennae in lateral view. B, head (left side) and right antennae in medial view. C, right Gn1 in medial view. D, carpal process of right Gn1 in medial view. E, coxae 1–3 and right Gn2 in lateral view.

part], fig. 115 (lower photograph). – J.L. Barnard, 1961: 96 (key). – De Broyer, 1983: 329, 339 [presumably, in part]. – Andres, 1990: 136, fig. 269. – Ren & Huang, 1991: 213, fig. 16. – Vinogradov, 1999: 1160, fig. 4.6. – Emison, 2000: 6 [in part, not figs 2–8 (= *E. giganteus s.l.*)]. – Andres *et al.*, 2002: 121 [in part], figs 7D–K, 8A, C–E [holotype], not fig. 8B, F, H–J (= *E. pontomedon*). – d'Udekem d'Acoz & Robert, 2008: 53 [in part]. – Baird *et al.*, 2011: 3443 [in part]. – Rauschert & Arntz, 2015: 64, pl. 57 (unnumbered fig.). – Peña Othaitz & Sorbe, 2020: 250 [in part].

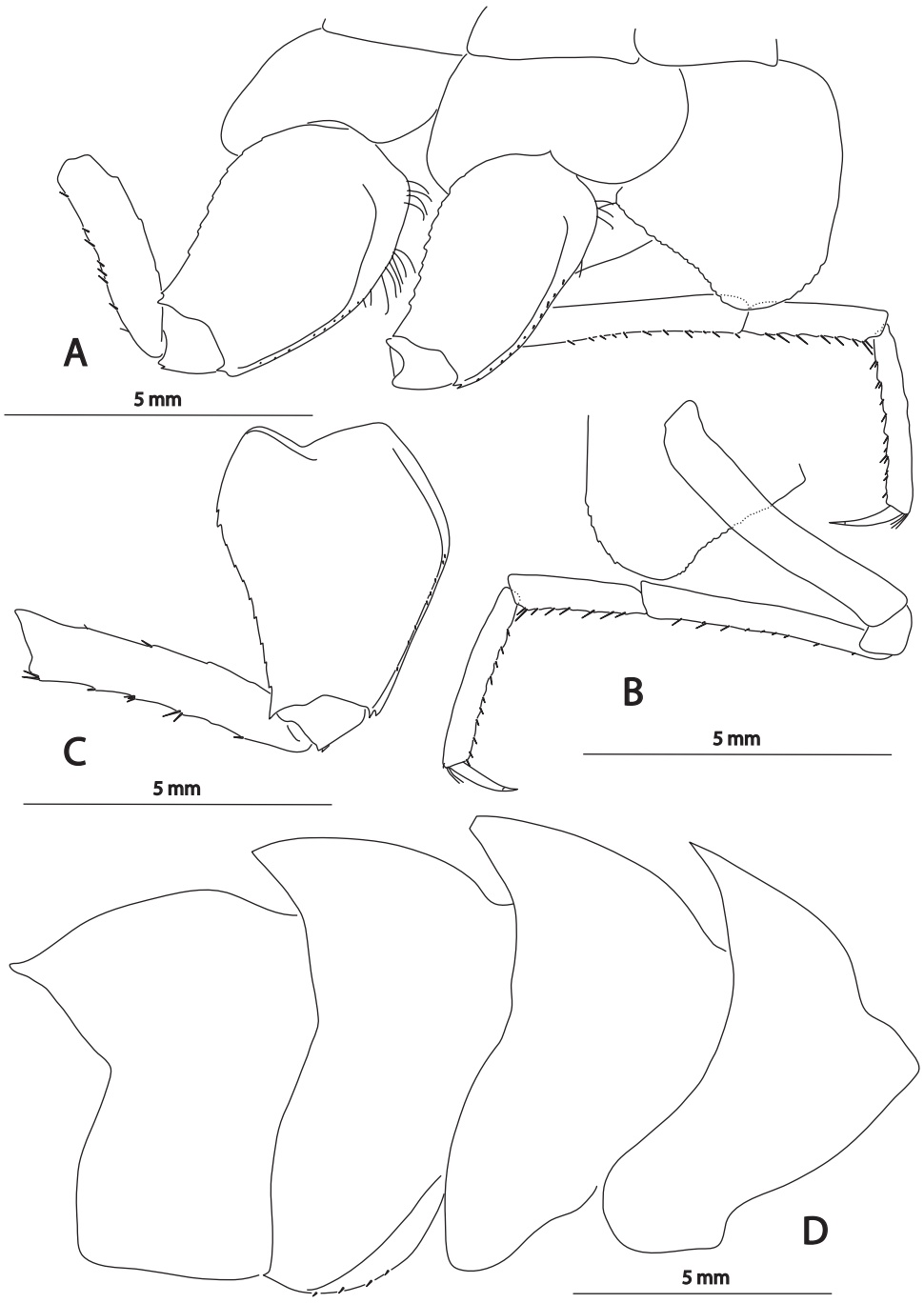

Figure 5. *Eusirus perdentatus*, ♀ holotype, RV *Pourquoi Pas?*, dredging station 15, Palmer Archipelago, *MNHN AM 831*. A, right P4–P5 in lateral view. B, right P4 in medial view. C, right P7. D, pereionite 7 and pleonites 1–3.

Eusirus splendidus Chilton, 1912: 492, pl. 2, fig. 20.

Eusirus perdentatus type marbré – Verheye, 2011: 94, pl. 1, figs A–B, pl. 2, figs A, C, E, G, I.

Eusirus cplx *perdentatus* marbled – d'Udekem d'Acoz & Verheye, 2013: 59, 63, fig. 3.8.3A.

Type material

RV *Pourquoi Pas?*, dredging station 15, Palmer Archipelago, in front of Port-Lockroy [coordinates of Port Lockroy: 64°49′31″S, 63°29′40″W], chenal de Roosen [Neumayer Channel], 60–70 m, dredge, 26

Figure 6. *Eusirus perdentatus*. Life colour pattern. A, B, ♀♀; C, sex indeterminate. A, B, ANT-XXIII/8, sta. 721-2 (A, RBINS, INV. 132538; B, RBINS, INV. 132517). C, ANT-XXIII/8, sta. 604-1 (RBINS, INV. 122631).

November 1900: one ♀ holotype, MNHN *AM 831* [only carcass part of appendages in alcohol; microscopic slides not retrieved].

Other material

ANT-XIX/3–4, station lost: one sp., RBINS, INV. 132555, extr. EPE3.

ANT-XXI/2, sta. 253-1, 71°04.89′S, 11°32.21′W to 71°04.30′S, 11°33.92′W, 295–309 m, 23 December 2003: one sp., RBINS, INV. 132562, extr. EC19, GenBank MT985577 (*COI*), MT945016 (*CytB*), MT945034 (ITS2). – Same sta.: one sp., RBINS, INV. 132568, extr. EC23, GenBank MT985580 (*COI*), MT945018 (*CytB*), MT945037 (ITS2). – Same sta.: one sp., RBINS, INV. 132571, extr. EC22, GenBank MT985579 (*COI*), MT945017 (*CytB*), MT945036 (ITS2). – ANT-XXI/2, sta. 276-1, 71°6.44′S, 11°27.76′W to 71°6.64′S, 11°27.28′W, 268–277 m, 28 December 2003: one sp., RBINS, INV. 132519, extr. ED7, GenBank MT985596 (*COI*). – Same sta.: one sp., RBINS, INV. 122643. – Same sta.: one sp., RBINS, INV. 132379-1 (carcass in alcohol) and 132379-2 to 132379-5 (four microscopic slides in Euparal).

ANT-XXIII/8, sta. 604-1, 61°20.52′S, 55°09.72′W to 61°20.11′S, 55°07.26′W, 286–407 m, 19 December 2006: one sp., RBINS, INV. 132379-1 (carcass in alcohol) and 132379-2 to 132379-5 (four microscopic slides in Euparal). – ANT-XXIII/8, sta. 605-1, 61°20.35′S, 55°29.16′W to 61°19.98′S, 55°32.67′W, 146–151 m, 19 December 2006: one sp., RBINS, INV. 122646. – ANT-XXIII/8, sta. 611-1, 60°58.90′S, 55°11.31′W to 60°58.52′S, 55°07.82′W, 215–297 m, 21 December 2006: one sp., RBINS, INV. 122639. – ANT-XXIII/8, sta. 642-1, 61°04.38′S, 55°59.81′W to 61°04.27′S, 55°58.88′W, 254 m, 27 December 2006: one sp., RBINS, INV. 132539, extr. ED28, GenBank MT985587 (*COI*), MT945021 (*CytB*), MT945041 (ITS2). – ANT-XXIII/8, sta. 721-2, 65°55.41′S, 60°34.01′W to 65°55.79′S, 60°33.96′W, 295–299 m, 20 January 2007: one sp., RBINS, INV. 122633. – Same sta.: one ♀, RBINS, INV. 132538, extr. ED29, GenBank MT985588 (*COI*), MT945022 (*CytB*), MT945042 (ITS2). – Same sta.: one ♀, RBINS, INV. 132517, extr. ED26, GenBank MT985585 (*COI*), MT945020 (*CytB*), MT945040 (ITS2). – ANT-XXIII/8, sta. 726-1, 64°30.86′S, 56°40.23′W to 64°31.16′S, 56°40.51′W, 197–199 m, 22 January 2007: one sp., RBINS, INV. 122649. – ANT-XXIII/8, sta. 726-4, 64°37.83′S, 56°42.10′W to 64°38.03′S, 56°42.57′W, 292 m, 23 January 2007: one sp., RBINS, INV. 122636. – Same sta.: one sp. dissected and mounted on ten microscopic slides in Euparal, RBINS, INV. 132398-1 to 132398-10.

ANT-XXIX/3, sta. 116-9, 62°33.79′S, 56°27.81′W to 62°33.71′S, 56°28.31′W, 248 m, 26 January 2013: two sps, RBINS, INV. 122857. – ANT-XXIX/3, sta. 185-3, 63°51.34′S, 55°41.11′W to 63°51.52′S, 55°41.43′W, 261–296 m, 19 February 2013: ten sps, RBINS, INV. 122843. – ANT-XXIX/3, sta. 185-4, 63°51.53′S, 55°40.74′W to 63°51.53′S, 55°40.43′W, 253–258 m, 19 February 2013: eight sps, RBINS, INV. 122831. – ANT-XXIX/3, sta. 188-4, 63°50.36′S, 55°37.42′W to 63°50.53′S, 55°37.52′W, 425–427 m, 20 February 2013: eight sps, RBINS, INV. 122850. – ANT-XXIX/3, sta. 193-8, 62°43.73′S, 57°29.04′W to 62°43.80′S, 57°29.40′W, 428–431 m, 23 February 2013: one sp., RBINS, INV. 138476, extr. MH3, GenBank MT985628 (*COI*), MT945023 (*CytB*), MT945060 (ITS2). – Same sta.: one ♀, RBINS, INV. 122805A, extr. MH5, GenBank MT985629 (*COI*), MT945024 (*CytB*), MT945061 (ITS2). – Same sta.: one sp., RBINS, INV. 122805B, extr. MH12, GenBank MT985621 (*COI*), MT945027 (*CytB*), MT945053 (ITS2). – Same sta.: one ♀, RBINS, INV. 122805C, extr. MH10. – Same sta.: one sp., RBINS, INV. 122805D, extr. MH8, GenBank MT985631 (*COI*), MT945026 (*CytB*). – Same sta.: one sp., RBINS, INV. 122805E, extr. MH7, GenBank MT985630 (*COI*), MT945025 (*CytB*). – ANT-XXIX/3, sta. 193-9, 62°43.50′S, 57°27.92′W to 62°43.53′S, 57°28.28′W, 420–431 m, 23 February 2013: six sps, RBINS, INV. 122845. – Same sta.: two sps, RBINS, INV. 122859. – ANT-XXIX/3, sta. 197-5, 62°44.73′S, 57°26.79′W to 62°45.05′S, 57°26.68′W,

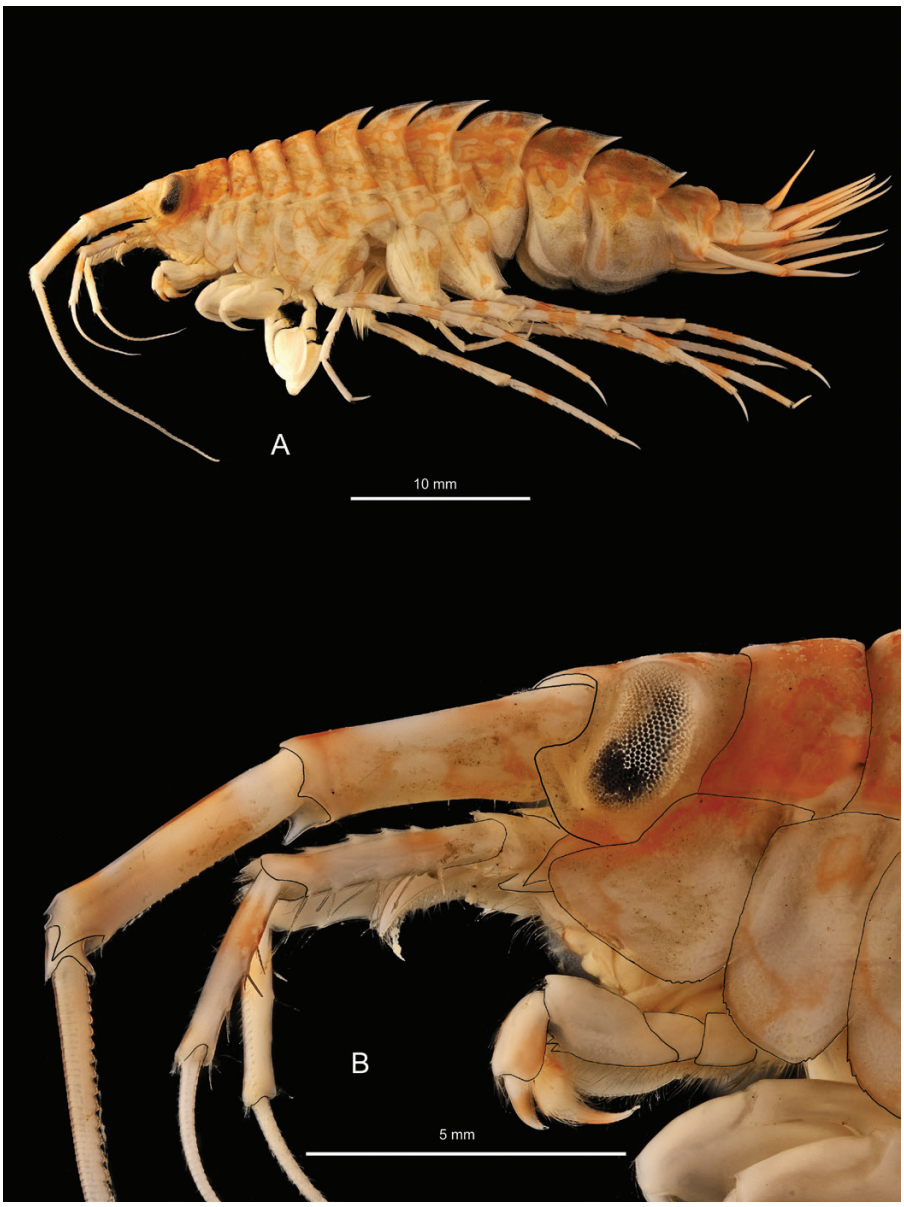

Figure 7. *Eusirus perdentatus*, ♀, ANT-XXIII/8, sta. 721-2 (RBINS, INV. 132538). A, lateral habitus. B, head, peduncle of A1 and A2, pereionite 1, coxae 1–2.

258–273 m, 25 February 2013: ten sps, RBINS, INV. 122851. – Same sta.: five sps., RBINS, INV. 122855. – ANT-XXIX/3, sta. 197-6, 62°45.05′S, 57°26.68′W to 62°45.09′S, 57°26.47′W, 210–222 m, 25 February 2013: one sp., RBINS, INV. 122860. – ANT-XXIX/3, sta. 199-4, 62°57.22′S, 58°14.60′W to 62°57.33′S, 58°14.95′W, 325–339 m, 27 February 2013: 17 sps, RBINS, INV. 122799. – Same sta.: three sps, RBINS, INV. 122808. – ANT-XXIX/3, sta. 204-2, 62°56.07′S, 57°58.14′W to 62°56.08′S, 57°58.51′W, 767–781 m, 28 February 2013: one sp., RBINS, INV. 122795. – ANT-XXIX/3, sta. 217-6, 62°53.45′S, 58°13.06′W to 62°53.42′S, 58°13.41′W, 461–483 m, 2 March 2013: one sp., RBINS, INV. 122816. – ANT-XXIX/3, sta. 224-3, 63°0.53′S, 58°35.67′W to 63°0.58′S, 58°36.11′W, 257–261 m, 4 March 2013: two sps, RBINS, INV. 122813.

R/V James Clark Ross, JR144 (BIOPEARL I), Elephant Island, sta. EI-EBS-4-Supra, 61.33544°S, 055.20379°W to 61.33637°S, 055.20901°W, 270 m, 12 March 2006: one sp., INV. 138473, extr. EB8, GenBank MT985572 (*COI*). – Same sta.: one sp., INV. 138474, extr. EB9, GenBank MT985573 (*COI*). – Same sta.: one sp., INV. 138471, extr. EB10, GenBank MT985570 (*COI*).

CEAMARC sta. 01 (lot 2323), Adélie Coast, 66.003882°S, 142.313777°E to 65.99601°S,

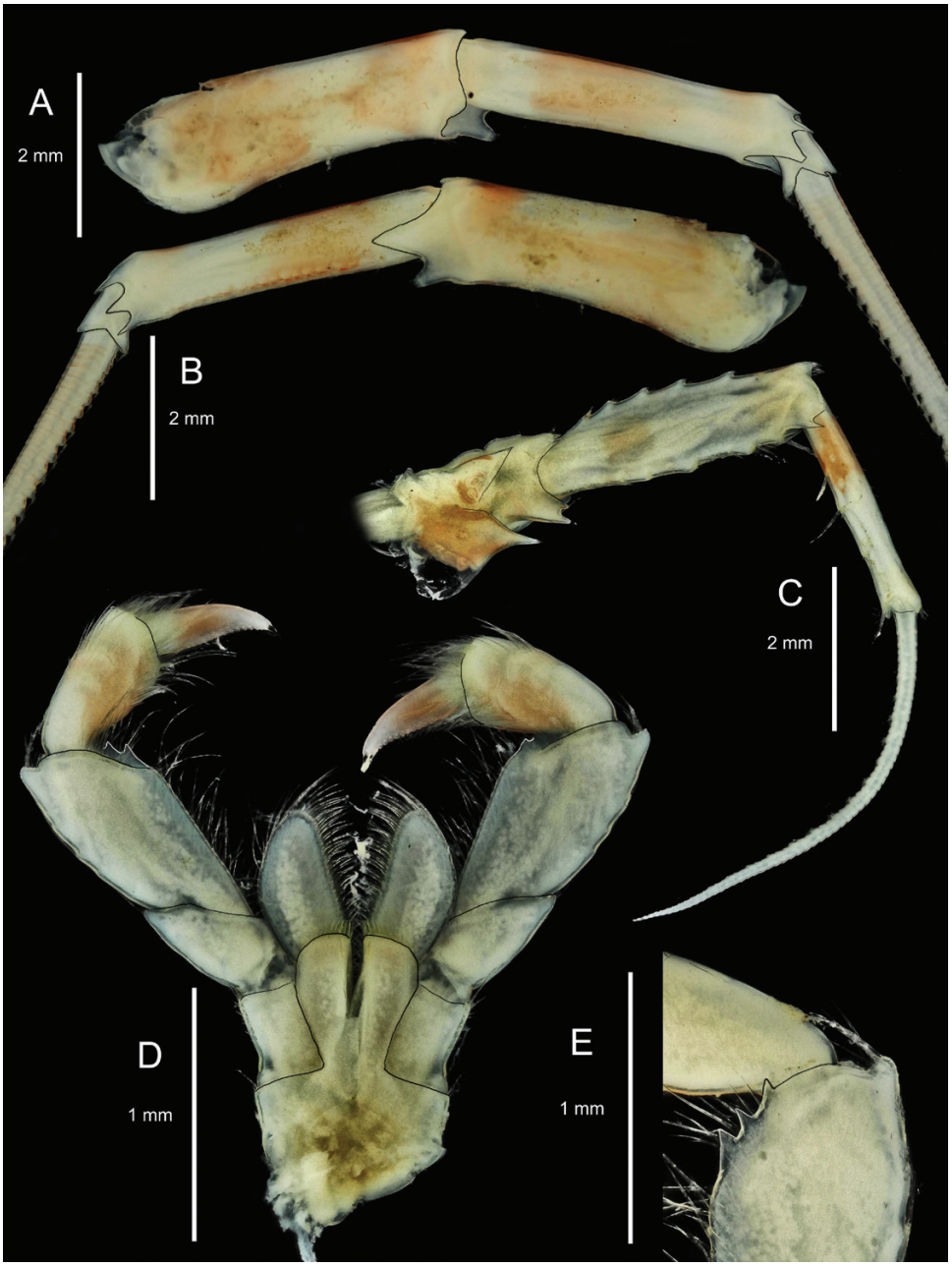

Figure 8. *Eusirus perdentatus*, ♀, ANT-XXIII/8, sta. 721-2 (RBINS, INV. 132538). A, peduncle of right A1 (lateral). B, peduncle of right A1 (medial). C, peduncle of right A2 (lateral). D, Mxp (oral side). E, palp of left Mxp (facial side), junction of articles 2 and 3.

142.35833°E, 228–240 m, 12 January 2008: one sp., MNHN-IU-2019-3361, extr. EE21, GenBank MT985598 (*COI*), MT945019 (*CytB*).

Description

(Based on female RBINS, INV. 132538; with reference to complementary illustrations of the holotype, MNHN *AM 831*).

Body dorsal armature (Figs 6, 7A): Pereionites 5–7 and pleonites 1–3 with mid-dorsal carina backwardly prolonged into strong tooth; dorsal profile of pleonite 3 distinctly sigmoid.

Epimeron 1 (Figs 5D, 14A): Narrow, tapering distally and posterodistally pointed, posteroventral margin nearly straight.

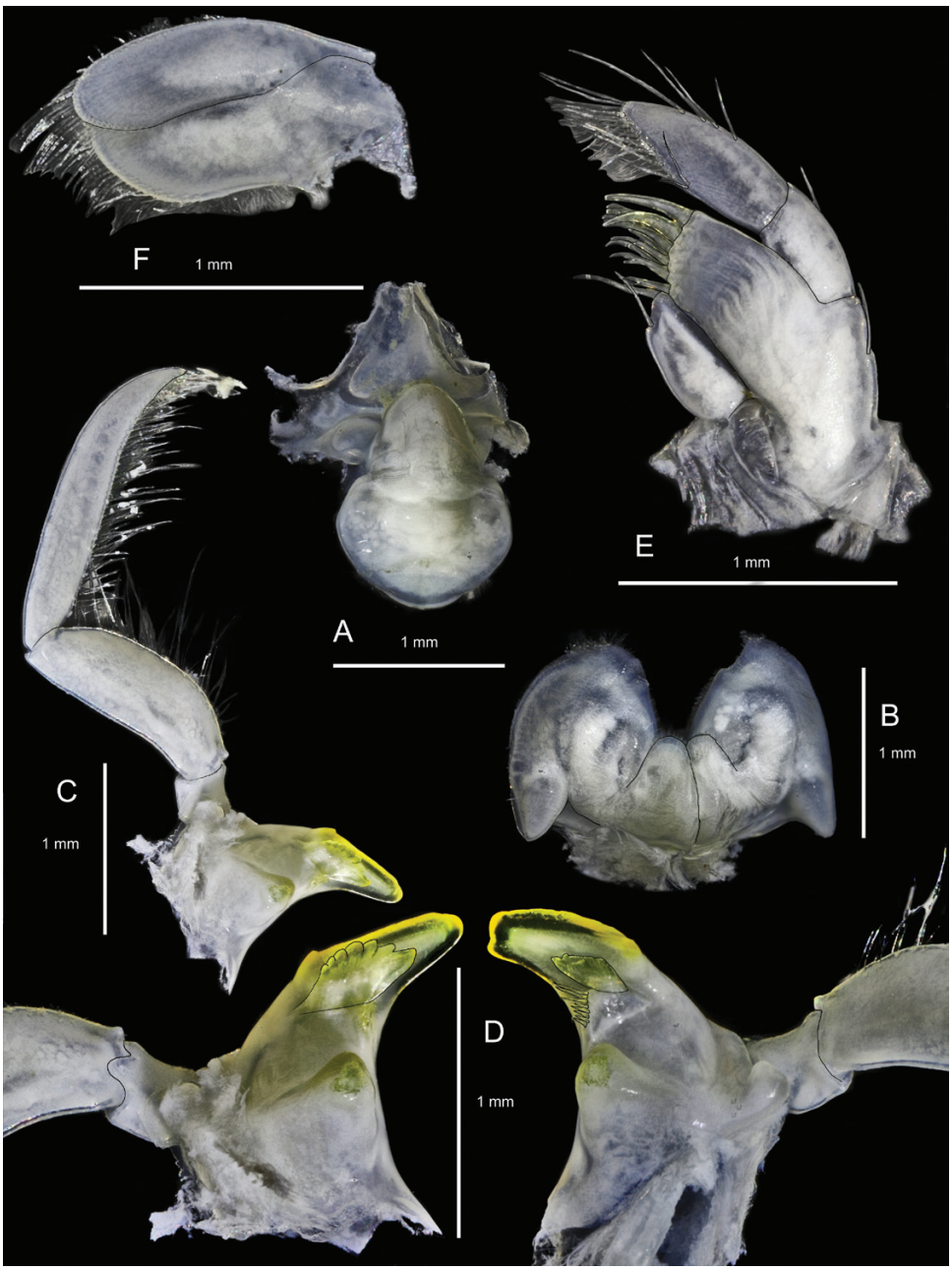

Figure 9. *Eusirus perdentatus*, ♀, ANT-XXIII/8, sta. 721-2 (RBINS, INV. 132538). A, upper lip and epistome. B, lower lip. C, left Md. D, corpus of left and right Md. E, left Mx1. F, left Mx2.

Epimeron 2 (Figs 5D, 14A): Ventral margin rounded, armed with spines, posterodistal angle toothed, and posterior margin sinuous.

Epimeron 3 (Figs 5D, 14A): Ventral margin slightly convex, small spines present, posterior margin gently convex, postero-inferior corner rectangular, finely serrate.

Urosomite 1 (Fig. 14B): With proximal depression followed by a mid-dorsal, sinuous carina, roundly sloping distally.

Head (Figs 4A, B, 7B): About as long as pereionites 1 and 2 combined. Rostrum short, downcurved, tip narrow but blunt, ventrally concave. Lateral lobe produced, subrectangular, unevenly rounded, apically

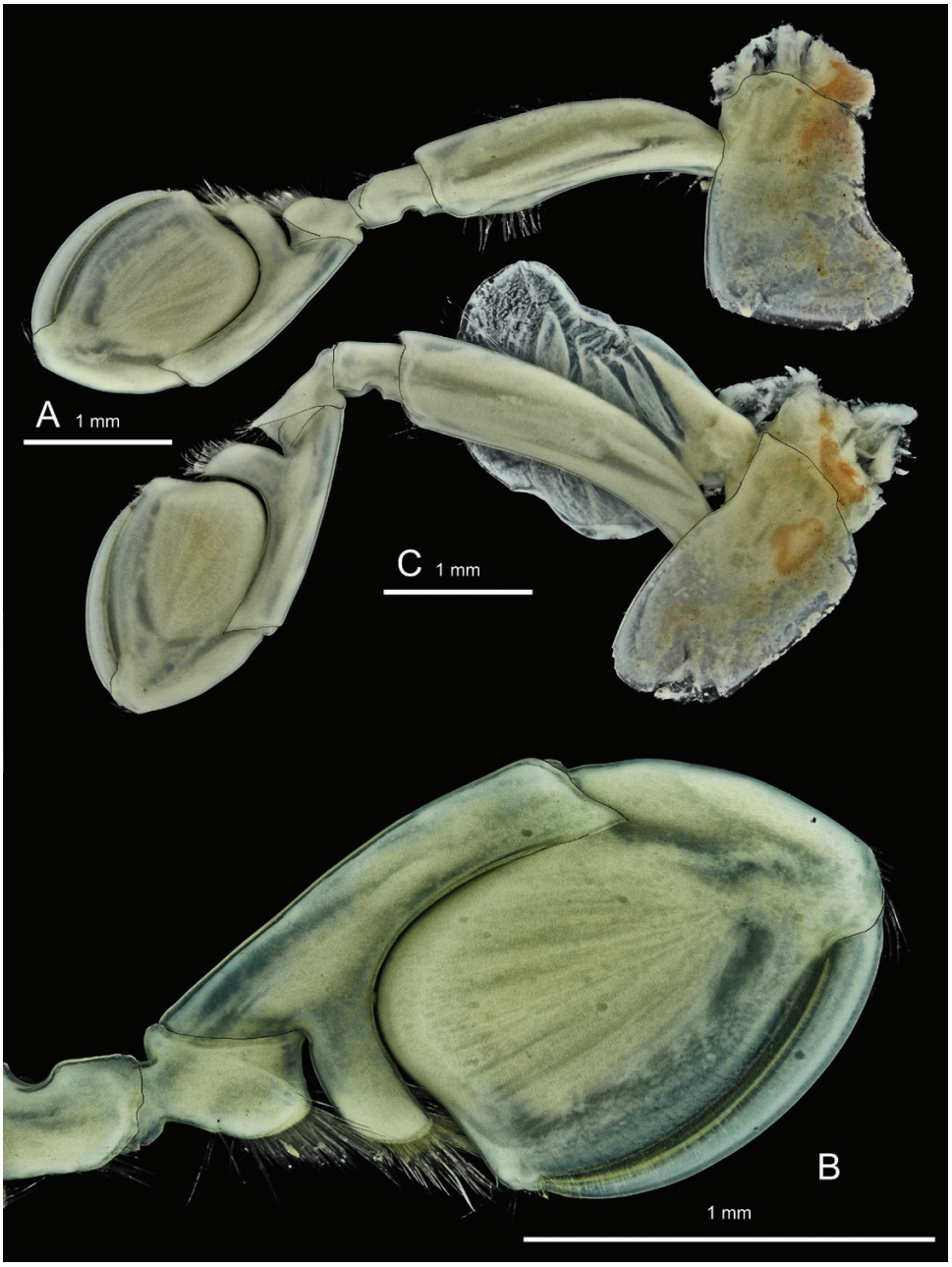

Figure 10. *Eusirus perdentatus*, ♀, ANT-XXIII/8, sta. 721-2 (RBINS, INV. 132538). A, right Gn1. B, chela of right Gn1. C, right Gn2.

blunt. Post-antennal sinus narrowly U-shaped. Post-antennal lobe shallow, forming a right angle. Ventral margin slightly concave. Eyes large, prominent, elongate, sub-reniform. Interocular space wide.

Antenna 1 (Figs 4A, B, 8A, B): Whole antenna conspicuously longer than whole antenna 2, shorter than body length. Peduncle of antenna 1 slightly longer than that of antenna 2. Peduncle article 1 (medial tooth included) 1.2× as long as article 2, 6× as long as article 3. Peduncle article 1 distally with ventrolateral tooth or angulose protrusion, with two medial teeth (long medial tooth and medium-sized ventromedial tooth). Peduncle article 2 distally with three ventrolateral teeth (most dorsal shortest, most ventral longest) and three subequal medial teeth. Article 3 with dorsal and ventral process. Accessory flagellum of one article, short, thin. Flagellum > 1.4× as long as total peduncle length (in another specimen 2.4× as long as total peduncle length). Calceoli

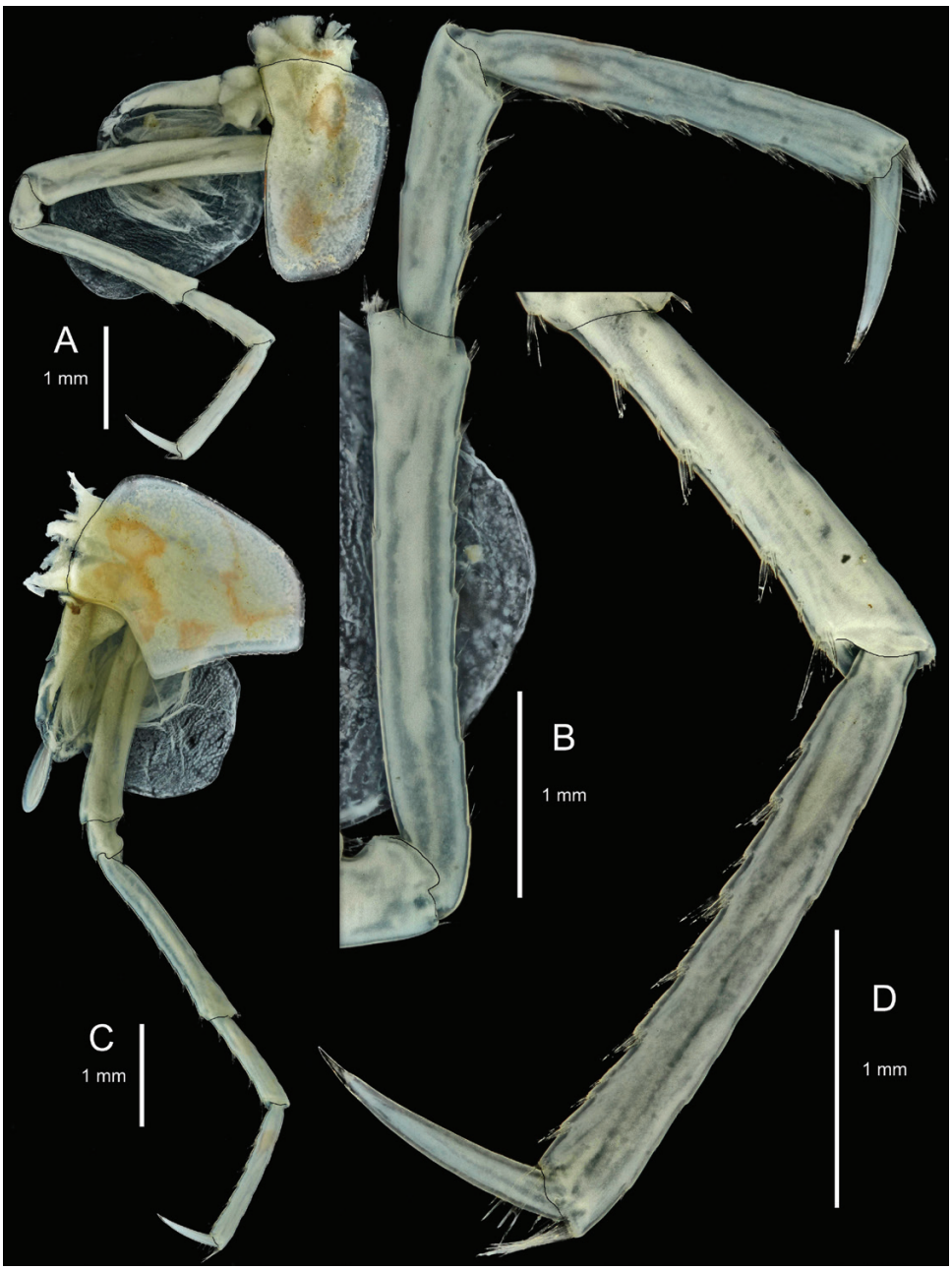

Figure 11. *Eusirus perdentatus*, ♀, ANT-XXIII/8, sta. 721-2 (RBINS, INV. 132538). A, right P3. B, merus, carpus, propodus and dactylus of right P3. C, right P4. D, carpus, propodus and dactylus of right P4.

ventrally present on peduncular articles 2 and 3 and on distoventral surface of flagellar articles.

Antenna 2 (Figs 4A, B, 8C): Peduncular article 4 1.2× as long as article 5, 2.5× broader than article 5, flattened, 3.6× as long as wide, with six dorsal teeth, of which one is in a distal position, with six ventral protrusions, one subdistal tooth and two distal denticles. Peduncular article 5 dorsally toothless and with short setae, ventrally with four groups of strong setae (last one in distal position) associated with weak protrusion. Calceoli ventrally present on distoventral surface of flagellar articles.

Upper lip [labrum] (Fig. 9A): Entire, ventrally rounded, slightly more prominent than straight epistome, separated by incision.

Figure 12. *Eusirus perdentatus*, ♀, ANT-XXIII/8, sta. 721-2 (RBINS, INV. 132538). A, right P5. B, dactylus and tip of propodus of right P5. C, right P6. D, dactylus and tip of propodus of right P6. E, right P7. F, dactylus and tip of propodus of right P7.

Lower lip [paragnath or hypopharynx] (Fig. 9B): Inner lobes small, outer lobes gaping, mandibular processes short, rounded.

Mandible (Fig. 9C, D): Left incisor long, with cutting edge smooth except for proximolateral tiny tooth; right incisor long, with cutting edge smooth except for proximal tiny tooth and blunt median tooth; left lacinia mobilis much larger than right one, with seven blunt teeth; right lacinia mobilis with margin straight and lined with 11 blunt and scarcely distinct teeth (the two most medial stronger); row of normally developed raker spines present; molar process columnar, but narrowing distally, triturative surface reduced. Palp three-articulated, attached midway, much longer than mandible body; article 1 short, without setae; article 2 0.7× as long as article 3, ventral margin expanded, heavily setose (D2-setae), distally constricted; article 3

Figure 13. *Eusirus perdentatus*, ♀, ANT-XXIII/8, sta. 721-2 (RBINS, INV. 132538). A, basis of right P5. B, propodus and dactylus of right P5. C, basis of right P6. D, propodus and dactylus of right P6. E, basis of right P7. F, propodus and dactylus of right P7.

falcate, ventral margin heavily setose (D3-setae), E3-setae short, B3 (grouped in transverse rows) present.

Maxilla 1 (Fig. 9E): Inner plate slender, oblong, subapically bearing one seta; outer plate with 12 spines, some bifid (both prongs long); palp two-articulated, article 1 0.6× as long as article 2, with one lateral seta; article 2 with one row of lateral setae and two rows of medial setae on distal half.

Maxilla 2 (Fig. 9F): Plates subequal in length, apically rounded; outer plate about half width of inner plate, with stiff setae distally; apical margin of inner plate fringed with shorter stiff setae.

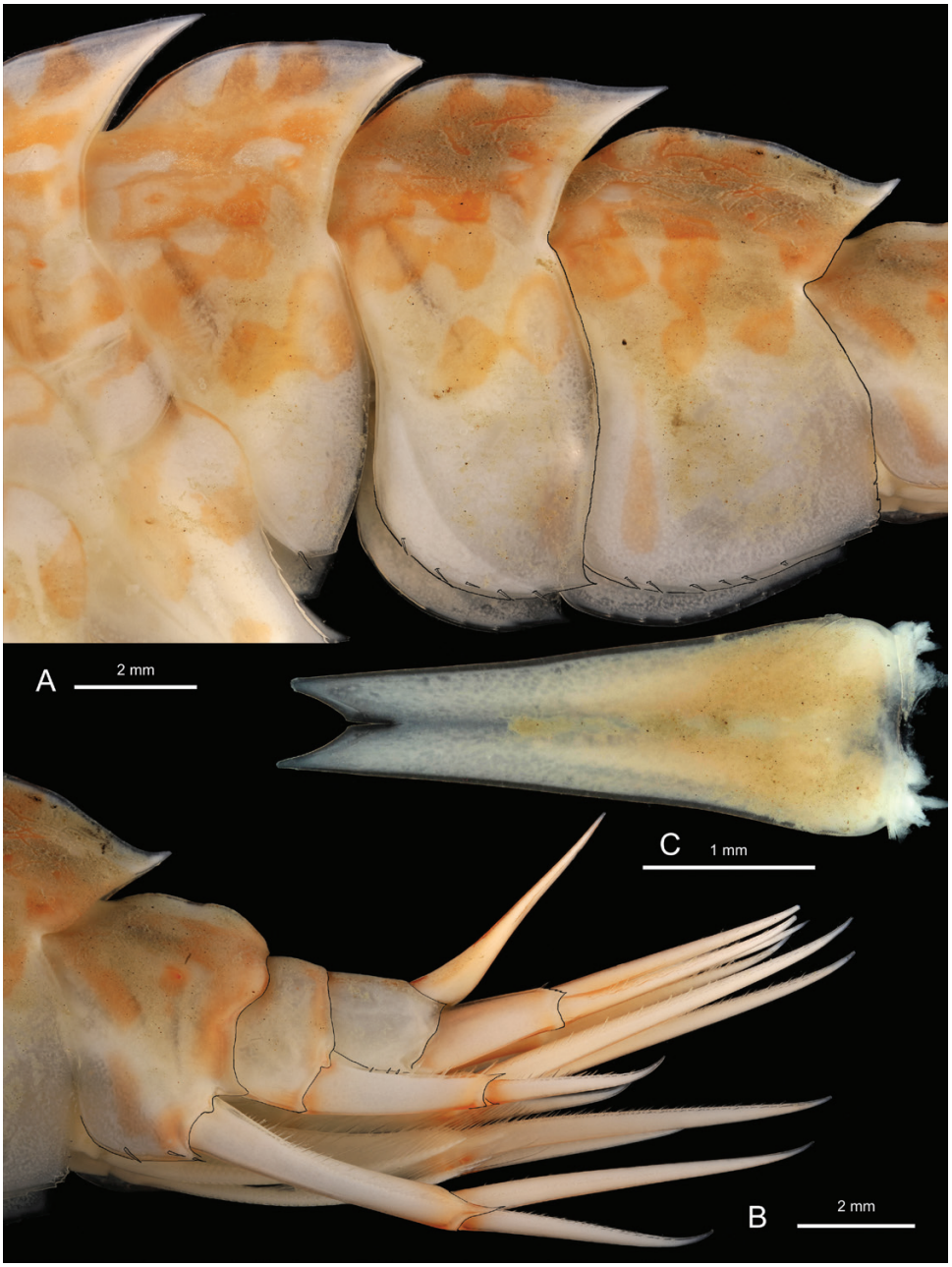

Figure 14. *Eusirus perdentatus*, ♀, ANT-XXIII/8, sta. 721-2 (RBINS, INV. 132538). A, pleosome. B, urosome. C, telson.

Maxilliped (Fig. 8D, E): Inner plate short (medially extending to end of palp article 1), distally and distolaterally densely armed with spines. Outer plate oblong (medially extending one-third to one-half length of palp article 2), laterally, apically and medially armed with long setae. Palp robust, four-articulated, articles 1 and 2 distally dilated; article 2 longest, article 1 sparsely setose. Dorsodistal corner of palp article 2 forming a tooth-like process, bearing fringe of setae; posterodistal corner (facial side) with three teeth. Palp article 3 regularly and strongly expanding distally, densely setose. Palp article 4 three-quarters of overall length of article 3, claw-like, unguis short, distal half of posterior margin armed with uniform, short spines.

Gnathopod 1 (Figs 4C, D, 10A, B): Subchelate, similar to but slightly shorter than gnathopod 2. Coxal plate about as deep as maximal height of corresponding pereionite, deeper than wide (ratio of

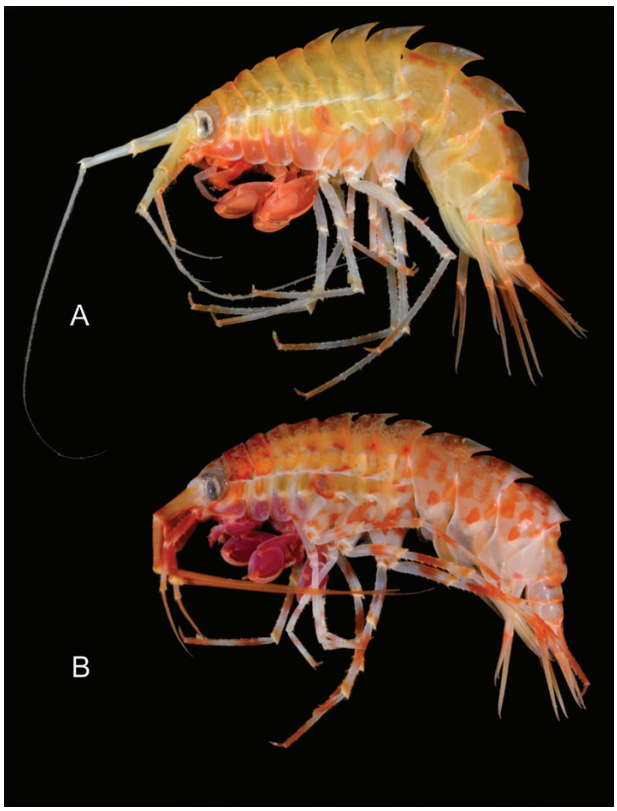

Figure 15. ***Eusirus pontomedon*****,** colour in life, paratypes (sex indeterminate). A, ANT-XXIX/3, sta. 188-4 (RBINS, INV. 122826 or 122844 or 122846). B, ANT-XXIX/3, sta. 196-8 (RBINS, INV. 122800 or 122821).

depth to width: 1.2), anteroventral angle produced into a broad rounded lobe, anterior margin concave, posterodistal angle irregularly, finely serrate. Basis weakly curved, proximally narrowed, sparsely setose. Ischium subrectangular, with deep U-shaped notch on anterior border, posterodistal margin setose. Merus subtriangular, about as long as ischium, posterodistal angle rounded and setose. Carpus lobe linguiform, broad, distally tapering, posterior margin regularly convex, clearly exceeding merus, distally setose; ratio of length to width of carpus lobe: 1.88 (length of lobe measured from tip to connection with merus). Propodus subrectangular; longest (transverse) axis 1.45 × length of anterior margin, posterior margin slightly concave; palm convex, longer than anterior margin, bearing shorter and longer setae, defined by a hump armed with rows of short to long spines. Dactylus falcate, reaching the hump.

Gnathopod 2 (Figs 4E, 10C): Subchelate. Coxal plate deeper than maximal height of corresponding pereionite, elliptic-rectangular, anterior and posterior border nearly parallel (weakly converging downwards), ventral margin rounded (tip of rounded lobe in posterior position), antero- and posteroventral angles with a few serrations; ratio of depth to width of coxal plate: 1.9. Basis weakly curved, proximally narrowed, sparsely setose. Ischium subrectangular, with deep U-shaped notch on anterior border, posterodistal margin almost not setose. Merus subtriangular, about as long as ischium, posterodistal angle produced into a tooth and setose. Carpus lobe linguiform, broad, distally tapering, posterior margin regularly convex, clearly exceeding merus, distally setose; ratio of length to width of carpus lobe: 1.4 (length of lobe measured from tip to connection with merus). Propodus subrectangular; longest (transverse) axis 1.3× length of anterior margin, posterior margin slightly concave; palm convex, longer than anterior margin, bearing shorter and longer setae, defined by a hump armed with rows of short to long spines. Dactylus falcate, reaching the hump.

Pereiopod 3 (Fig. 11A, B): Coxal plate deeper than maximal height of corresponding pereionite, subrectangular, anterior and posterior border nearly parallel (weakly converging downwards), ventral margin nearly straight (tip of rounded lobe in posterior position), antero- and posteroventral angles with a few serrations; ratio to depth to width of coxal plate: 1.8. Merus 6× as long as wide, 1.9× as long as carpus, 1.35× as long as propodus, with four anterior groups of spines (one in distal position) and ten posterior groups of spines; carpus 3.7× as long as wide, 0.71× as long as propodus, with three (groups of) minute anterior spines and five groups of posterior spines; propodus 6.8× as long as wide, with six anterior groups of spines (which are minute except for those of the distal group) and 11 posterior groups of spines; dactylus long and narrow, 0.48× as long as propodus and 0.67× as long as carpus, 6.8× as long as wide.

Pereiopod 4 (Figs 5A, B, 11C, D): Coxal plate deeper than maximal height of corresponding pereionite, 1.3× as deep as wide, pentagonal; anterodorsal margin nearly straight; anteroventral margin straight; anterodorsal and anteroventral margin connecting with low curve ornate with serrations; connection between anterodorsal and anteroventral border (ventral tip of coxa) forming a blunt right angle in photographed specimen [tip of coxa rounded in holotype]; posteroventral border weakly concave and serrate; posterodorsal border distinctly concave; connection between posteroventral and posterodorsal border forming a right angle. Leg similar to P3, but merus, carpus and propodus a bit longer. Merus 6.4× as long as wide, 1.9× as long as carpus, 1.32× as long as propodus, with five anterior groups of spines (one in distal position) and 11 posterior groups of spines;

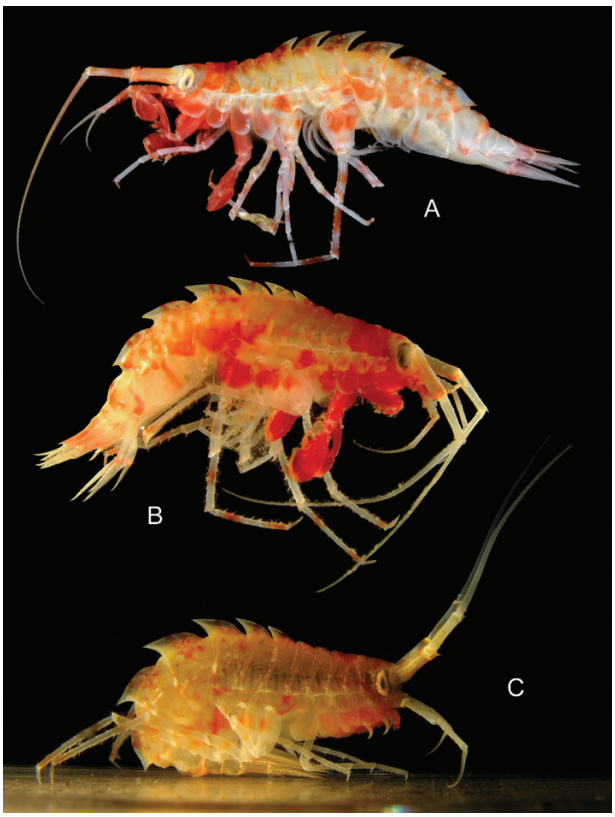

Figure 16. ***Eusirus pontomedon***, colour in life, paratypes (sex indeterminate). A, ANT-XXIX/3, sta. 185-3 (RBINS, INV. 122833). B, ANT-XXIII/8, sta. 604-1 (RBINS, INV. 122635). C, ANT-XXIII/8, sta. 603-5 (RBINS, INV. 132556).

carpus 4.5× as long as wide, 0.72× as long as propodus, with three (groups of) minute anterior spines and seven groups of posterior spines; propodus 7.8× as long as wide, with nine anterior groups of spines (which are minute except for those of the distal group) and 12 posterior groups of spines; dactylus long and narrow, 0.44× as long as propodus and 0.61× as long as carpus, 7.2× as long as wide.

Pereiopod 5–7 relationships (Fig. 12A, C, E): Pereiopods 5–7 similar, long, slender; P5 shortest, P6 and P7 subequal. Basis increasing in length from P5 to P7.

Pereiopod 5 (Figs 5A, 12A, B, 13A, B): Coxal plate less deep than maximal height of corresponding pereionite, bilobed, posterior lobe longest. Basis 1.6× as long as wide, 0.85× as long as carpus, anterior margin nearly straight on most of its length, setose on proximal 0.3, spinose on distal 0.7, with two small distal teeth, posterior border expanded, distinctly serrate (about ten serrations), proximal 0.3 convex, distal 0.7 nearly straight (weakly concave), posterodistal corner forming a right angle; ischium short, with strong anterodistal tooth and strong posterodistal tooth, with two anterior (groups of) spines; merus 4.6× as long as wide, spinose on both sides; carpus 5.9× as long as wide, 1.2× as long as merus, spinose on both sides; propodus 13.3× as long as wide, 1.7× as long as merus, spinose on both sides; dactylus 8.5× as long as wide, 0.21× as long as propodus.

Pereiopod 6 (Figs 5A, 12C, D, 13C, D): Coxal plate less deep than maximal height of corresponding pereionite, bilobed, posterior lobe longest. Basis 1.6× as long as wide, 0.81× as long as carpus, anterior margin convex, setose on proximal 0.3, spinose on distal 0.7, with two small distal teeth, posterior border expanded, distinctly serrate (~11 serrations), proximal 0.3 convex, distal 0.7 nearly straight (weakly concave), posterodistal corner produced into a tooth; ischium short, with strong anterodistal tooth and strong posterodistal tooth, with one anterior spine; merus 5.2× as long as wide, spinose on both sides; carpus 6.6× as long as wide, 1.2× as long as merus, spinose on both sides; propodus 14.3× as long as wide, 1.6× as long as merus, spinose on both sides; dactylus (tip of unguis damaged) 7.9× as long as wide, 0.24× as long as propodus.

Pereiopod 7 (Figs 2C, 9E, F, 10E, F): Coxal plate less deep than maximal height of corresponding pereionite, unilobed. Basis 1.4× as long as wide, 0.85× as long as carpus, anterior margin with angular discontinuity on proximal 0.4, weakly convex and setose on proximal 0.4, straight and spinose on distal 0.6, with two small distal teeth, posterior border expanded, distinctly serrate (11 serrations), proximal 0.3 convex, distal 0.7 concave, posterodistal corner produced into a tooth; ischium short, with strong anterodistal tooth and strong posterodistal tooth, with one anterior spine; merus 4.9× as long as wide, spinose on both sides; carpus 7.4× as long as wide, 1.1× as long as merus, spinose on both sides; propodus 14.5× as long as wide, 1.5× as long as merus, spinose on both sides; dactylus (tip of unguis damaged) 9.6× as long as wide, 0.24× as long as propodus.

Coxal gills: From gnathopod 2 to pereiopod 7, proximally voluminous, sack-like (partly pleated), distally lamellate; with oblong accessory gill.

Oostegites: From gnathopod 2 to pereiopod 5, narrowly elliptic.

Pleopods: Without special characters.

Uropod 1 (Fig. 14B): Reaching level of uropod 2 and slightly overreaching uropod 3. Peduncle longer than

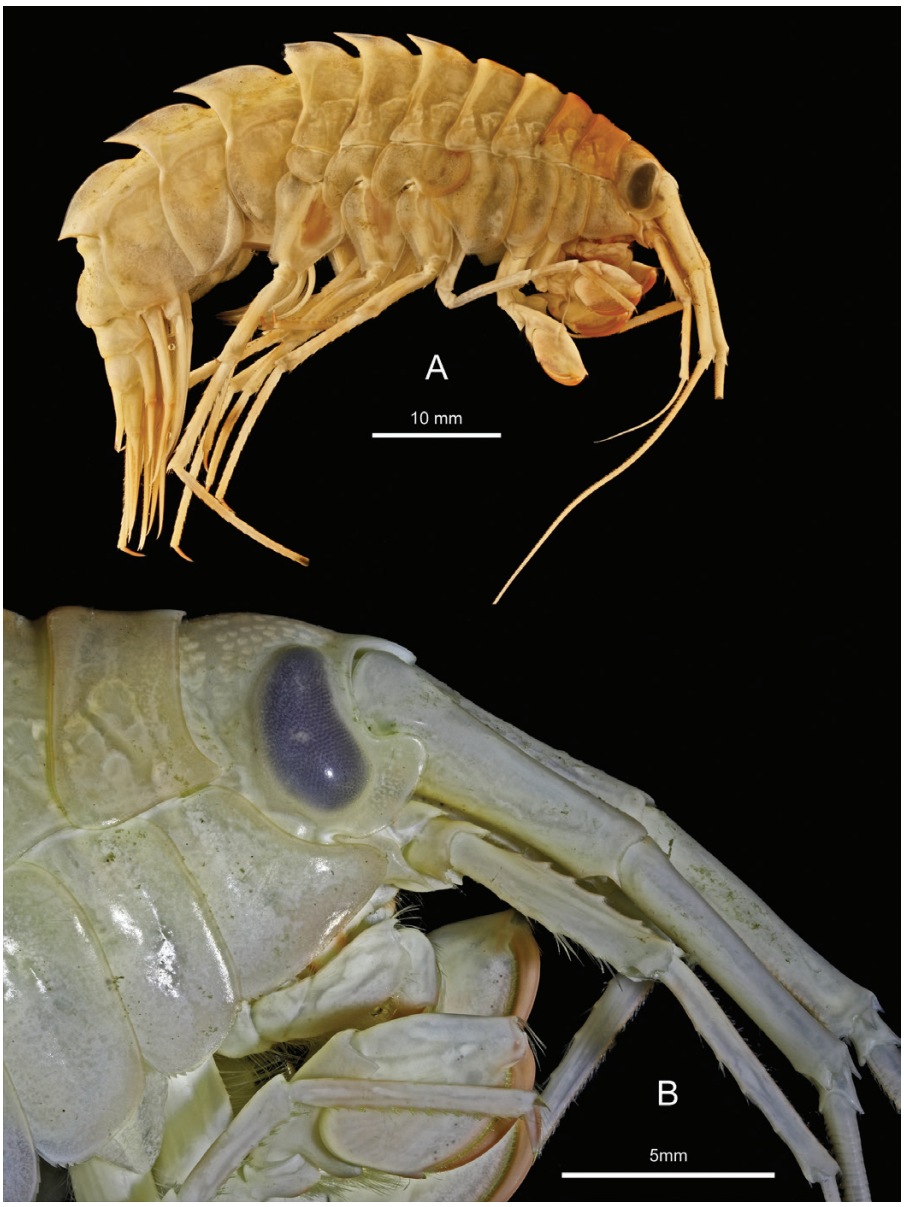

Figure 17. ***Eusirus pontomedon***, ♀ holotype, ANT-XXIX/3, sta. 193-8 (removed from RBINS, INV. 122797, now RBINS *INV. 150107*). A, habitus. B, head, peduncle of A1 and A2, pereionite 1, coxae 1–3.

outer ramus and shorter than inner ramus, with dorsal borders spinose; inner ramus 1.4× length of outer ramus; rami spinose.

Uropod 2 (Fig. 14B): Peduncle 1.1× as long as outer ramus, with dorsal borders spinose; inner ramus 2.2× as long as outer; rami spinose.

Uropod 3 (Fig. 14B): Lateral subdistal spine present; distolateral tip with three teeth; inner ramus weakly exceeding outer ramus; rami spinose.

Telson (Fig. 14C): Long, slender, tapering distad, cleft; exceeding half of rami of uropod 3. Telson length 2.9× its breadth. Cleft 18% of length, distally gaping, lobes apically acute.

Colour pattern (Fig. 6): Body, antennae, coxae of all pereiopods and bases of pereiopods with ivory background richly dappled with coalescent rounded spots, which are marginally crimson red, the colour fading to pink towards the centre in most spots; mouthparts white, with a few pink or red marks;

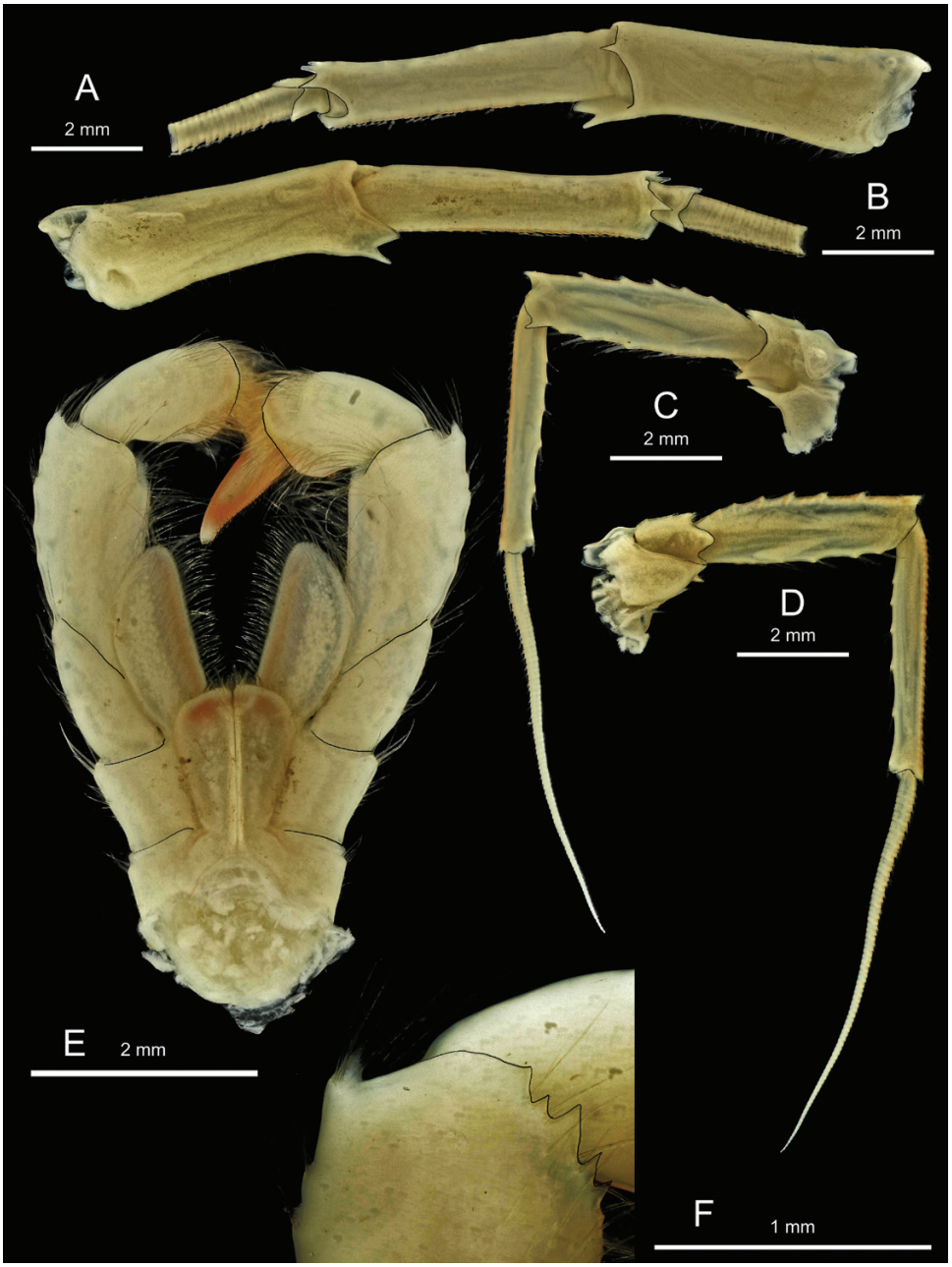

Figure 18. ***Eusirus pontomedon***, ♀ holotype, ANT-XXIX/3, sta. 193-8 (removed from RBINS, INV. 122797, now RBINS *INV. 150107*). A, peduncle of left A1 (lateral). B, peduncle of left A1 (medial). C, peduncle of left A2 (lateral). D, peduncle of left A2 (medial). E, Mxp (oral side). F, palp of right Mxp (facial side), junction of articles 2 and 3.

gnathopods white, usually (but not always) tinged with pink; slender part of walking pereiopods white, with irregular red transverse stripes or spots; tail fan more or less tinged with red or pink; eyes golden or silver in life (turning black in alcohol). In subadult females, ripe ovaries appear as blue by transparency. This highly characteristic colour pattern is constant.

Body length: The largest specimens examined were 50 mm long. The one used for description was 41 mm long.

Distribution and bathymetric range

Palmer Archipelago (holotype) (Chevreux, 1912, 1913), South Orkney Islands (Chilton, 1912, as *Eusirus splendidus* Chilton, 1912), South Shetland Islands,

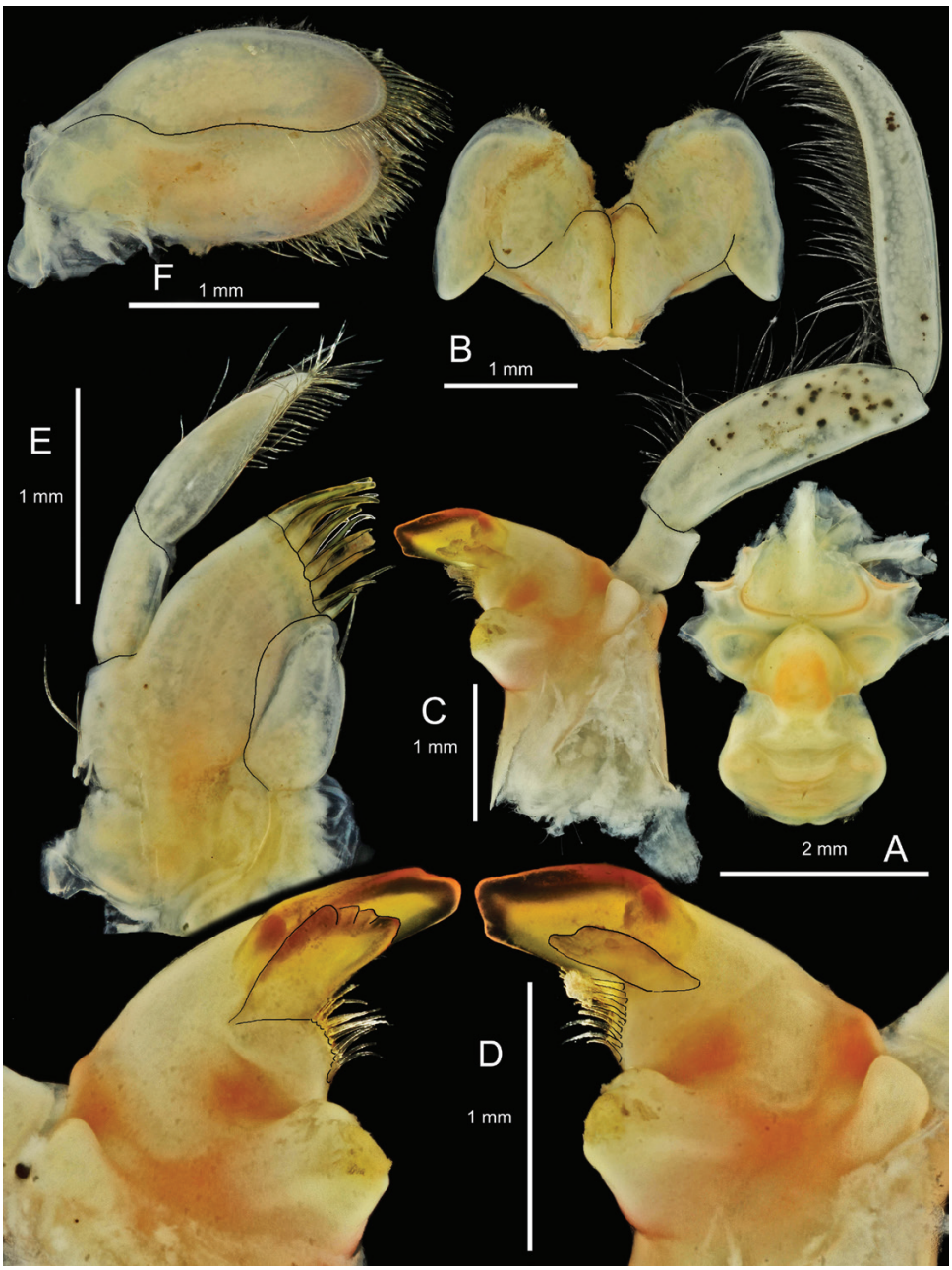

Figure 19. ***Eusirus pontomedon***, ♀ holotype, ANT-XXIX/3, sta. 193-8 (removed from RBINS, INV. 122797, now RBINS *INV. 150107*). A, upper lip and epistome. B, lower lip. C, right Md. D, corpus of left and right Md. E, right Mx1. F, right Mx2.

Bransfield Strait, tip of the Antarctic Peninsula, Larsen B, eastern shelf of the Weddell Sea, Adélie Coast (present material). Shallowest station: 60–70 m (holotype). Deepest station 767–781 m, but all other specimens were collected at depths shallower than 500 m.

Remarks

Illustrations of the holotype of *Eusirus perdentatus* are given in the papers by Chevreux (1913) and Andres *et al.* (2002) and in the present paper. We looked at the carcass and the pieces of the holotype preserved in alcohol, but the microscopic slides made by Chevreux were not retrieved. The characteristics of its articles 4 and 5 of the antenna 2, and that of the dactylus of its pereiopod 4, make its identity clear. The colour description given by Chevreux (1913) is another good indication of the identity of the holotype: 'corps blanchâtre, tigré de rouge' [body whitish, with a red tiger-like colour pattern]. The colour pattern of

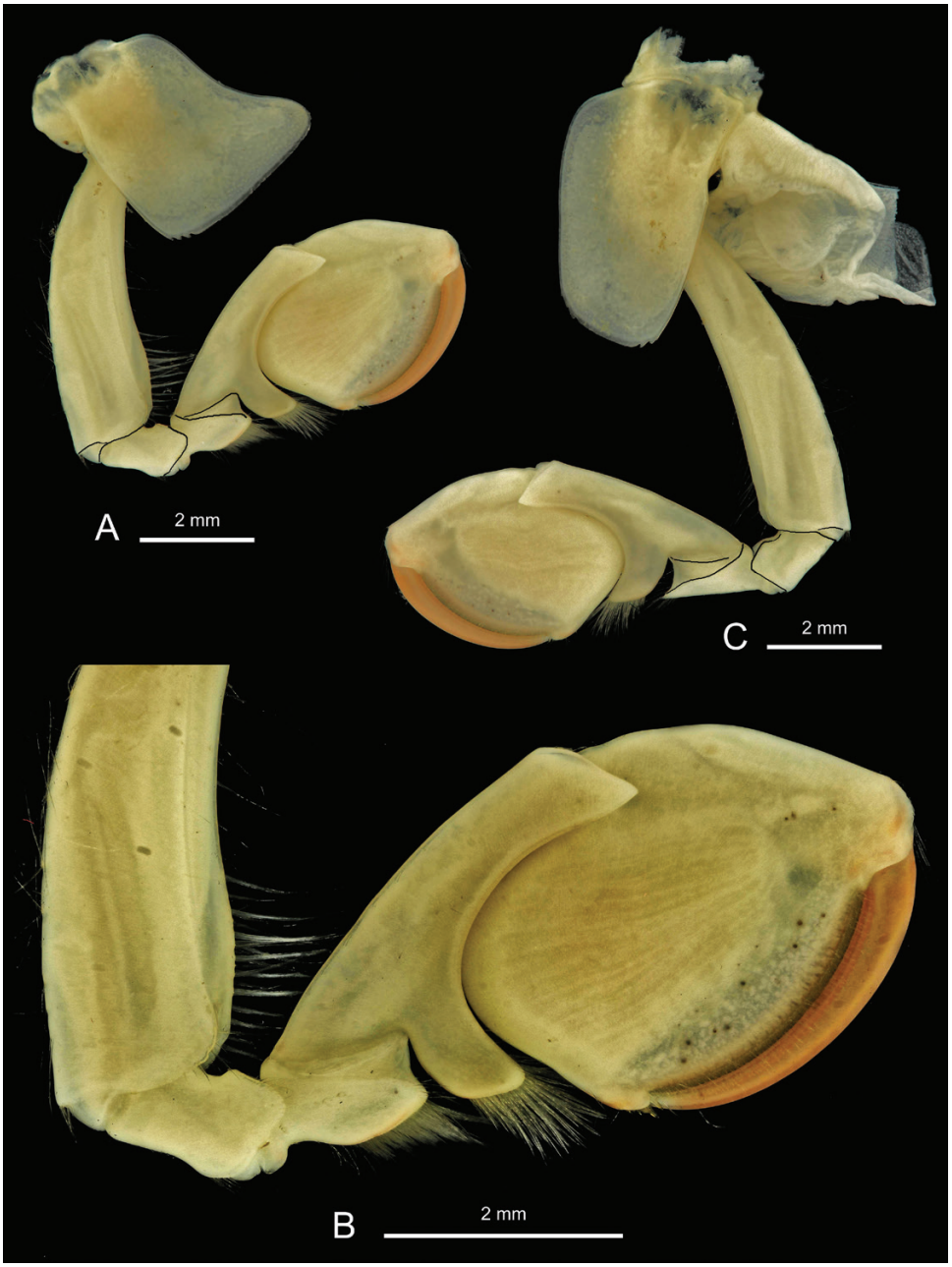

Figure 20. ***Eusirus pontomedon***, ♀ holotype, ANT-XXIX/3, sta. 193-8 (removed from RBINS, INV. 122797, now RBINS *INV. 150107*). A, right Gn1. B, distal part of Gn1. C, left Gn2.

the closely related *E. pontomedon* can be spotted with orange-red on a yellowish (not whitish) background, but much less contrasted than in *E. perdentatus* (not tiger-like) and it quickly fades in alcohol, whereas in the case of *E. perdentatus,* it can persist for a few years. *Eusirus splendidus* Chilton, 1912 illustrated by Chilton (1912) is *E. perdentatus*, because it has long dactyli on pereiopods 3 and 4. *Eusirus perdentatus* Chevreux, 1912 has priority over *Eusirus splendidus* Chilton, 1912, because it was published earlier the same year [Chilton (1912) is himself citing Chevreux (1912)].

EUSIRUS PONTOMEDON SP. NOV.

(FIGS 15–24)

Zoobank registration: urn:lsid:zoobank.org:pub:055688C7-A2E1-4C0D-BE45-57058B3AB67A

Eusirus perdentatus – K.H. Barnard, 1932: 188 [in part], ? fig. 115 (upper photograph). – Emison, 2000:

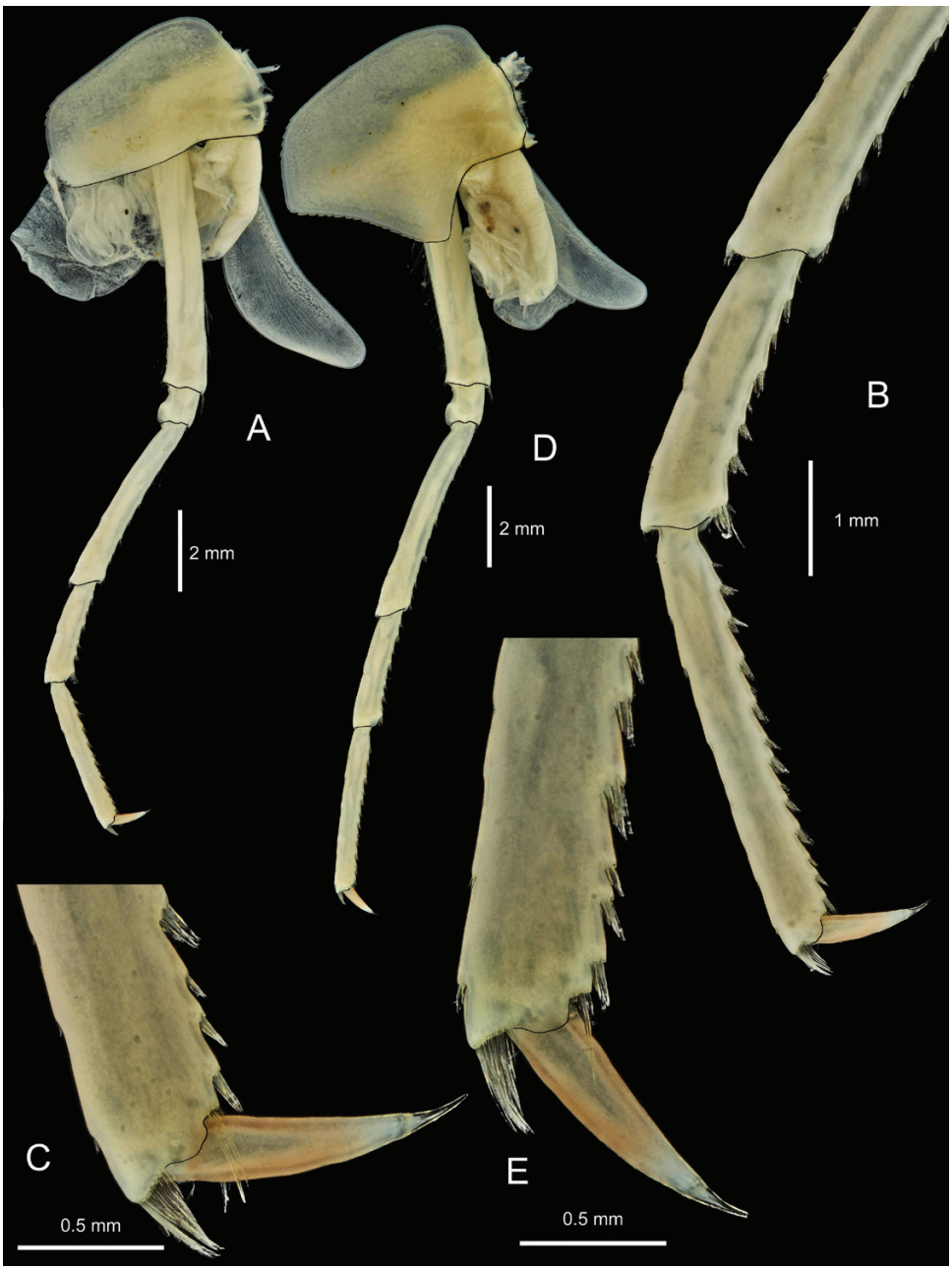

Figure 21. ***Eusirus pontomedon***, ♀ holotype, ANT-XXIX/3, sta. 193-8 (removed from RBINS, INV. 122797, now RBINS *INV. 150107*). A, left P3. B, distal half of left P3. C, dactylus of left P3. D, left P4. E, dactylus of left P4.

6 [in part, not figs 2–8 (= *E. giganteus s.l.*)]. – Andres *et al.*, 2002: 121 [in part], figs 8B, F, H–J, not figs 7D–K, 8A, C–E (= *E. perdentatus*). – d'Udekem d'Acoz & Robert, 2008: 53 [in part]. – Baird *et al.*, 2011: 3443 [in part]. – Peña Othaitz & Sorbe, 2020: 250 [in part].

Eusirus perdentatus type tacheté – Verheye, 2011: 94, pl. 1, figs C–E, 96, pl. 2, figs B, D, F, H, J.

Eusirus cplx *perdentatus* spotted – d'Udekem d'Acoz & Verheye, 2013: 59, 63, fig. 3.8.3B.

Eusirus sp. aff. *perdentatus* Rauschert & Arntz, 2015: 64, plate 57 (unnumbered fig.).

Type material

ANT-XXIX/3, Bransfield Strait, sta. 193-8, 62°43.73′S, 57°29.04′W to 62°43.80′S, 57°29.40′W, 428–431 m, Agassiz trawl, 23 February 2013: one subadult ♀ **Holotype**, RBINS, *INV. 150107*, extr. MH17, GenBank MT985623 (*COI*), MT944994 (*CytB*), MT945055 (ITS2).

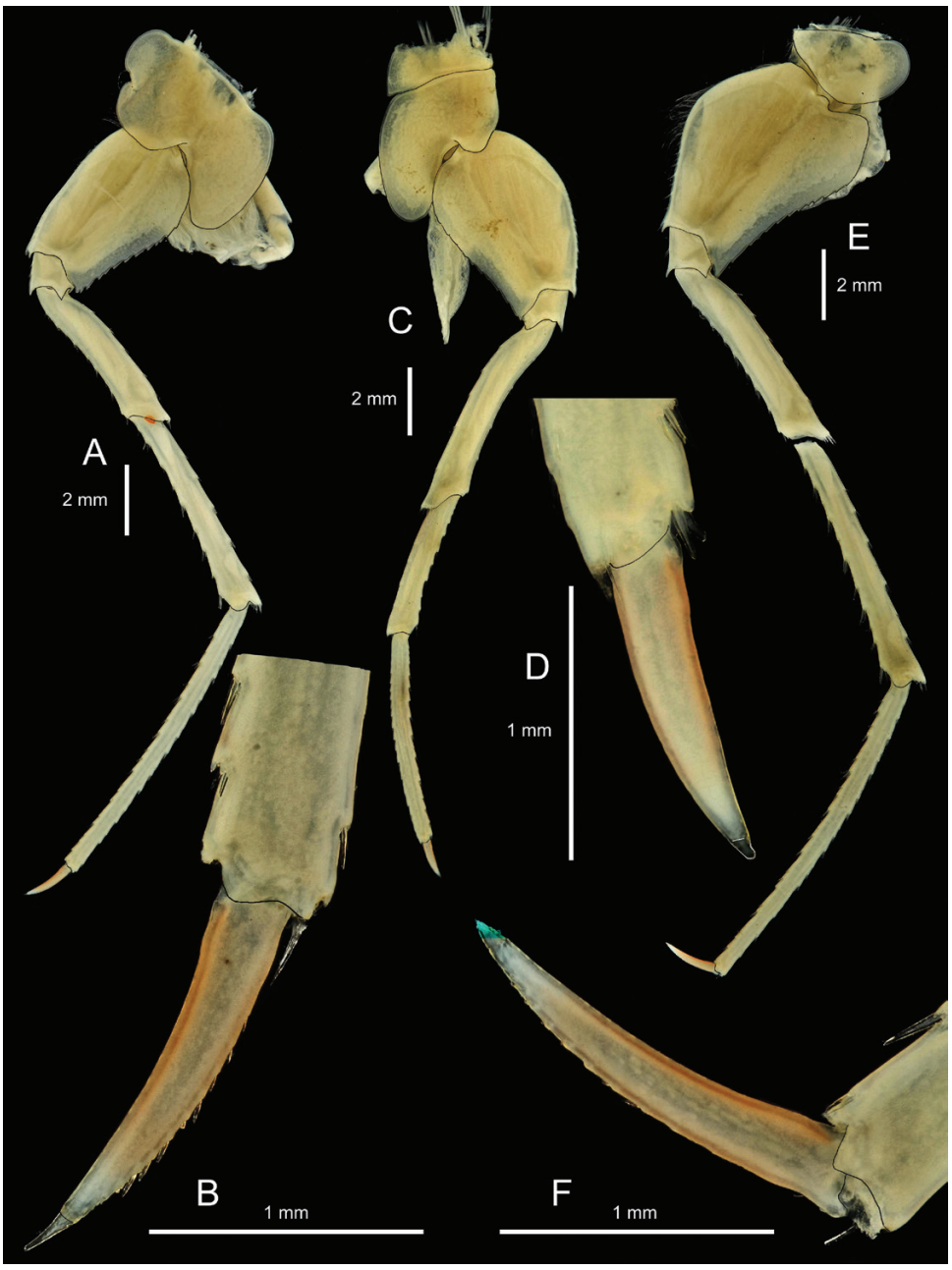

Figure 22. ***Eusirus pontomedon***, ♀ holotype, ANT-XXIX/3, sta. 193-8 (removed from RBINS, INV. 122797, now RBINS *INV. 150107*). A, left P5. B, dactylus of left P5. C, right P6 (carpus, propodus and dactylus abdnormally short and, presumably, regenerated). D, dactylus of right P6. E, left P7. F, dactylus of left P7.

ANT-XIX/3–4, sta. 103-1, 61°44.88′S, 58°01.54′W to 61°45.54′S, 57°58.15′W, 107–111 m, 13 February 2002: one paratype, RBINS, INV. 132557, extr. EPE9. – ANT-XIX/3–4, sta. 106-1, 61°38.17′S, 57°32.66′W to 61°38.05′S, 57°36.39′W, 424–427 m, 14 February 2002: one paratype, RBINS, INV. 132513, extr. ED6, GenBank MT985595 (*COI*), MT945009 (*CytB*), MT945044 (ITS2).

ANT-XXI/2, sta. 293-1, 72°51.90′S, 19°39.31′W to 72°52.07′S, 19°39.62′W, 518–542 m, 31 December 2003: one paratype, RBINS, INV. 132524, extr. EC11, GenBank MT985574 (*COI*), MT945006 (*CytB*), MT945033 (ITS2). – Same sta.: one paratype, RBINS, INV. 132527. – ANT-XXI-2, sta. 308-1, 72°50.18′S, 19°35.94′W to 72°50.09′S, 19°35.82′W, 295–309 m, 2 January 2004: one paratype, RBINS, INV. 132526, extr.

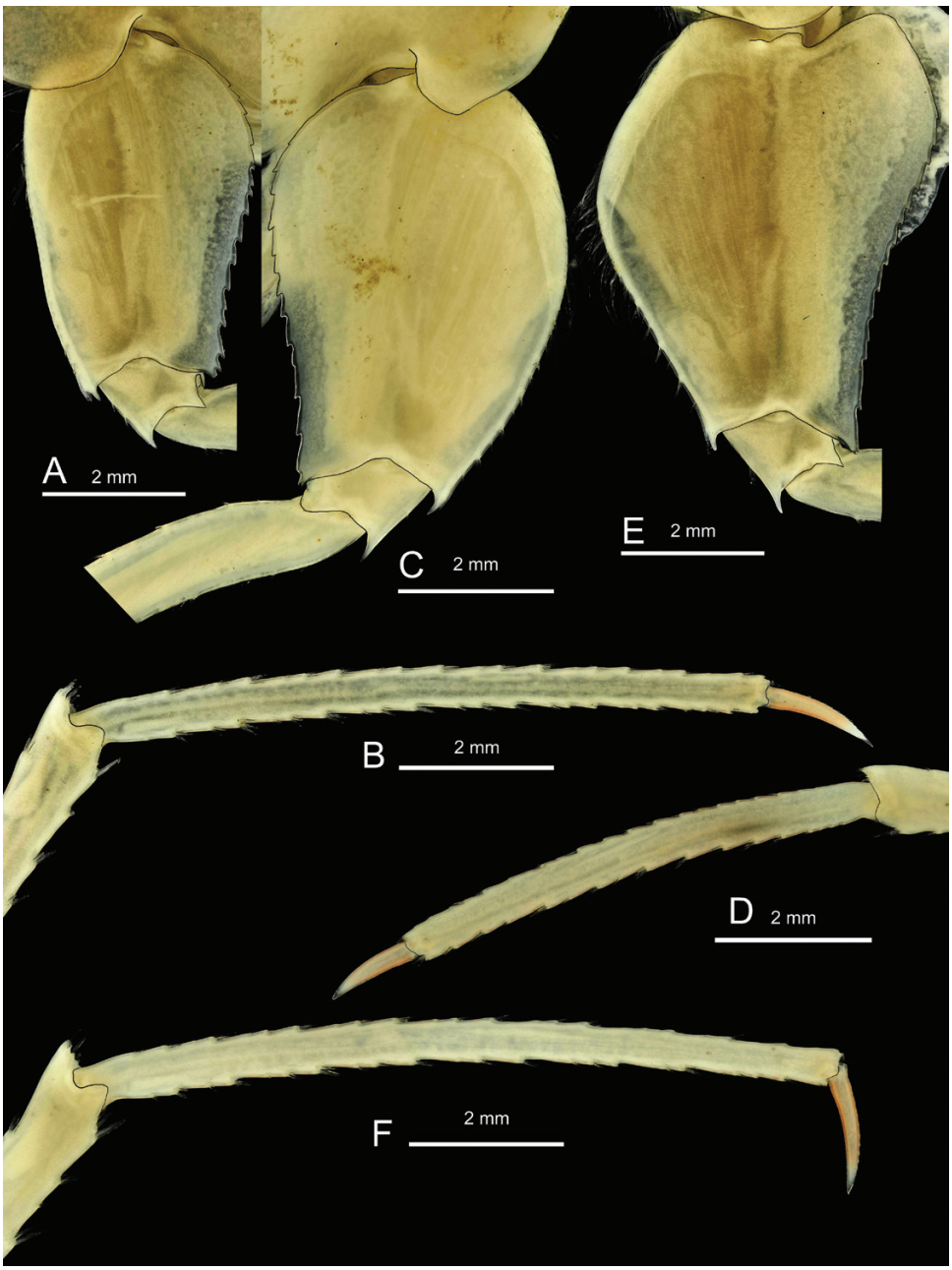

Figure 23. ***Eusirus pontomedon***, ♀ holotype, ANT-XXIX/3, sta. 193-8 (removed from RBINS, INV. 122797, now RBINS *INV. 150107*). A, basis of left P5. B, propodus and dactylus of left P5. C, basis of right P6. D, propodus and dactylus of right P6 (abnormally short and, presumably, regenerated). E, basis of left P7. F, propodus and dactylus of left P7.

EC2, GenBank MT985578 (*COI*), MT945007 (*CytB*), MT945035 (ITS2).

ANT-XXIII/8, sta. 603-5, 70°30.99′S, 08°48.08′W to 70°30.40′S, 08°48.13′W, 274–297 m, 7 December 2006: one paratype, RBINS, INV. 132556, extraction EPE12. – ANT-XXIII/8, sta. 604-1, 61°20.52′S, 55°09.72′W to 61°20.11′S, 55°07.26′W, 286–407 m, 19 December 2006: one paratype, RBINS, RBINS, INV. 122635. – ANT-XXIII/8, sta. 604-1, 61°20.52′S, 55°09.72′W to 61°20.11′S, 55°07.26′W, 286–407 m, 19 December 2006: one paratype, RBINS, INV. 122645 (carcass) and INV. 132380-1 to 132380-5 (five microscopic slides in Euparal). – ANT-XXIII/8, sta. 605-1, 61°20.35′S, 55°29.16′W to 61°19.98′S, 55°32.67′W, 146–151 m, 19 December 2006: one paratype, RBINS, INV. 122648. – ANT-XXIII-8, sta. 608-1, 61°11.34′S, 54°43.17′W to 61°11.80′S, 54°40.05′W, 284–293 m, 20 December 2006: two paratypes, RBINS, INV. 122628. – ANT-XXIII-8, sta. 661-2, 61°39.29′S,

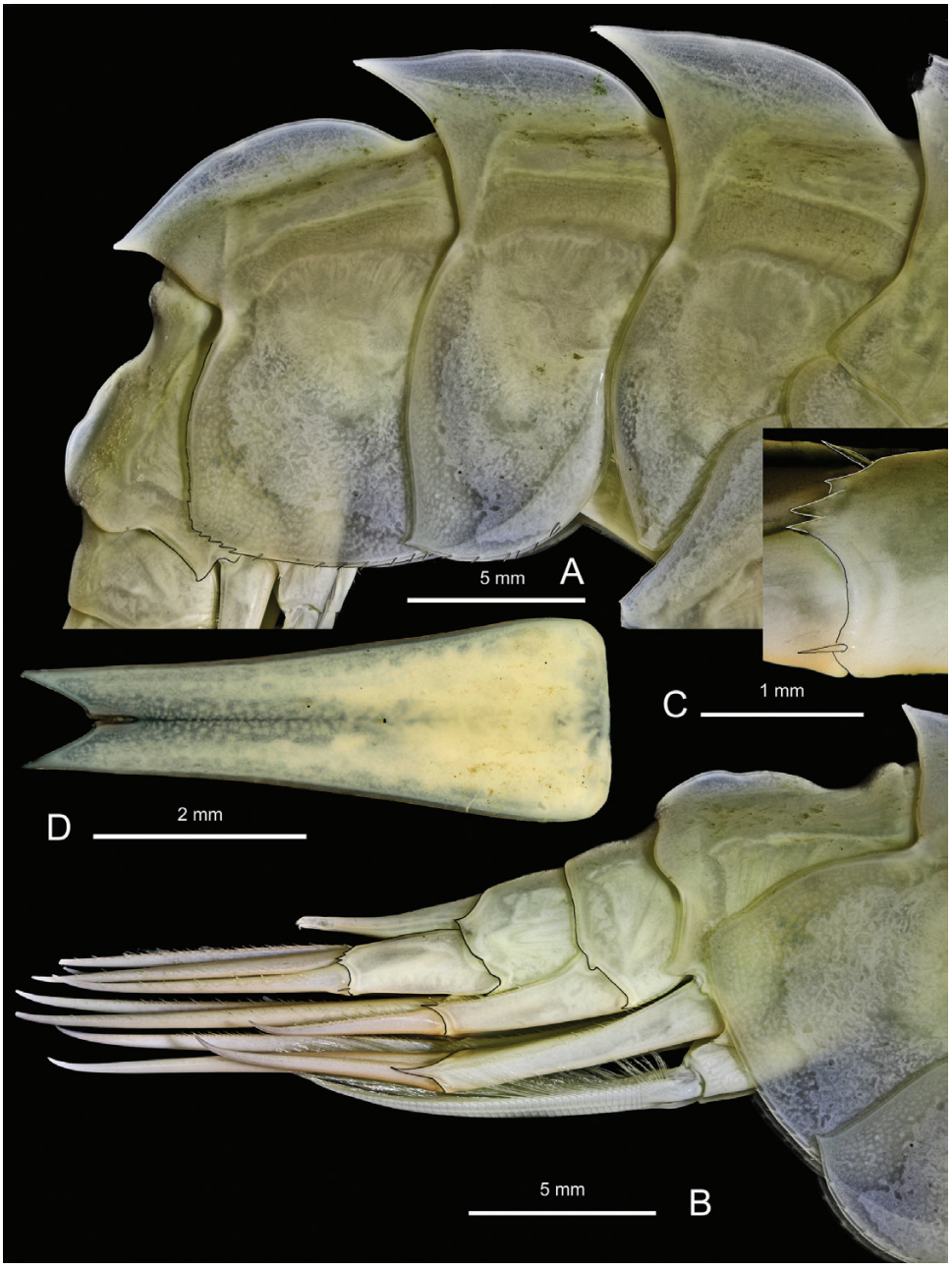

Figure 24. ***Eusirus pontomedon***, ♀ holotype, ANT-XXIX/3, sta. 193-8 (removed from RBINS, INV. 122797, now RBINS *INV. 150107*). A, pleosome. B, urosome. C, tip of peduncle of urosome 3. D, telson.

57°02.89′W to 61°39.20′S, 57°04.75′W, 466–467 m, 30 December 2006: two paratypes, RBINS, INV. 121704. – ANT-XXIII/8, sta. 663-1, 61°38.18′S, 57°33.17′W to 61°38.02′S, 57°37.16′W, 432–434 m, 30 December 2006: one paratype, RBINS, INV. 122638 (carcass) and INV. 132399-1 to 132399-17 (17 microscopic slides in Euparal). – ANT-XXIII/8, sta. 694-1, 63°00.10′S, 58°07.40′W to 62°59.96′S, 58°03.51′W, 220–268 m, 6 January 2007: one paratype, RBINS, INV. 122637.

ANT-XXIV-2, sta. 48-1, 70°23.94′S, 8°19.14′W to 70°23.89′S, 8°18.67′W, 595–602 m, 12 January 2008: one paratype, RBINS, INV. 132512, extr. ED5, GenBank MT985594 (*COI*), MT945008 (*CytB*), MT945043 (ITS2).

ANT-XXIX/3, sta. 118-4, 62°25.95′S, 56°17.26′W to 62°33.71′S, 56°28.31′W, 464–437 m, 27 January 2013: one paratype, RBINS, INV. 122803. – ANT-XXIX/3, sta. 162-7, 63°58.78′S, 56°46.24′W to 63°59.02′S, 56°46.26′W,

214–216 m, 10 February 2013: one paratype, RBINS, INV. 122854. – ANT-XXIX/3, sta. 185-3, 63°51.34′S, 55°41.11′W to 63°51.52′S, 55°41.43′W, 261–296 m, 19 February 2013: one paratype, RBINS, INV. 122833. ANT-XXIX/3, sta. 185-4, 63°51.53′S, 55°40.74′W to 63°51.53′S, 55°40.43′W, 253–255 m, 19 February 2013: one paratype, RBINS, INV. 122835. – ANT-XXIX/3, sta. 188-4, 63°50.36′S, 55°37.42′W to 63°50.53′S, 55°37.52′W, 425–427 m, 20 February 2013: one paratype, RBINS, INV. 122826. – Same sta.: one paratype, RBINS, INV. 122844. – Same sta.: one paratype, RBINS, INV. 122846. – ANT-XXIX/3, sta. 193-8, 62°43.73′S 57°29.04′W to 62°43.80′S 57°29.40′W, 428–431 m, 23 February 2013: one subadult ♀ paratype [telson illustrated], RBINS, INV. 150108, extr. MH22, GenBank MT985624 (*COI*), MT944991 (*CytB*), MT945056 (ITS2). – Same sta.: one paratype, RBINS, INV. 122797A, extr. MH16, GenBank MT985622 (*COI*), MT945014 (*CytB*), MT945054 (ITS2). – Same sta.: one paratype, RBINS, INV. 122797B, extr. MH27, GenBank MT985627 (*COI*), MT944993 (*CytB*), MT945059 (ITS2). – Same sta.: one paratype, RBINS, INV. 122797C, extr. MH23, GenBank MT985625 (*COI*), MT944992 (*CytB*), MT945057 (ITS2). – Same sta.: one paratype, RBINS, INV. 122797D, extr. MH24, GenBank MT985626 (*COI*), MT944995 (*CytB*), MT945058 (ITS2). – Same sta.: one paratype, RBINS, INV. 122797E, extr. MH13. – Same sta.: one paratype, RBINS, INV. 122847. – ANT-XXIX/3, sta. 193-9, 62°43.50′S, 57°27.92′W to 62°43.53′S, 57°28.28′W, 420–431 m, 23 February 2013: nineteen paratypes, RBINS, INV. 122809. – Same sta.: twelve paratypes, RBINS, INV. 122825. – ANT-XXIX/3, sta. 196-8, 62°47.80′S, 57°5.35′W to 62°47.63′S, 57°5.63′W, 542–580 m, 24 February 2013: ten paratypes, RBINS, INV. 122800. – Same sta.: one paratype, RBINS, INV. 122821. – ANT-XXIX/3, sta. 199-4, 62°57.22′S, 58°14.60′W to 62°57.33′S, 58°14.95′W, 325–339 m, 27 February 2013: two paratypes, RBINS, INV. 122810. – ANT-XXIX/3, sta. 217-6, 62°53.45′S, 58°13.06′W to 62°53.42′S, 58°13.41′W, 461–483 m, 2 March 2013: ten paratypes, RBINS, INV. 122798. – Same sta.: forty-four paratypes, RBINS, INV. 122802. – ANT-XXIX/3, sta. 217-7, 62°53.64′S, 58°12.52′W to 62°53.64′S, 58°12.37′W, 387–395 m, 2 March 2013: two paratypes, RBINS, INV. 122823. – ANT-XXIX/3, sta. 227-2, 62°55.83′S, 58°41.09′W to 62°55.76′S, 58°41.46′W, 562–564 m, 5 March 2013: thirty-seven paratypes, RBINS, INV. 122811.

CEAMARC, Adélie Coast, sta. 47 (lot 1245), 67.0677°S, 144.66187°E to 67.036803°S, 144.67242°E, 180–205 m, 30 December 2007: one paratype, reg. no. MNHN-IU-2019–3355, extr. EE31, GenBank MT985605 (*COI*), MT944998 (*CytB*), MT945045 (ITS2). – CEAMARC, Adélie Coast, sta. 79 (lot 3678), 65.706925°S, 140.597385°E to 65.693818°S, 140.538905°E, 419–667 m, 18 January 2008: one paratype, reg. no. MNHN-IU-2019-3356, extr. EE6, GenBank MT985607 (*COI*), MT944999 (*CytB*). – CEAMARC, Adélie Coast, sta. 79 (lot 3678), 65.706925°S, 140.597385°E to 65.693818°S, 140.538905°E, 419–667 m, 18 January 2008: one paratype, reg. no. MNHN-IU-2019-3357, extr. EE7, GenBank MT985608 (*COI*), MT945000 (*CytB*), MT945046 (ITS2). – CEAMARC, Adélie Coast, sta. 79 (lot 3678), 65.706925°S, 140.597385°E to 65.693818°S, 140.538905°E, 419–667 m, 18 January 2008: one paratype, reg. no. MNHN-IU-2019-3357, extr. EE8, GenBank MT985608 (*COI*), MT945000 (*CytB*), MT945046 (ITS2). – CEAMARC, Adélie Coast, sta. 79 (lot 3678), 65.706925°S, 140.597385°E to 65.693818°S, 140.538905°E, 420–668 m, 18 January 2008: one paratype, reg. no. MNHN-IU-2019-3358, extr. EF13, GenBank MT985610 (*COI*), MT945002 (*CytB*), MT945047 (ITS2).

Description

(Based on female holotype RBINS, *INV. 150107*, except for telson: female paratype RBINS INV. 150108).

Body dorsal armature (Figs 15, 16, 17A): Pereionites 5–7 and pleonites 1–3 with mid-dorsal carina backwardly prolonged into strong tooth; dorsal profile of pleonite 3 sigmoid.

Epimeron 1 (Figs 16A, 24A): Narrow, tapering distally and posterodistally pointed, posteroventral margin straight.

Epimeron 2 (Fig. 24A): Ventral margin rounded, armed with spines, posterodistal angle toothed, and posterior margin sinuous.

Epimeron 3 (Fig. 24A): Ventral margin slightly convex, small spines present, posterior margin gently convex, postero-inferior corner rectangular, finely serrate.

Urosomite 1 (Fig. 24B): With proximal depression followed by a mid-dorsal, sinuous carina, roundly sloping distally.

Head (Fig. 17B): About as long as pereionites 1 and 2 combined. Rostrum short, downcurved, tip narrow but blunt, ventrally concave. Lateral lobe produced, subrectangular, unevenly rounded, apically blunt. Post-antennal sinus narrowly U-shaped. Post-antennal lobe shallow, forming a right angle. Ventral margin slightly concave. Eyes large, prominent, elongate, subreniform. Interocular space wide.

Antenna 1 (Fig. 15A, B): Whole antenna 1 conspicuously longer than whole antenna 2, shorter than body length. Peduncle of antenna 1 slightly longer than that of antenna 2. Peduncle article 1 (medial tooth included)

1.1× as long as article 2, 7× as long as article 3. Peduncle article 1 distally with ventrolateral tooth, with two medial teeth of similar size. Peduncle article 2 distally with three ventrolateral teeth (most dorsal shortest, most ventral longest) and three subequal medial teeth (two broken off on illustrated antenna). Article 3 with dorsal and ventral process. Accessory flagellum of one article, short, thin. Flagellum more than 1.8× as long as total peduncle length. Calceoli ventrally present on peduncular articles 2 and 3 and on distoventral surface of flagellar articles.

Antenna 2 (Fig. 18C, D): Peduncular article 4 0.95× as long as article 5, 2.0× broader than article 5, flattened, 3.6× as long as wide, with seven dorsal teeth, of which one is in distal position, with six ventral protrusions (some indistinct), one subdistal tooth and distal denticle. Peduncular article 5 dorsally toothless and with short setae, ventrally with six groups of strong setae (last one in distal position) associated with weak protrusion. Calceoli ventrally present on distoventral surface of flagellar articles.

Upper lip [labrum] (Fig. 19A): Entire, ventrally rounded, with shallow median notch, slightly more prominent than straight epistome, separated by incision.

Lower lip [paragnath or hypopharynx] (Fig. 19B): Inner lobes small, outer lobes gaping, mandibular processes short, rounded.

Mandible (Fig. 19C, D): Left incisor long, with cutting edge smooth except for proximolateral tooth; right incisor long, with cutting edge smooth except for proximal tooth and blunt median tooth; left lacinia mobilis much larger than right one, with four blunt teeth (most medial one largest and separated from others by shallow notch); right lacinia mobilis with margin irregular; row of normally developed raker spines present; molar process columnar, but narrowing distally, triturative surface reduced. Palp three-articulated, attached midway, much longer than mandible body; article 1 short, without setae; article 2 0.7× as long as article 3, ventral margin expanded, heavily setose (D2-setae), distally constricted; article 3 falcate, ventral margin heavily setose (D3-setae), E3-setae short, B3 (grouped in transverse rows) present.

Maxilla 1 (Fig. 19E): Inner plate slender, oblong, subapically bearing one seta; outer plate with 11 spines, some bifid (accessory prongs short); palp two-articulated, article 1 0.6× as long as article 2, article 2 with one row of lateral setae and two rows of medial setae on distal half.

Maxilla 2 (Fig. 19F): Plates subequal in length, apically rounded; outer plate about half width of inner plate, with stiff setae distally; apical margin of inner plate fringed with shorter stiff setae.

Maxilliped (Fig. 18E, F): Inner plate short (medially extending to end of palp article 1), distally and distolaterally densely armed with spines. Outer plate oblong (medially extending one-third to one-half length of palp article 2), laterally, apically and medially armed with long setae. Palp robust, four-articulated, articles 1 and 2 distally dilated; article 2 longest, article 1 sparsely setose. Dorsodistal corner of palp article 2 forming a tooth-like process, bearing fringe of setae; prosterodistal corner (facial side) with four or five teeth. Palp article 3 regularly and strongly expanding distally, densely setose. Palp article 4 three-quarters of overall length of article 3, claw-like, unguis short, distal half of posterior margin armed with uniform, short spines.

Gnathopod 1 (Fig. 20A, B): Subchelate, similar to but slightly shorter than gnathopod 2. Coxal plate about as deep as maximal height of corresponding pereionite, deeper than wide (ratio of depth to width: 1.3), anteroventral angle produced into a broad rounded lobe, anterior margin concave, posterodistal angle with three serrations. Basis weakly curved, proximally narrowed, sparsely setose. Ischium subrectangular, with deep U-shaped notch on anterior border, posterodistal margin setose. Merus subtriangular, about as long as ischium, posterodistal angle rounded and setose. Carpus lobe linguiform, broad, distally tapering, posterior margin regularly convex, clearly exceeding merus, distally setose; ratio of length to width of carpus lobe: 1.57 (length of lobe measured from tip to connection with merus). Propodus subrectangular; longest (transverse) axis 1.24× length of anterior margin, posterior margin slightly concave; palm convex, longer than anterior margin, bearing shorter and longer setae, defined by a hump armed with rows of short to long spines. Dactylus falcate, reaching the hump.

Gnathopod 2 (Fig. 20C): Subchelate. Coxal plate slightly deeper than maximal height of corresponding pereionite, subrectangular, anterior and posterior border weakly converging downwards, ventral margin weakly convex (tip of rounded lobe in posterior position), antero- and posteroventral angles with three and two serrations, respectively; ratio of depth to width of coxal plate: 1.9. Basis weakly curved, proximally narrowed, sparsely setose. Ischium subrectangular, with deep U-shaped notch on anterior border, posterodistal margin almost not setose. Merus

subtriangular, about as long as ischium, posterodistal angle produced into a tooth and setose. Carpus lobe linguiform, broad, distally tapering, posterior margin regularly convex, clearly exceeding merus, distally setose; ratio of length to width of carpus lobe: 1.0 (length of lobe measured from tip to connection with merus). Propodus subrectangular; longest (transverse) axis 1.2× length of anterior margin, posterior margin slightly concave; palm convex, longer than anterior margin, bearing shorter and longer setae, defined by a hump armed with rows of short to long spines. Dactylus falcate, reaching the hump.

Pereiopod 3 (Fig. 21A–C): Coxal plate slightly deeper than maximal height of corresponding pereionite, subrectangular, anterior and posterior border distinctly converging downwards, ventral margin nearly straight (tip of rounded lobe in posterior position), antero- and posteroventral angles with a four serrations; ratio of depth to width of coxal plate: 1.6. Merus 6.1× as long as wide, 1.7× as long as carpus, 1.23× as long as propodus, with nine anterior groups of tiny (hard to see) spines (one in distal position) and ten posterior groups of spines; carpus 3.8× as long as wide, 0.72× as long as propodus, with four (groups of) tiny anterior spines and seven groups of posterior spines; propodus 7.4× as long as wide, with eight anterior groups of spines (which are minute except for those of the distal group) and 15 posterior groups of spines; dactylus short and robust, 0.28× as long as propodus and 0.39× as long as carpus, 4.6× as long as wide.

Pereiopod 4 (Fig. 21D, E): Coxal plate slightly deeper than maximal height of corresponding pereionite, 1.3× as deep as wide, pentagonal; anterodorsal margin nearly straight; anteroventral margin straight; anterodorsal and anteroventral margin connecting with low curve ornate with five serrations; connection between anterodorsal and anteroventral border (ventral tip of coxa) forming a blunt right angle; posteroventral border weakly concave and serrate; posterodorsal border distinctly concave; connection between posteroventral and posterodorsal border forming a right angle. Leg similar to P3, but merus, carpus and propodus a bit longer. Merus 6.7× as long as wide, 1.7× as long as carpus, 1.25× as long as propodus, with ten anterior groups of tiny (hard to see) spines (one in distal position) and 13 posterior groups of spines; carpus 4.3× as long as wide, 0.73× as long as propodus, with six (groups of) minute anterior spines and nine groups of posterior spines; propodus 7.6× as long as wide, with 11 anterior groups of spines (which are minute except for those of the distal group) and 15 posterior groups of spines; dactylus short and robust, 0.26× as long as propodus and 0.36× as long as carpus, 4.4× as long as wide.

Pereiopod 5–7 relationships (Fig. 22A, C, E): Pereiopods 5–7 similar, long, slender; pereiopod 5 shortest, pereiopod 6 and pereiopod 7 subequal. Basis increasing in length from pereiopod 5 to pereiopod 7 [carpus, propodus and dactylus of pereiopod 6 illustrated abnormally short and probably regenerated].

Pereiopod 5 (Figs 22A, B, 23A, B): Coxal plate less deep than maximal height of corresponding pereionite, bilobed, posterior lobe longest. Basis 1.6× as long as wide, 0.73× as long as carpus, anterior margin nearly straight for most of its length, setose on proximal 0.3, spinose on distal 0.7, with two small distal teeth, posterior border expanded, distinctly serrate (13 serrations), proximal 0.3 convex, distal 0.7 nearly straight (weakly concave), posterodistal corner forming a right angle; ischium short, with strong anterodistal tooth and strong posterodistal tooth, with two anterior (groups of) spines; merus 4.4× as long as wide, spinose on both sides; carpus 6.7× as long as wide, 1.3× as long as merus, spinose on both sides; propodus 14.2× as long as wide, 1.7× as long as merus, spinose on both sides; dactylus 5.6× as long as wide, 0.13× as long as propodus; dactylus with spinose posterior border.

Pereiopod 6 (Figs 22C, D, 23C, D): Coxal plate less deep than maximal height of corresponding pereionite, bilobed, posterior lobe longest. Basis 1.5× as long as wide, anterior margin convex, setose on proximal 0.3, spinose on distal 0.7, with two small distal teeth, posterior border expanded, distinctly serrate (14 serrations), proximal 0.3 convex, distal 0.7 nearly straight (weakly concave), posterodistal corner produced into a tooth; ischium short with strong anterodistal tooth and strong posterodistal tooth, with one anterior spine; carpus, propodus and dactylus of pereiopod 6 illustrated abnormally short and probably regenerated.

Pereiopod 7 (Figs 22E, F, 23E, F): Coxal plate less deep than maximal height of corresponding pereionite, unilobed. Basis 1.4× as long as wide, 0.81× as long as carpus, anterior margin with angular discontinuity on proximal 0.5, weakly convex and setose on proximal 0.5, straight and spinose on distal 0.5, with two small distal teeth, posterior border expanded, distinctly serrate (13 serrations), proximal 0.3 convex, distal 0.7 concave, posterodistal corner produced into a tooth; ischium short, with strong anterodistal tooth and strong posterodistal tooth, with one anterior spine; merus 5.5× as long as wide, spinose on both sides; carpus 7.4× as long as wide, 1.2× as long as merus, spinose on both sides; propodus 15.2× as long as wide,

1.5× as long as merus, spinose on both sides; dactylus 6.6× as long as wide, 0.18× as long as propodus.

Coxal gills: From gnathopod 2 to pereiopod 7, proximally voluminous, sack-like (partly pleated), distally lamellate; with oblong accessory gill.

Oostegites: From gnathopod 2 to pereiopod 5, narrowly elliptic.

Pleopods: Without special characters.

Uropod 1 (Fig. 24B): Not reaching level of uropod 2 and uropod 3. Peduncle longer than outer ramus and shorter than inner ramus, with dorsal borders spinose; inner ramus 1.6× length of outer ramus; rami spinose.

Uropod 2 (Fig. 24B): Peduncle 1.0× as long as outer ramus, with dorsal borders spinose; inner ramus 2.2× as long as outer; rami spinose.

Uropod 3 (Fig. 24B, C): Lateral subdistal spine present; distolateral tip with three teeth; inner ramus weakly exceeding outer ramus; rami spinose.

Telson (Fig. 24D): Long, slender, tapering distally, cleft; not reaching half of rami of uropod 3. Telson length 2.9× its breadth. Cleft 19% of length, distally gaping, lobes apically acute.

Colour pattern (Figs 15, 16): Body, antennae, coxae of all pereiopods and bases of pereiopods with a dominant orange or orange-red colour forming a moderately to weakly contrasted (sometimes indistinct) mottled pattern, and with few areas whitish (especially on epimeral plates and bases of pereiopods 5–7); lower half of coxae 1–4 and anterior part of coxa 5 tinged with pink or red (intensity variable); mouthparts and gnathopods deep pink or red; slender part of walking pereiopods whitish, with tip orange and often with orange transverse stripes; tail fan orange or whitish, with traces of orange; eyes silver to golden in life (turning black in alcohol).

Body length: The holotype, which is one of the largest specimens examined, was 75 mm long.

Etymology

From Greek Ποντομέδων: lord of the sea, a byname of Poseidon). The name, which is a noun in apposition, alludes to the large size, the vibrant coloration and the magnificent crested adornment of this predatory Antarctic amphipod, for which we found the title of lord of (Antarctic) seas fitting.

Distribution and bathymetric range

Elephant Island, north-east of King George Island, Bransfield Strait, Joinville Island, James Ross Island, Dundee Island, eastern shelf of the Weddell Sea, Adélie Coast (material examined), Ross Sea (DNA sequences from Baird *et al.*, 2011). The shallowest recorded station was 107–111 m and the deepest 595–602 m.

Biology

All specimens were collected with trawls and dredges, indicating that it is a benthic *Eusirus* species. The stomach of the holotype was full of amphipod fragments, which indicates that it is carnivorous.

Remarks

Eusirus pontomedon is similar to *E. perdentatus*. Both species were systematically confused in the past. They were even confused by Andres *et al.* (2002), whose illustrated specimens of '*Eusirus perdentatus*' included both genuine *E. perdentatus* (the holotype) and *E. pontomedon* (more recently collected specimens). The colour pattern of both species is different, allowing an easy separation of living specimens on board research vessels. The identification of alcohol-preserved, discoloured specimens is much more difficult. The most reliable and easiest diagnostic character is the length and width of the dactylus of pereiopods 3 and 4: they are long and slender in *E. perdentatus* and short and broad in *E. pontomedon*. Other differences include: article 4 of antenna 2 is a bit longer than article 5 in *E. perdentatus* and slightly shorter in *E. pontomedon*. The anterior angle of coxa 1 is more broadly rounded in *E. perdentatus* than in *E. pontomedon*. The posterior lobe of the carpus of gnathopods 1 and 2 is a bit narrower in *E. perdentatus* than in *E. pontomedon*. The proportion of the propodus of gnathopods 1–2 is slightly different. The ratio of the depth of coxa to height of corresponding body segment for coxae 1–4 is a bit higher in *E. perdentatus* than in *E. pontomedon*. The ratio of the length of dactylus to propodus in pereiopods 5–7 is a bit higher *E. perdentatus* than in *E. pontomedon*, but this difference is much less evident than in pereiopods 3 and 4 and might not apply to juveniles.

It is also important to point out that some 'forms' of the *Eusirus giganteus* complex have a colour pattern similar to that of *E. pontomedon* (d'Udekem d'Acoz & Verheye, 2013). These taxa can easily be confused, especially if they are not compared side by side. In the *E. giganteus* complex, the four distal articles of pereiopods 3–7 are distinctly more slender than in *E. pontomedon*, and the propodus of pereiopods 3 and 4 is nearly as long as the merus instead of being distinctly shorter.

KEY TO SPECIES AND SPECIES COMPLEXES OF ANTARCTIC *EUSIRUS*

A provisional key of Antarctic *Eusirus* is presented herein in order to summarize the current state of knowledge. However, it has to be noted that additional taxa within this clade might be species complexes, such as *E. giganteus* (Baird *et al.*, 2011; present study) and the morphologically similar *E. antarcticus*, *Eusirus bouvieri* Chevreux, 1911 and *Eusirus laticarpus* Chevreux, 1906 (Verheye, 2011). '*Eusirus perdentatus* P1' was not included in this key because it is known only from genetic sequences, and its phenotype is unknown. *Eusirus laevis* Walker, 1903, which is known only from a 4 mm juvenile (Walker, 1903), possibly being the juvenile of a species currently known under another name, was also excluded.

1. Pleonites 1 and 2 with posterodorsal tooth: *Eusirus* group *antarcticus* 2
   - Pereionite 7 to pleonite 2 with posterodorsal tooth ..... *Eusirus microps* Walker, 1906
   - Pereionite 5 to pleonite 3 with posterodorsal tooth: crested *Eusirus* 3
2. Medial border of article 2 of maxilliped not distally toothed; posterior border of epimeron 3 minutely serrate; urosomite 3 lateral posterodistal corner angular or produced into one tooth; telson cleft for 0.40–0.45 of its length; live specimens richly mottled in orange ..... *Eusirus antarcticus* Thomson, 1880 [the name *E. antarcticus* is herein applied to the species diagnosed as such in the literature]
   - Medial border of article 2 of maxilliped not distally toothed; posterior border of epimeron 3 smooth (only the posteroventral corner bears a few serrations); urosomite 3 lateral posterodistal corner angular or produced into one tooth; colour of live specimens uniform and dull, often yellowish ..... *Eusirus laticarpus* Chevreux, 1906
   - Medial border of article 2 of maxilliped distally with two to four teeth; posterior border of epimeron 3 minutely serrate; urosomite 3 lateral posterodistal corner with more than one tooth; telson cleft for 0.16 of its length in adults (≤ 0.24 in immatures); body pale brownish; legs and antennae with some reddish brown stripes ..... *Eusirus bouvieri* Chevreux, 1911
3. Epimeron 1 narrow; article 5 of peduncle of antenna 2 longer, equal or scarcely shorter than article 4; propodus of gnathopods not elongate in the palmar axis; propodus of pereiopods 3 and 4 not tapering distad; basis of pereiopod 7 posteriorly with many serrations 4
   - Epimeron 1 broad; article 5 of peduncle of antenna 2 distinctly shorter than article 4; propodus of gnathopods elongate in the palmar axis; propodus of pereiopods 3 and 4 tapering distad; basis of pereiopod 7 posteriorly with a few weak crenellations ..... *Eusirus propeperdentatus* Andres, 1979
4. Merus of pereiopods 3 and 4 1.25–1.35× as long as propodus; propodus of pereiopods 3 and 4 robust (6.8–7.6× as long as wide) 5
   - Merus of pereiopods 3 and 4 1.04–1.08× as long as propodus; propodus of pereiopods 3 and 4 slender (13.2–16.8× as long as wide) ..... *Eusirus giganteus* Andres, Lörz & Brandt, 2002
5. Dactylus of pereiopods 3 and 4 long and narrow (~7× as long as wide in adults and subadults); body and coxae and basis of pereiopods with contrasted purplish red marbling on a white background; coxae 1–4 without pink hue on their posterior half; gnathopods usually white or pale pink ..... *Eusirus perdentatus* Chevreux, 1912
   - Dactylus of pereiopods 3 and 4 short and robust (~4.5× as long as wide in adults and subadults); body and coxae and basis of pereiopods orange with a moderately contrasted mottled pattern or nearly uniform in colour; coxae 1–4 without pink hue on their posterior half; gnathopods usually with strong red or purple pigmentation ..... *Eusirus pontomedon*

EUSIRUS SP.

Eusirus perdentatus P1 – Baird *et al.*, 2011: 3443–3444.

Distribution

Endemic to the Ross Sea.

Remarks

The third species of the *E. perdentatus* complex is endemic to the Ross Sea, or at least it has not yet been recorded anywhere else. However, the specimens sequenced by Baird *et al.* (2011) were not available

for the present study, and their morphology could therefore not be examined.

DISCUSSION

Performance of the methods

The exploration of the shortcomings of DNA-based methods led to the conclusion that inferences regarding species boundaries based on genetic data alone will often be inadequate; hence, the need to place genetic approaches in a wider context that includes delimitation with non-genetic sources of data (Knowles & Carstens, 2007; Schlick-Steiner *et al.*, 2009; Carstens *et al.*, 2013). All DNA-based methods incorporate models that are imperfect imitations of biological reality and, as such, make a number of simplifying assumptions, any one of which could be violated in a particular system (Carstens *et al.*, 2013). Many authors therefore agree that taxonomic changes should not be made solely on the results of these methods (Lohse, 2009; Esselstyn *et al.*, 2012; Puillandre *et al.*, 2012b; Talavera *et al.*, 2013; Zhang *et al.*, 2013; Blair & Bryson, 2017).

In the present study, bPTP did not perform well overall, delimiting an unrealistically high number of poorly supported putative species (22–36), especially within *E. pontomedon* (11–19) (Figs 1, 2). Within the *E. giganteus* complex, the delimitations produced by GMYC based on *CytB* and ITS2 trees were well supported and consistent with other methods (ABGD, mPTP and TCS unconnected haplotype networks; Figs 1, 3). However, GMYC also failed to recognize *E. pontomedon* as a single species (Figs 1, 2). It appears that bPTP and GMYC have difficulty in locating the threshold point in the data, i.e. the transition in rates of branching events (GMYC) or in the mean expected number of substitutions per site, reflected by branch lengths (bPTP), between inter- and intraspecific portions of the tree.

Both GMYC and (b)PTP define a single threshold point for all delimited species in the phylogeny. This is problematic in the case of significant variation in intraspecific genetic diversity among species, because the threshold point between coalescent and speciation processes will be variable. Such variation can have different causes, such as different population sizes or demographic history. In the present study, sampling is highly uneven within the *E. perdentatus* complex, with many more sequences covering a wider geographical area sampled for *E. pontomedon* (16 stations in five regions) compared with sister species (e.g. six stations in four regions for *E. perdentatus* and only one station for P1). Sampling bias is therefore likely to be responsible, at least in part, for the comparatively much higher number of haplotypes (Fig. 3) and intraspecific pairwise distances (Supporting Information, Table S2) observed in *E. pontomedon*.

Varying levels of intraspecific genetic diversity among species are known to decrease the accuracy of (b)PTP and GMYC (Lohse, 2009; Esselstyn *et al.*, 2012; Zhang *et al.*, 2013; Ahrens *et al.*, 2016; Blair & Bryson, 2017; Kapli *et al.*, 2017). Therefore, the large difference in the inferred number of species between bPTP and mPTP is likely to be attributable to the increased accuracy of the latter method in the case of uneven sampling (Blair & Bryson, 2017; Kapli *et al.*, 2017). The mPTP method indeed fits multiple exponential branch length distributions to species, in order to account for different rates of coalescence in heterogeneous datasets (Kapli *et al.*, 2017). The ABGD method is based solely on genetic distances calculated between each pair of sequences and allows for the exploration of a range of thresholds and different levels of intraspecific genetic distances (Puillandre *et al.*, 2012a, b). As such, the bias resulting from uneven sampling appears to be reduced, although this issue requires further exploration (Puillandre *et al.*, 2012b). This reduction in bias is also suggested by the closer match between delimitation schemes resulting from ABGD and mPTP observed here, but also in previous studies (e.g. Blair & Bryson, 2017; Correa *et al.*, 2017; Kapli *et al.*, 2017; Huang *et al.*, 2019; Martínez-Arce *et al.*, 2020). Increasing the sampling effort to minimize differences in specimen numbers between putative species could reduce the potential biases witnessed here in bPTP and GMYC.

Tree-based methods (GMYC, bPTP and mPTP) are applied on single loci, thereby poorly supported nodes and/or non-monophyly in gene trees can render results unreliable (Esselstyn *et al.*, 2012; Fujisawa & Barraclough, 2013; Kapli *et al.*, 2017). Many of the putative species delimited by bPTP and GMYC are not supported clades (Figs 1, 2). In order for these tree-based methods to be able to assign individuals to species correctly, all species must be monophyletic on the gene trees (Esselstyn *et al.*, 2012). Polyphyletic species will be either delimited into smaller groups or delimited with other, nested species (Kapli *et al.*, 2017). In the present study, the *COI* dataset alone did not contain enough phylogenetic information to recover *E. pontomedon* and *E.* cf. *giganteus* G1 (in the ML tree used for mPTP; see Supporting Information, Fig. S3.C) as monophyletic, preventing their delimitation as single putative species by tree-based methods (Fig. 2). These results further exemplify that, although the DNA barcode region was generally found useful for 'quick start' taxonomic exploration (Hebert *et al.*, 2003; Kekkonen & Hebert, 2014; Martínez-Arce *et al.*, 2020), species delineation based solely on single-locus

mitochondrial DNA data is exposed to interpretational risk (Funk & Omland, 2003; Lohse, 2009; Dupuis *et al.*, 2012; Talavera *et al.*, 2013).

In the present case study, non-genetic data (here, morphological analyses) were an essential contribution to the delimitation of species, especially regarding uncertainties and conflicts that arose when applying DNA-based methods to the genetically heterogeneous *E. perdentatus* complex.

Underestimated diversity within crested *Eusirus*

The present study formally explores species boundaries within crested *Eusirus* and, following up from the results of Baird *et al.* (2011), confirms that hidden diversity is present within both nominal species, *E. perdentatus* and *E. giganteus*. Reconstruction of statistical parsimony networks based on our extended datasets revealed unconnected networks corresponding to those shown by Baird *et al.* (2011), namely G1–G4 within the *E. giganteus* complex, with G4 being split into G4a and G4b for the two mitochondrial genes, and P1–P3 within the *E. perdentatus* complex (Fig. 3). Additionally, the DNA-based species delimitation methods applied here overall identified each of those clades as separate putative species (Figs 1, 2). Likewise, species complexes have been revealed by molecular studies in almost every Antarctic group that has been studied to date (Grant & Linse, 2009). The present study adds to the literature (e.g. Held, 2003; Held & Wägele, 2005; Linse *et al.*, 2007; Raupach *et al.*, 2007; Mahon *et al.*, 2008; Thornhill *et al.*, 2008; Janosik & Halanych, 2010; Krabbe *et al.*, 2010; Allcock *et al.*, 2011; Schüller, 2011; Hemery *et al.*, 2012) to highlight our incomplete knowledge of the biodiversity of the Southern Ocean.

Most of the abovementioned molecular studies, including Baird *et al.* (2011) for crested *Eusirus*, suggest the presence of previously undetected cryptic species. However, species are only cryptic to human perception owing to the lack of conspicuous differences in outward appearance, based on the data at hand (Pfenninger & Schwenk, 2007). In many cases, such species are likely to be separated readily by morphological variation that was previously assumed to be intraspecific (Sáez & Lozano, 2005). The fact that high diversity and intricate diagnostic morphological characters make identification of those species challenging without independent information calls for integrative taxonomy. For Antarctic marine taxa, which are difficult to maintain in aquaria and observe *in situ*, genetic and geographical data are usually the most accessible complementary sources of information. Thereby, the combination of phylogeographical and/or DNA-based species delimitation analyses with morphological descriptions and/or morphometric analyses is increasingly used to uncover species diversity within such problematic 'pseudocryptic' complexes (e.g. Janosik & Halanych, 2010; Dettaï *et al.*, 2011; Weis *et al.*, 2014; Dömel *et al.*, 2019; for amphipods: d'Udekem d'Acoz & Verheye, 2017; d'Udekem d'Acoz *et al.*, 2018).

The present study also exemplifies the relevance of integrative taxonomy to resolve species complexes. The true *E. perdentatus* and the newly described *E. pontomedon* can be distinguished by their colour pattern (respectively, 'marbled' and 'spotted'), a trait that is quickly lost in alcohol-preserved specimens, and other relatively inconspicuous character states, the most distinct being the length and robustness of the dactylus of pereiopods 3 and 4: long and slender for *E. perdentatus* vs. short and robust for *E. pontomedon*. Likewise, all four to five putative species within the *E. giganteus* complex are morphologically very similar, but preliminary observation reveals the existence of different colour morphs (Fig. 2; d'Udekem d'Acoz & Verheye, 2013), of which at least some exhibit minor morphological differences (d'Udekem d'Acoz C., unpublished data). In order to translate the DNA-based entities ('putative species') consistently recovered by the various methods within the *E. giganteus* complex into formal species, a detailed morphological analysis, such as the one provided here for the *E. perdentatus* complex, is therefore advocated.

Additional evidence for the sympatric occurrence of some of these (putative) species (notably, *E. perdentatus* and *E. pontomedon*, in addition to G2 and G4) is presented here, with specimens occasionally being collected in the same trawls and their bathymetric range overlapping widely. As suggested by Baird *et al.* (2011), the existence of the proposed *Eusirus* species in sympatry implies that they might exploit different ecological niches. Ecological niche modelling is underutilized in species delimitation (Carstens *et al.*, 2013), but is an appealing perspective in such cases, because it would enable an assessment of the environmental differentiation between putative lineages (e.g. Florio *et al.*, 2012; Zhou *et al.*, 2012).

Circum-Antarctic distributions?

The discovery of overlooked species often leads to the restriction of the previously recorded distributional ranges. For instance, before the widespread use of molecular techniques in taxonomy, many taxa were recorded as circum-Antarctic. This led to the assumption that this biogeographical pattern was common in the Southern Ocean because of a combination of factors that could have homogenizing effects on the faunal communities (Arntz *et al.*, 1997, 2005; Clarke & Johnston, 2003), i.e. a continuous

continental shelf (Griffiths *et al.*, 2009), uniform physical conditions across the continental shelf (Arntz & Gallardo, 1994) and oceanographic currents (Orsi *et al.*, 1993, 1995; Fahrbach *et al.*, 1994; Linse *et al.*, 2007). But progressively, from the almost-routine application of genetic techniques to a large number of Antarctic samples, more and more evidence has emerged that truly circum-Antarctic species are uncommon (Stoddart, 2010).

Numerous molecular studies have shown that recorded circum-Antarctic species are composed of two or more regionally restricted (pseudo)-cryptic species (e.g. Held, 2003; Held & Wägele, 2005; Raupach & Wägele, 2006; Mahon *et al.*, 2008; Thornhill *et al.*, 2008; Brandão *et al.*, 2010; Arango *et al.*, 2011; Verheye *et al.*, 2016). This was generally explained by interdependent factors related to both the biology of the organism and environmental factors. Among the biological factors are the lack of pelagic stages, the low mobility of adults (Hoffman *et al.*, 2010) and/or restricted trophic niches. Regarding environmental factors, glacial cycles (Clarke & Crame, 1989, 1997; Clarke *et al.*, 1992; Allcock & Strugnell, 2012) and the Antarctic Circumpolar Current (Pearse & Bosch, 1994; Pearse *et al.*, 2009) both potentially acted as drivers of speciation for poorly dispersive species, whereas the patchiness of suitable habitats also contributes to such distribution patterns (Raguá-Gil *et al.*, 2004; Gutt *et al.*, 2013; d'Udekem d'Acoz & Verheye, 2017). On the contrary, molecular studies confirming true circumpolarity are fewer and usually concern species with a strictly pelagic lifestyle and/or planktotrophic developmental stage (e.g. Raupach *et al.*, 2010; Bortolotto *et al.*, 2011; Hemery *et al.*, 2012; Moore *et al.*, 2018), while only a handful concern benthic brooders (Arango *et al.*, 2011; Strugnell *et al.*, 2012; Collins *et al.*, 2018).

In amphipods, all of which are brooders, currently 22% of all benthic to benthopelagic species are recorded as circum-Antarctic, i.e. with a distributional range covering at least three widely separated localities around the continent (De Broyer & Jażdżewska, 2014). Although almost all of these species that have been studied with molecular tools have been shown to be complexes of locally restricted species (e.g. Lörz *et al.*, 2009; Havermans *et al.*, 2011, 2013; Verheye *et al.*, 2016), a few were confirmed as circum-Antarctic (e.g. Havermans *et al.*, 2011; d'Udekem d'Acoz *et al.*, 2018), including '*Eusirus* cf. *perdentatus* P3' (Baird *et al.*, 2011), i.e. *E. pontomedon*. The present study shows that the genuine *E. perdentatus* can also be interpreted as potentially circum-Antarctic, being found in all sampled locations, except for the Ross Sea, but noting that samples from the Ross Sea were scarce, meaning that this could be a sampling bias. In the *E. giganteus* complex, all putative species (clades G1–G4) have widespread distributions, including at least one location in the Weddell Sea (Peninsula and/or eastern Weddell Sea) and one distant location (Adélie Coast and/or Ross Sea). To sum up, most crested *Eusirus* studied here, except for the possible Ross Sea endemic *E.* aff. *perdentatus* P1, appear to have widespread to circum-Antarctic distributions.

The extent of contemporary species distributions is directly related to the mobility of the species and the effectiveness of the physical barriers to surmount, e.g. currents, geographical distance and deep stretches (Leese *et al.*, 2010). Population genetic analyses of species of the *E. perdentatus*/*giganteus* complexes indicated high population differentiation between the different sampled locations around the continent, suggesting limited gene flow, as is expected for brooders (Baird *et al.*, 2011). However, the remarkable extent of their contemporary distributions indicates that, compared with most other benthic amphipods, they still appear mobile. Species of the *E. perdentatus*/*giganteus* complexes are presumed to be benthic to benthopelagic carnivorous predators, although because of the past confusion between the different species, it is unclear which ecological observations were based on which species (Klages & Gutt, 1990; Klages, 1993; Emison, 2000; Dauby *et al.*, 2001; Graeve *et al.*, 2001; Nelson *et al.*, 2001; Nyssen *et al.*, 2005; Krapp *et al.*, 2008). *Eusirus giganteus s.l.* specimens were observed swimming upwards in the water column to prey on krill and then 'parachuting' themselves back to the bottom (De Broyer C., pers. com.). One *E. perdentatus s.l.* was collected under pack ice, 240 m above the ocean floor (Krapp *et al.*, 2008). The latter observations show that (at least some of) these species are good swimmers that can occasionally be found in the water column and even at the surface, under ice. Pelagic drift of any type is still considered the most effective dispersal mechanism (Thatje, 2012). In Antarctica, shelf species partly or completely living in the water column might disperse via the East-wind drift (a current flowing close to the continent and all around, except in the Peninsula area) and regionally via the Weddell and Ross Sea gyres (Leese *et al.*, 2010; Janosik *et al.*, 2011; Hemery *et al.*, 2012; Riesgo *et al.*, 2015).

Such phylogeographical analyses are essential to improve our understanding of the contemporary distributions of Antarctic marine organisms and how they are achieved, i.e. their means of dispersal. Ultimately, comprehensive species occurrence data are needed for predicting the impacts of environmental changes and establishing management strategies for the region (Brasier *et al.*, 2017).

ACKNOWLEDGEMENTS

The CAML-CEAMARC cruise of RSV *Aurora Australis* (IPY project no. 53) was supported by the Australian Antarctic Division, the Japanese Science Foundation and the Institut polaire français Paul Émile Victor (IPEV) (programme ICOTA). The material belongs to the Muséum National d'Histoire Naturelle, Paris and was partly transferred to us by Christoph Held (Alfred-Wegener-Institut–Helmoltz-Zentrum für Polar- und Meeresforschung). Many thanks to Helena Baird (Monash University, Clayton, Victoria, Australia) and Glenn Johnstone [Australian Antarctic Division (AAD)] for the helpful correspondence and for organizing transfer of CEAMARC specimens from the AAD. The authors wish to thank Huw Griffiths and Katrin Linse (British Antarctic Survey) for giving us access to the material collected by the RRS *James Clark Ross*. The travel expenses of the authors during ANT-XXIX/3 were funded by the Fonds Léopold III. We would like to thank our scientific colleagues, the crew and the captain of the RV *Polarstern* for their fruitful collaboration during various Antarctic cruises. We wish to thank the editor of the journal and the anonymous reviewer for helpful comments and improvements of this manuscript. This publication is registered as ANDEEP contribution no. 219, contribution no. 45 to the vERSO project (Belgian Federal Science Policy Office, contract no. BR/132/A1/vERSO) and contribution no. 20 to the RECTO project (BELSPO, contract no. BR/154/A1/RECTO).

REFERENCES

Ahrens D, Fujisawa T, Krammer HJ, Eberle J, Fabrizi S, Vogler AP. 2016. Rarity and incomplete sampling in DNA-based species delimitation. *Systematic Biology* **65:** 478–494.

Allcock AL, Barratt I, Eléaume M, Linse K, Norman MD, Smith PJ, Steinke D, Stevens DW, Strugnell JM. 2011. Cryptic speciation and the circumpolarity debate: a case study on endemic Southern Ocean octopuses using the COI barcode of life. *Deep Sea Research Part II: Topical Studies in Oceanography* **58:** 242–249.

Allcock AL, Strugnell JM. 2012. Southern Ocean diversity: new paradigms from molecular ecology. *Trends in Ecology & Evolution* **27:** 520–528.

Andres HG. 1990. Amphipoda. In: Sieg J, Wägele JW, eds. *Fauna der Antarktis*. Berlin & Hamburg: Paul Parey, 133–143.

Andres HG, Lörz AN, Brandt A. 2002. A common but undescribed huge species of *Eusirus* Krøyer, 1845 (Crustacea, Amphipoda, Eusiridae) from Antarctica. *Mitteilungen aus der Hamburgischen Zoologischen Museum und Institut* **99:** 109–126.

Arango CP, Soler-Membrives A, Miller KJ. 2011. Genetic differentiation in the circum-Antarctic sea spider *Nymphon australe* (Pycnogonida; Nymphonidae). *Deep Sea Research Part II: Topical Studies in Oceanography* **58:** 212–219.

Arntz WE, Brey T. 2005. The expedition ANTARKTIS XXI/2 (BENDEX) of RV "*Polarstern*" in 2003/2004. *Berichte zur Polar- und Meeresforschungen* **503:** 1–149.

Arntz WE, Gallardo VA. 1994. Antarctic benthos: present position and future prospects. In: Hempel G, ed. *Antarctic science: global concerns*. Berlin, Heidelberg: Springer Berlin Heidelberg, 243–277.

Arntz WE, Gutt J, Klages JP. 1997. Antarctic marine biodiversity. In: Battaglia B, Valencia J, Walton D, eds. *Antarctic communities: species, structure and survival*. Cambridge: Cambridge University Press, 3–14.

Arntz WE, Thatje S, Gerdes D, Gili JM, Gutt J, Jacob U, Montiel A, Orejas C, Teixido N. 2005. The Antarctic-Magellan connection: macrobenthos ecology on the shelf and upper slope, a progress report. *Scientia Marina* **69:** 237–269.

Baird HP, Miller KJ, Stark JS. 2011. Evidence of hidden biodiversity, ongoing speciation and diverse patterns of genetic structure in giant Antarctic amphipods. *Molecular Ecology* **20:** 3439–3454.

Barnard JL. 1961. Gammaridean Amphipoda from depths of 400 to 6000 meters. *Galathea Report* **5:** 23–128.

Barnard KH. 1930. Crustacea. Part XI. Amphipoda. British Antarctic ("Terra Nova") Expedition, 1910. Natural history report. *Zoology* **8:** 307–454.

Barnard KH. 1932. Amphipoda. *Discovery Reports* **5:** 1–326.

Barnes DKA, Peck LS. 2008. Vulnerability of Antarctic shelf biodiversity to predicted regional warming. *Climate Research* **37:** 149–163.

Bathmann U. 2010. The expedition of the research vessel "Polarstern" to the Antarctic in 2007/2008 (ANT-XXIV/2). *Berichte zur Polar- und Meeresforschungen* **604:** 1–200.

Blair C, Bryson RW Jr. 2017. Cryptic diversity and discordance in single-locus species delimitation methods within horned lizards (Phrynosomatidae: Phrynosoma). *Molecular Ecology Resources* **17:** 1168–1182.

Borchsenius F. 2009. *FastGap 1.2*. Aarhus: Department of Biosciences, Aarhus University. Available at: http://www.aubot.dk/FastGap_home.htm

Bortolotto E, Bucklin A, Mezzavilla M, Zane L, Patarnello T. 2011. Gone with the currents: lack of genetic differentiation at the circum-continental scale in the Antarctic krill *Euphausia superba*. *BMC Genetics* **12:** 32.

Brandão SN, Sauer J, Schön I. 2010. Circumantarctic distribution in Southern Ocean benthos? A genetic test using the genus *Macroscapha* (Crustacea, Ostracoda) as a model. *Molecular Phylogenetics and Evolution* **55:** 1055–1069.

Brasier MJ, Harle J, Wiklund H, Jeffreys RM, Linse K, Ruhl HA, Glover AG. 2017. Distributional patterns of polychaetes across the West Antarctic based on DNA barcoding and particle tracking analyses. *Frontiers in Marine Science* **4:** 356.

Brecko J, Mathys A, Dekoninck W, Leponce M, VandenSpiegel D, Semal P. 2014. Focus stacking: comparing commercial top-end set-ups with a semi-automatic

low budget approach. A possible solution for mass digitization of type specimens. *ZooKeys* **464:** 1–23.

Cardoso A, Vogler AP. 2005. DNA taxonomy, phylogeny and Pleistocene diversification of the *Cicindela hybrida* species group (Coleoptera: Cicindelidae). *Molecular Ecology* **14:** 3531–3546.

Carstens BC, Pelletier TA, Reid NM, Satler JD. 2013. How to fail at species delimitation. *Molecular Ecology* **22:** 4369–4383.

Chen H, Strand M, Norenburg JL, Sun S, Kajihara H, Chernyshev AV, Maslakova SA, Sundberg P. 2010. Statistical parsimony networks and species assemblages in Cephalotrichid nemerteans (Nemertea). *PLoS One* **5:** e12885.

Chevreux E. 1912. Deuxième expédition dans l'Antarctique, dirigée par le Dr. Charcot. 1908–1910. Diagnoses d'amphipodes nouveaux. *Bulletin du Muséum National d'Histoire Naturelle* **18:** 208–218.

Chevreux E. 1913. Amphipodes. In: Masson et Cie, eds. *Deuxième expédition Antarctique française (1908–1910) commandée par le Dr. Jean Charcot, sciences naturelles: documents scientifiques*. Paris: L. Joubin, 79–186.

Chilton C. 1912. The Amphipoda of the Scottish national Antarctic expedition. *Transactions of the Royal Society of Edinburgh* **48:** 455–520, pls 1–2.

Chown SL, Clarke A, Fraser CI, Cary SC, Moon KL, McGeoch MA. 2015. The changing form of Antarctic biodiversity. *Nature* **522:** 431–438.

Chown SL, Lee JE, Hughes KA, Barnes J, Barrett PJ, Bergstrom DM, Convey P, Cowan DA, Crosbie K, Dyer G, Frenot Y, Grant SM, Herr D, Kennicutt MC 2nd, Lamers M, Murray A, Possingham HP, Reid K, Riddle MJ, Ryan PG, Sanson L, Shaw JD, Sparrow MD, Summerhayes C, Terauds A, Wall DH. 2012. Conservation. Challenges to the future conservation of the Antarctic. *Science* **337:** 158–159.

Clarke A, 2008. Antarctic marine benthic diversity: patterns and processes. *Journal of Experimental Marine Biology and Ecology* **366:** 48–55.

Clarke A, Crame JA. 1989. The origin of the Southern Ocean marine fauna. In: Crame JA, ed. *Origins and evolution of the Antarctic biota*. Cambridge: Geological Society London Special Publications Vol. 47: 253–268.

Clarke A, Crame JA. 1992. The Southern Ocean benthic fauna and climate change: a historical perspective. *Philosophical Transactions of the Royal Society B: Biological Sciences* **338:** 299–309.

Clarke A, Crame JA. 1997. Diversity, latitude and time: patterns in the shallow sea. In: Ormond RFG, ed. *Marine biodiversity*. Cambridge: Cambridge University Press, 122–147.

Clarke A, Johnston NM. 2003. Antarctic marine benthic biodiversity. In: Gibson RN, Atkinson RJA, eds. *Oceanography and marine biology, an annual review*. London: CRC Press, 47–114.

Clarke A, Murphy EJ, Meredith MP, King JC, Peck LS, Barnes DK, Smith RC. 2007. Climate change and the marine ecosystem of the western Antarctic Peninsula. *Philosophical transactions of the Royal Society B: Biological Sciences* **362:** 149–166.

Clement M, Posada D, Crandall KA. 2000. TCS: a computer program to estimate gene genealogies. *Molecular Ecology* **9:** 1657–1659.

Collins EE, Galaska MP, Halanych KM, Mahon AR. 2018. Population genomics of *Nymphon australe* Hodgson, 1902 (Pycnogonida, Nymphonidae) in the Western Antarctic. *The Biological Bulletin* **234:** 180–191.

Correa C, Vásquez D, Castro-Carrasco C, Zúñiga-Reinoso Á, Ortiz JC, Palma RE. 2017. Species delimitation in frogs from South American temperate forests: The case of *Eupsophus*, a taxonomically complex genus with high phenotypic variation. *PLoS One* **12:** e0181026.

Costello MJ, Bouchet P, Boxshall G, Fauchald K, Gordon D, Hoeksema BW, Poore GC, van Soest RW, Stöhr S, Walter TC, Vanhoorne B, Decock W, Appeltans W. 2013. Global coordination and standardisation in marine biodiversity through the World Register of Marine Species (WoRMS) and related databases. *PLoS One* **8:** e51629.

Dauby P, Scailteur Y, De Broyer C. 2001. Trophic diversity within the eastern Weddell Sea amphipod community. *Hydrobiologia* **443:** 69–86.

De Broyer C. 1983. *Recherches sur la systématique et l'évolution des crustacés amphipodes gammarides antarctiques et subantarctiques*. Louvain-la-Neuve: Université Catholique de Louvain.

De Broyer C, Clarke A, Koubbi P, Pakhomov E, Scott F, Vanden Berghe E, Danis B. (eds.) 2020. *Register of Antarctic marine species*. Available at: http://www.marinespecies.org/rams

De Broyer C, Danis B. 2011. How many species in the Southern Ocean? Towards a dynamic inventory of the Antarctic marine species. *Deep Sea Resarch Part II: Topical Studies in Oceanography* **58:** 5–17.

De Broyer C, Jażdżewska A. 2014. Biogeographic patterns of Southern Ocean benthic amphipods. In: De Broyer C, Koubbi P, Griffiths H, Raymond B, d'Udekem d'Acoz C, Van de Putte A, Danis B, David B, Grant S, Gutt J, Held C, Hosie G, Huettmann F, Post A, Ropert-Coudert Y, eds. *Biogeographic atlas of the Southern Ocean*. Cambridge: Scientific Committee on Antarctic Research, 155–165.

De Broyer C, Lowry JK, Jażdżewski K, Robert H. 2007. Catalogue of the gammaridean and corophiidean Amphipoda (Crustacea) of the Southern Ocean with distribution and ecological data. In: De Broyer C, ed. *Synopsis of the Amphipoda of the Southern Ocean*. Brussels: Institut Royal des Sciences Naturelles de Belgique, 1–325.

DeSalle R, Egan MG, Siddall M. 2005. The unholy trinity: taxonomy, species delimitation and DNA barcoding. *Philosophical Transactions of the Royal Society B: Biological Sciences* **360:** 1905–1916.

Dettaï A, Adamowizc SJ, Allcock L, Arango CP, Barnes DK, Barratt I, Chenuil A, Couloux A, Cruaud C, David B, Denis F, Denys G, Díaz A, Eléaume M, Féral J-P, Froger A, Gallut C, Grant R, Griffiths H, Held C, Hemery LG, Hosie G, Kuklinski P, Lecointre G, Linse K, Lozouet P, Mah C, Monniot F, Norman MD,

O'Hara T, Ozouf-Costaz C, Piedallu C, Pierrat B, Poulin E, Puillandre N, Riddle M, Samadi S, Saucède T, Schubart C, Smith PJ, Stevens DW, Steinke D, Strugnell J, Tarnowska K, Wadley V, Améziane N. 2011. DNA barcoding and molecular systematics of the benthic and demersal organisms of the CEAMARC survey. *Polar Science* **5:** 298–312.

Dömel JS, Macher TH, Dietz L, Duncan S, Mayer C, Rozenberg A, Wolcott K, Leese F, Melzer RR. 2019. Combining morphological and genomic evidence to resolve species diversity and study speciation processes of the *Pallenopsis patagonica* (Pycnogonida) species complex. *Frontiers in Zoology* **16:** 1–29.

Dornburg A, Santini F, Alfaro ME. 2008. The influence of model averaging on clade posteriors: an example using the triggerfishes (Family Balistidae). *Systematic Biology* **57:** 905–919.

Dupuis JR, Roe AD, Sperling FA. 2012. Multi-locus species delimitation in closely related animals and fungi: one marker is not enough. *Molecular Ecology* **21:** 4422–4436.

Emison WB. 2000. Revision of *Eusirus perdentatus* Chevreux, 1912 and *E. propeperdentatus* Andres, 1979 (Crustacea: Amphipoda). *ANARE Reports* **145:** 1–80.

Esselstyn JA, Evans BJ, Sedlock JL, Anwarali Khan FA, Heaney LR. 2012. Single-locus species delimitation: a test of the mixed Yule-coalescent model, with an empirical application to Philippine round-leaf bats. *Proceedings of the Royal Society B: Biological Sciences* **279:** 3678–3686.

Ezard T, Fujisawa T, Barraclough T. 2009. *Splits: SPecies' LImits by Threshold Statistics. R package version 1.0-11/r29 15*. Available at: http://R-Forge.R-project.org/projects/splits/

Fahrbach E, Rohardt G, Schröder M, Strass V. 1994. Transport and structure of the Weddell Gyre. *Annales Geophysicae* **12:** 840–855.

Florio AM, Ingram CM, Rakotondravony HA, Louis EE, Raxworthy CJ. 2012. Detecting cryptic speciation in the widespread and morphologically conservative carpet chameleon (*Furcifer lateralis*) of Madagascar. *Journal of Evolutionary Biology* **25:** 1399–1414.

Folmer O, Black M, Hoeh W, Lutz R, Vrijenhoek R. 1994. DNA primers for amplification of mitochondrial Cytochrome C oxidase subunit I from diverse metazoan invertebrates. *Molecular marine biology and biotechnology* **3:** 294–299.

Fujisawa T, Barraclough TG. 2013. Delimiting species using single-locus data and the Generalized Mixed Yule Coalescent approach: a revised method and evaluation on simulated data sets. *Systematic Biology* **62:** 707–724.

Funk DJ, Omland KE. 2003. Species-level paraphyly and polyphyly: frequency, causes, and consequences, with insights from animal mitochondrial DNA. *Annual Review of Ecology, Evolution, and Systematics* **34:** 397–423.

Fütterer D, Brandt A, Poore G. 2003. The expeditions ANTARKTIS-XIX/3–4 of the research vessel Polarstern in 2002: (ANDEEP I and II: Antarctic benthic deep-sea biodiversity – colonization history and recent community patterns). *Berichte zur Polar- und Meeresforschung* **470:** 1–174.

Graeve M, Dauby P, Scailteur Y. 2001. Combined lipid, fatty acid and digestive tract content analyses: a penetrating approach to estimate feeding modes of Antarctic amphipods. *Polar Biology* **24:** 853–862.

Grant RA, Griffiths HJ, Steinke D, Wadley V, Linse K. 2011. Antarctic DNA barcoding: a drop in the ocean? *Polar Biology* **34:** 775–780.

Grant RA, Linse K. 2009. Barcoding Antarctic biodiversity: current status and the CAML initiative, a case study of marine invertebrates. *Polar Biology* **32:** 1629.

Griffiths HJ. 2010. Antarctic marine biodiversity – what do we know about the distribution of life in the Southern Ocean? *PLoS One* **5:** e11683.

Griffiths HJ, Barnes DKA, Linse K. 2009. Towards a generalized biogeography of the Southern Ocean benthos. *Journal of Biogeography* **36:** 162–177.

Griffiths HJ, Danis B, Clarke A. 2011. Quantifying Antarctic marine biodiversity: the SCAR-MarBIN data portal. *Deep Sea Resarch Part II: Topical Studies in Oceanography* **58:** 18–29.

Gutt J. 2008. The expedition ANTARKTIS-XXIII/8 of the research vessel "Polarstern" in 2006/2007. *Berichte zur Polar- und Meeresforschungen* **569:** 1–152.

Gutt J. 2013. The expedition of the research vessel "Polarstern" to the Antarctic in 2013 (ANTXXIX/3). *Berichte zur Polar- und Meeresforschungen* **665:** 1–154.

Gutt J, Barnes D, Lockhart SJ, Van de Putte A. 2013. Antarctic macrobenthic communities: A compilation of circumpolar information. *Nature Conservation* **4:** 1–13.

Gutt J, Bertler N, Bracegirdle TJ, Buschmann A, Comiso J, Hosie G, Isla E, Schloss IR, Smith CR, Tournadre J, Xavier JC. 2015. The Southern Ocean ecosystem under multiple climate change stresses – an integrated circumpolar assessment. *Global Change Biology* **21:** 1434–1453.

Gutt J, Sirenko BI, Smirnov I, Arntz WE. 2004. How many macrozoobenthic species might inhabit the Antarctic shelf? *Antarctic Science* **16:** 11–16.

Hart MW, Keever CC, Dartnall AJ, Byrne M. 2006. Morphological and genetic variation indicate cryptic species within Lamarck's little sea star, *Parvulastra* (=*Patiriella*) exigua. *The Biological Bulletin* **210:** 158–167.

Hart MW, Sunday J. 2007. Things fall apart: biological species form unconnected parsimony networks. *Biology Letters* **3:** 509–512.

Havermans C, Nagy ZT, Sonet G, De Broyer C, Martin P. 2011. DNA barcoding reveals new insights into the diversity of Antarctic species of *Orchomene sensu lato* (Crustacea: Amphipoda: Lysianassoidea). *Deep Sea Resarch Part II: Topical Studies in Oceanography* **58:** 230–241.

Havermans C, Sonet G, d'Udekem d'Acoz C, Nagy ZT, Martin P, Brix S, Riehl T, Agrawal S, Held C. 2013. Genetic and morphological divergences in the cosmopolitan deep-sea amphipod *Eurythenes gryllus* reveal a diverse abyss and a bipolar species. *PLoS One* **8:** e74218.

Hebert PDN, Cywinska A, Ball SL, deWaard JR. 2003. Biological identifications through DNA barcodes. *Proceedings of the Royal Society B: Biological Sciences* **270:** 313–322.

Held C. 2003. Molecular evidence for cryptic speciation within the widespread Antarctic crustacean *Ceratoserolis*

trilobitoides (Crustacea, Isopoda). *Antarctic Biology in a Global Context* **305:** 1–5.

Held C, Wägele JW. 2005. Cryptic speciation in the giant Antarctic isopod *Glyptonotus antarcticus* (Isopoda, Valvifera, Chaetiliidae). *Scientia Marina* **69:** 175–181.

Hemery LG, Eléaume M, Roussel V, Améziane N, Gallut C, Steinke D, Cruaud C, Couloux A, Wilson NG. 2012. Comprehensive sampling reveals circumpolarity and sympatry in seven mitochondrial lineages of the Southern Ocean crinoid species *Promachocrinus kerguelensis* (Echinodermata). *Molecular Ecology* **21:** 2502–2518.

Hernando M, Schloss IR, Malanga G, Almandoz GO, Ferreyra GA, Aguiar MB, Puntarulo S. 2015. Effects of salinity changes on coastal Antarctic phytoplankton physiology and assemblage composition. *Journal of Experimental Marine Biology and Ecology* **466:** 110–119.

Hoffman JI, Peck LS, Linse K, Clarke A. 2010. Strong population genetic structure in a broadcast-spawning Antarctic marine invertebrate. *The Journal of Heredity* **102:** 55–66.

Huang XC, Su JH, Ouyang JX, Ouyang S, Zhou CH, Wu XP. 2019. Towards a global phylogeny of freshwater mussels (Bivalvia: Unionida): species delimitation of Chinese taxa, mitochondrial phylogenomics, and diversification patterns. *Molecular Phylogenetics and Evolution* **130:** 45–59.

Janosik AM, Halanych KM. 2010. Unrecognized Antarctic biodiversity: a case study of the genus *Odontaster* (Odontasteridae; Asteroidea). *Integrative and Comparative Biology* **50:** 981–992.

Janosik AM, Mahon AR, Halanych KM. 2011. Evolutionary history of Southern Ocean *Odontaster* sea star species (Odontasteridae; Asteroidea). *Polar Biology* **34:** 575–586.

Joly S, Stevens MI, van Vuuren BJ. 2007. Haplotype networks can be misleading in the presence of missing data. *Systematic Biology* **56:** 857–862.

Kapli P, Lutteropp S, Zhang J, Kobert K, Pavlidis P, Stamatakis A, Flouri T. 2017. Multi-rate Poisson tree processes for single-locus species delimitation under maximum likelihood and Markov chain Monte Carlo. *Bioinformatics* **33:** 1630–1638.

Kekkonen M, Hebert PD. 2014. DNA barcode-based delineation of putative species: efficient start for taxonomic workflows. *Molecular Ecology Resources* **14:** 706–715.

Klages M. 1993. Distribution, reproduction and population dynamics of the Antarctic gammaridean amphipod *Eusirus perdentatus* Chevreux, 1912 (Crustacea). *Antarctic Science* **5:** 349–359.

Klages M, Gutt J. 1990. Observations on the feeding behaviour of the Antarctic gammarid *Eusirus perdentatus* Chevreux, 1912 (Crustacea: Amphipoda) in aquaria. *Polar Biology* **10:** 359–364.

Knowles LL, Carstens BC. 2007. Delimiting species without monophyletic gene trees. *Systematic Biology* **56:** 887–895.

Knust R, Gerdes D, Mintenbeck K. 2012. The expedition of the research vessel "Polarstern" to the Antarctic in 2011 (ANT-XXVII/3) (CAMBIO). *Berichte zur Polar- und Meeresforschungen* **644:** 1–200.

Knust R, Schröder M. 2014. The expedition PS82 of the research vessel Polarstern to the southern Weddell Sea in 2013/2014. *Berichte zur Polar- und Meeresforschungen* **680:** 1–155.

Krabbe K, Leese F, Mayer C, Tollrian R, Held C. 2010. Cryptic mitochondrial lineages in the widespread pycnogonid *Colossendeis megalonyx* Hoek, 1881 from Antarctic and Subantarctic waters. *Polar Biology* **33:** 281–292.

Krapp RH, Berge J, Flores H, Gulliksen B, Werner I. 2008. Sympagic occurrence of eusirid and lysianassoid amphipods under Antarctic pack ice. *Deep Sea Research Part II: Topical Studies in Oceanography* **55:** 1015–1023.

Krapp-Schickel T, De Broyer C. 2014. Revision of *Leucothoe* (Amphipoda, Crustacea) from the Southern Ocean: a cosmopolitanism concept is vanishing. *European Journal of Taxonomy* **80:** 1–55.

Kumar S, Stecher G, Tamura K. 2016. MEGA7: molecular evolutionary genetics analysis version 7.0 for bigger datasets. *Molecular Biology and Evolution* **33:** 1870–1874.

Lanfear R, Calcott B, Ho SY, Guindon S. 2012. Partitionfinder: combined selection of partitioning schemes and substitution models for phylogenetic analyses. *Molecular Biology and Evolution* **29:** 1695–1701.

Leese F, Agrawal S, Held C. 2010. Long-distance island hopping without dispersal stages: transportation across major zoogeographic barriers in a Southern Ocean isopod. *Die Naturwissenschaften* **97:** 583–594.

Leese F, Held C. 2008. Identification and characterization of microsatellites from the Antarctic isopod *Ceratoserolis trilobitoides*: nuclear evidence for cryptic species. *Conservation Genetics* **9:** 1369–1372.

Linse K, Cope T, Lörz AN, Sands C. 2007. Is the Scotia Sea a centre of Antarctic marine diversification? Some evidence of cryptic speciation in the circum-Antarctic bivalve *Lissarca notorcadensis*. *Polar Biology* **30:** 1059–1068.

Lohse K. 2009. Can mtDNA barcodes be used to delimit species? A response to Pons *et al*. (2006). *Systematic Biology* **58:** 439–442.

Lörz AN, Held C. 2004. A preliminary molecular and morphological phylogeny of the Antarctic Epimeriidae and Iphimediidae (Crustacea, Amphipoda). *Molecular Phylogenetics and Evolution* **31:** 4–15.

Lörz AN, Maas EW, Linse K, Coleman CO. 2009. Do circum-Antarctic species exist in peracarid Amphipoda? A case study in the genus *Epimeria* Costa, 1851 (Crustacea, Peracarida, Epimeriidae). *Zookeys* **18:** 91–128.

Lowry JK, Stoddart H. 1993. Crustacea Amphipoda: Lysianassoids from Philippine and Indonesian waters. In: Betsch J-M, Bouchet P, Erard C, Justine J-L, eds. *Mémoires du Muséum national d'Histoire naturelle. Résultats des campagnes MUSORSTOM, volume 10*. Paris: G.D.R. Ecoprophyce and ORSTOM, 55–109.

Mahon AR, Arango CP, Halanych KM. 2008. Genetic diversity of *Nymphon* (Arthropoda: Pycnogonida: Nymphonidae) along the Antarctic Peninsula with a focus on *Nymphon australe* Hodgson 1902. *Marine Biology* **155:** 315–323.

Martínez-Arce A, De Jesús-Navarrete A, Leasi F. 2020. DNA barcoding for delimitation of putative Mexican marine nematodes species. *Diversity* **12:** 1–16.

Miller MA, Pfeiffer W, Schwartz T. 2010. Creating the CIPRES Science Gateway for inference of large phylogenetic trees. *Gateway Computing Environments Workshop (GCE)* **2010:** 1–8.

Monaghan MT, Wild R, Elliot M, Fujisawa T, Balke M, Inward DJ, Lees DC, Ranaivosolo R, Eggleton P, Barraclough TG, Vogler AP. 2009. Accelerated species inventory on Madagascar using coalescent-based models of species delineation. *Systematic Biology* **58:** 298–311.

Moore JM, Carvajal JI, Rouse GW, Wilson NG. 2018. The Antarctic Circumpolar Current isolates and connects: Structured circumpolarity in the sea star *Glabraster antarctica*. *Ecology and Evolution* **8:** 10621–10633.

Morando M, Avila LJ, Sites JW Jr. 2003. Sampling strategies for delimiting species: genes, individuals, and populations in the *Liolaemus elongatus-kriegi* complex (Squamata: Liolaemidae) in Andean–Patagonian South America. *Systematic Biology* **52:** 159–185.

Múrias dos Santos A, Cabezas MP, Tavares AI, Xavier R, Branco M. 2016. TcsBU: a tool to extend TCS network layout and visualization. *Bioinformatics* **32:** 627–628.

Nelson MM, Mooney BD, Nichols PD, Phleger CF. 2001. Lipids of Antarctic Ocean amphipods: food chain interactions and the occurrence of novel biomarkers. *Marine Chemistry* **73:** 53–64.

Nyssen F, Brey T, Dauby P, Graeve M. 2005. Trophic position of Antarctic amphipods—enhanced analysis by a 2-dimensional biomarker assay. *Marine Ecology Progress Series* **300:** 135–145.

Orr JC, Fabry VJ, Aumont O, Bopp L, Doney SC, Feely RA, Gnanadesikan A, Gruber N, Ishida A, Joos F, Key RM, Lindsay K, Maier-Reimer E, Matear R, Monfray P, Mouchet A, Najjar RG, Plattner GK, Rodgers KB, Sabine CL, Sarmiento JL, Schlitzer R, Slater RD, Totterdell IJ, Weirig MF, Yamanaka Y, Yool A. 2005. Anthropogenic ocean acidification over the twenty-first century and its impact on calcifying organisms. *Nature* **437:** 681–686.

Orsi AH, Nowlin WD, Whithworth T III. 1993. On the circulation and stratification of the Weddell Gyre. *Deep Sea Research Part I: Oceanographic Research Papers* **40:** 169–203.

Orsi AH, Whitworth T III, Nowlin WD. 1995. On the meridional extent and fronts of the Antarctic Circumpolar Current. *Deep Sea Research Part I: Oceanographic Research Papers* **42:** 641–673.

Padial JM, Miralles A, De la Riva I, Vences M. 2010. The integrative future of taxonomy. *Frontiers in Zoology* **7:** 16.

Paradis E, Claude J, Strimmer K. 2004. APE: analyses of phylogenetics and evolution in R language. *Bioinformatics* **20:** 289–290.

Pearse J, Mooi R, Lockhart SJ, Brandt A. 2009. Brooding and species diversity in the Southern Ocean: selection for brooders or speciation within brooding clades? In: Krupnik I, Lang MA, Miller SE, eds. *Smithsonian at the Poles: contributions to International Polar Year science*. Washington: Smithsonian Institution Scholarly Press, 181–196.

Pearse JS, Bosch I. 1994. Brooding in the Antarctic: Östergren had it nearly right. In: David B, Guille A, Feral J-P, Roux M, eds. *Echinoderms through time*. Rotterdam: A. A. Balkema, 111–120.

Peña Othaitz J, Sorbe JC. 2020. *Eusirus bonnieri* sp. nov. (Crustacea: Amphipoda: Eusiridae), a new deep species from the southeastern Bay of Biscay (NE Atlantic Ocean). *Zootaxa* **4751:** 238–256.

Pfenninger M, Schwenk K. 2007. Cryptic animal species are homogeneously distributed among taxa and biogeographical regions. *BMC Evolutionary Biology* **7:** 121.

Pons J, Barraclough TG, Gomez-Zurita J, Cardoso A, Duran DP, Hazell S, Kamoun S, Sumlin WD, Vogler AP. 2006. Sequence-based species delimitation for the DNA taxonomy of undescribed insects. *Systematic Biology* **55:** 595–609.

Posada D. 2008. jModelTest: phylogenetic model averaging. *Molecular Biology and Evolution* **25:** 1253–1256.

Powell JR. 2012. Accounting for uncertainty in species delineation during the analysis of environmental DNA sequence data. *Methods in Ecology and Evolution* **3:** 1–11.

Puillandre N, Lambert A, Brouillet S, Achaz G. 2012a. ABGD, Automatic Barcode Gap Discovery for primary species delimitation. *Molecular Ecology* **21:** 1864–1877.

Puillandre N, Modica MV, Zhang Y, Sirovich L, Boisselier MC, Cruaud C, Holford M, Samadi S. 2012b. Large-scale species delimitation method for hyperdiverse groups. *Molecular Ecology* **21:** 2671–2691.

Raguá-Gil JM, Gutt J, Clarke A, Arntz WE. 2004. Antarctic shallow-water mega-epibenthos: shaped by circumpolar dispersion or local conditions? *Marine Biology* **144:** 829–839.

Rambaut A, Drummond AJ, Xie D, Baele G, Suchard MA. 2018. Posterior summarisation in Bayesian phylogenetics using Tracer 1.7. *Systematic Biology* **67:** 901–904.

Raupach MJ, Malyutina M, Brandt A, Wägele JW. 2007. Molecular data reveal a highly diverse species flock within the munnopsoid deep-sea isopod *Betamorpha fusiformis* (Barnard, 1920) (Crustacea: Isopoda: Asellota) in the Southern Ocean. *Deep Sea Research Part II: Topical Studies in Oceanography* **54:** 1820–1830.

Raupach MJ, Thatje S, Dambach J, Rehm P, Misof B, Leese F. 2010. Genetic homogeneity and circum-Antarctic distribution of two benthic shrimp species of the Southern Ocean, *Chorismus antarcticus* and *Nematocarcinus lanceopes*. *Marine Biology* **157:** 1783–1797.

Raupach MJ, Wägele JW. 2006. Distinguishing cryptic species in Antarctic Asellota (Crustacea: Isopoda) – a preliminary study of mitochondrial DNA in *Acanthaspidia drygalskii*. *Antarctic Science* **18:** 191–198.

Rauschert M, Arntz WE. 2015. *Antarctic macrozoobenthos: a field guide to the invertebrates living at the Antarctic seafloor*. Bremen: Arntz & Rauschert Selbstverlag.

Ren X, Huang L. 1991. Studies on Gammaridea and Caprellidea (Crustacea: Amphipoda) from the northwest waters off the Antarctic Peninsula. *Studia Marina Sinica* **32:** 185–323.

Riesgo A, Taboada S, Avila C. 2015. Evolutionary patterns in Antarctic marine invertebrates: an update on molecular studies. *Marine Genomics* **23:** 1–13.

Ronquist F, Huelsenbeck JP. 2003. MrBayes 3: Bayesian phylogenetic inference under mixed models. *Bioinformatics* **19:** 1572–1574.

Sáez AG, Lozano E. 2005. Body doubles. *Nature* **433:** 111.

Schlick-Steiner BC, Steiner FM, Seifert B, Stauffer C, Christian E, Crozier RH. 2009. Integrative taxonomy: a multisource approach to exploring biodiversity. *Annual Review of Entomology* **55:** 421–438.

Schloss IR, Abele D, Moreau S, Demers S, Bers AV, González O, Ferreyra GA. 2012. Response of phytoplankton dynamics to 19-year (1991–2009) climate trends in Potter Cove (Antarctica). *Journal of Marine Systems* **92:** 53–66.

Schüller M. 2011. Evidence for a role of bathymetry and emergence in speciation in the genus *Glycera* (Glyceridae, Polychaeta) from the deep eastern Weddell Sea. *Polar Biology* **34:** 549–564.

Simmons MP, Ochoterena H. 2000. Gaps as characters in sequence-based phylogenetic analyses. *Systematic Biology* **49:** 369–381.

Stamatakis A. 2014. RAxML version 8: a tool for phylogenetic analysis and post-analysis of large phylogenies. *Bioinformatics* **30:** 1312–1313.

Stoddart M. 2010. 'Antarctic biology in the 21st century – Advances in, and beyond the international polar year 2007–2008'. *Polar Sciences* **4:** 97–101.

Strugnell JM, Watts PC, Smith PJ, Allcock AL. 2012. Persistent genetic signatures of historic climatic events in an Antarctic octopus. *Molecular Ecology* **21:** 2775–2787.

Talavera G, Dincă V, Vila R. 2013. Factors affecting species delimitations with the GMYC model: insights from a butterfly survey. *Methods in Ecology and Evolution* **4:** 1101–1110.

Thatje S. 2012. Effects of capability for dispersal on the evolution of diversity in Antarctic benthos. *Integrative and Comparative Biology* **52:** 470–482.

Thomson GM. 1880. New species of Crustacea from New Zealand. *Annals and Magazine of Natural History* **6:** 1–6.

Thornhill DJ, Mahon AR, Norenburg JL, Halanych KM. 2008. Open-ocean barriers to dispersal: a test case with the Antarctic Polar Front and the ribbon worm *Parborlasia corrugatus* (Nemertea: Lineidae). *Molecular Ecology* **17:** 5104–5117.

d'Udekem d'Acoz C. 2008. Systematic and ecological diversity of amphipods. *Berichte zur Polar- und Meeresforschung* **569:** 48–56.

d'Udekem d'Acoz C. 2010. Contribution to the knowledge of European Liljeborgiidae (Crustacea, Amphipoda), with considerations on the family and its affinities. *Bulletin de l'Institut Royal des Sciences Naturelles de Belgique / Bulletin van het Koninklijk Belgisch Instituut voor Natuurwetenschappen* **80:** 127–259.

d'Udekem d'Acoz C, Robert H. 2008. Systematic and ecological diversity of amphipods. **569:** 48–56.

d'Udekem d'Acoz C, Schön I, Robert H. 2018. The genus *Charcotia* Chevreux, 1906 in the Southern Ocean, with the description of a new species (Crustacea, Amphipoda, Lysianassoidea). *Belgian Journal of Zoology* **148:** 31–82.

d'Udekem d'Acoz C, Verheye ML. 2013. Taxocoenoses of amphipod crustaceans. *Berichte zur Polar- und Meeresforschung* **665:** 57–67.

d'Udekem d'Acoz C, Verheye ML. 2017. *Epimeria* of the Southern Ocean with notes on their relatives (Crustacea, Amphipoda, Eusiroidea). *European Journal of Taxonomy* **359:** 1–553.

Vaidya G, Lohman DJ, Meier R. 2011. SequenceMatrix: concatenation software for the fast assembly of multi-gene datasets with character set and codon information. *Cladistics* **27:** 171–180.

Verheye ML. 2011. *Systématique et diversité génétique des Eusirus de l'Océan Austral (Crustacea, Amphipoda, Eusiridae). Mémoire présenté en vue de l'obtention du diplôme de Master en Biologie des Organismes et Ecologie*. Louvain-la-Neuve: Université Catholique de Louvain-la-Neuve.

Verheye ML, Backeljau T, d'Udekem d'Acoz C. 2016. Looking beneath the tip of the iceberg: diversification of the genus *Epimeria* on the Antarctic shelf (Crustacea, Amphipoda). *Polar Biology* **39:** 925–945.

Vinogradov G. 1999. Amphipoda. In: Boltovskoy D, ed. *South Atlantic Zooplankton*. Leiden: Backhuys Publishers, 1141–1240.

Vogler AP, Monaghan MT. 2007. Recent advances in DNA taxonomy. *Journal of Zoological Systematics and Evolutionary Research* **45:** 1–10.

Walker AO. 1903. Amphipoda of the "Southern Cross" Antarctic expedition. *Journal of the Linnean Society of London, Zoology* **29:** 38–64.

Weis A, Meyer R, Dietz L, Dömel JS, Leese F, Melzer RR. 2014. *Pallenopsis patagonica* (Hoek, 1881) – a species complex revealed by morphology and DNA barcoding, with description of a new species of *Pallenopsis* Wilson, 1881. *Zoological Journal of the Linnean Society* **170:** 110–131.

Wiens JJ, Penkrot TA. 2002. Delimiting species using DNA and morphological variation and discordant species limits in spiny lizards (*Sceloporus*). *Systematic Biology* **51:** 69–91.

Will KW, Mishler BD, Wheeler QD. 2005. The perils of DNA barcoding and the need for integrative taxonomy. *Systematic Biology* **54:** 844–851.

Xavier JC, Brandt A, Ropert-Coudert Y, Badhe R, Gutt J, Havermans C, Jones C, Costa ES, Lochte K, Schloss IR, Kennicutt MC II, Sutherland WJ. 2016. Future challenges in Southern Ocean ecology research. *Frontiers in Marine Science* **3:** 94.

Zhang J, Kapli P, Pavlidis P, Stamatakis A. 2013. A general species delimitation method with applications to phylogenetic placements. *Bioinformatics* **29:** 2869–2876.

Zhou WW, Wen Y, Fu J, Xu YB, Jin JQ, Ding L, Min MS, Che J, Zhang YP. 2012. Speciation in the *Rana chensinensis* species complex and its relationship to the uplift of the Qinghai-Tibetan Plateau. *Molecular Ecology* **21:** 960–973.

SUPPORTING INFORMATION

Additional Supporting Information may be found in the online version of this article at the publisher's web-site:

Table S1. Sampling details for the sequenced *Eusirus* specimens, including expedition, station, locality, geographical coordinates and GenBank accession numbers. N/A, data not available.
Table S2. Intraclade mean uncorrected *p*-distances (above) and corrected distances (below) in bold on the diagonal. Interclade mean uncorrected *p*-distances above the diagonal and corrected distances below. Distances were calculated for the following datasets: (A) *COI*; (B) *CytB*; and (C) ITS2. Corrected distances were computed respectively under the following substitution models: TrNef+G (G = 0.15), K80+G (G = 0.18) and Tamura-3-p+G (G = 0.22).
Figure S1. Results of the Bayesian implementation of the Poisson tree processes model (bPTP) analyses applied on the following Bayesian inference (BI) individual gene trees (produced with MrBayes): A, *CytB*; B, ITS2; and C, *COI*.
Figure S2. Results of the general mixed Yule coalescent (GMYC) analyses applied on the following individual ultrametric gene trees (produced with BEAST): A, *CytB*; B, ITS2; and C, *COI*.
Figure S3. Results of the multi-rate Poisson tree processes (mPTP) analyses applied on the following maximum likelihood (ML) individual gene trees (produced with RaxML): A, *CytB*; B, ITS2; and C, *COI*.
Figure S4. Results of the automatic barcode gap discovery (ABGD) analyses.